

# NANOPARTICLE-INDUCED GENE-SILENCING FOR THE SUPPRESSION OF INFLAMMATION

## **Dissertation**

To fulfill the  
requirements for the degree of  
**“doctor rerum naturalium” (Dr. rer.nat.)**

Submitted to the  
Council of the Faculty of Medicine  
of the Friedrich Schiller University Jena

By Elena Müller, M.Sc.

born on October 9<sup>th</sup>, 1992 in Lauf a. d. Pegnitz

Peer reviewers

- |                                 |                                         |
|---------------------------------|-----------------------------------------|
| 1. Prof. Dr. Ingrid Hilger      | Friedrich Schiller University Jena      |
| 2. Apl. Prof. Dr. Ignacio Rubio | Friedrich Schiller University Jena      |
| 3. Prof. Dr. Dagmar Fischer     | Friedrich-Alexander-University Erlangen |

Day of public thesis defense: October 18<sup>th</sup>, 2022

# Contents

Abbreviations .....	VI
Abstract .....	1
Zusammenfassung .....	2
1 Introduction .....	3
1.1 Inflammation .....	3
1.2 NF- $\kappa$ B .....	5
1.3 RNA interference .....	10
1.4 Calcium phosphate nanoparticles as transfection agents .....	12
2 Aims of the study .....	15
3 Materials & Methods .....	18
3.1 Materials .....	18
3.1.1 Nanoparticles .....	18
3.1.2 Cell lines .....	22
3.1.3 Animals .....	22
3.1.4 Used equipment and devices .....	22
3.1.5 Consumption items .....	23
3.1.6 Chemicals .....	24
3.1.7 Antibodies .....	27
3.1.8 Kits .....	29
3.1.9 Buffer and solutions .....	29
3.1.10 Software .....	30
3.2 Methods .....	31
3.2.1 Cell lines and culture conditions .....	31
3.2.2 Nanoparticle uptake and cell viability .....	31
3.2.3 Characterization of targets on immune cells for decorated nanoparticles and their specific uptake in these cells .....	32
3.2.4 Intracellular localization of nanoparticles after cellular uptake .....	32
3.2.5 Inhibition of nanoparticle uptake pathways in monocytes .....	33
3.2.6 Incubation of inflamed cells with siRNA-loaded nanoparticles .....	33

## Contents

---

3.2.7	p65 gene expression after incubation with siRNA-loaded nanoparticles.....	34
3.2.8	p65 protein expression after incubation with siRNA-loaded nanoparticles.....	35
3.2.9	Cytokine secretion after incubation with siRNA-loaded nanoparticles .....	35
3.2.10	Induction of colitis in mice and treatment with nanoparticles.....	36
3.2.11	Biodistribution of nanoparticles .....	37
3.2.12	Assessment of colitis severity by clinical disease parameters .....	38
3.2.13	Detection of inflammation marker Lipocalin-2 in feces .....	38
3.2.14	Preparation of tissue sections and immunostaining .....	39
3.2.15	<i>Ex vivo</i> colon cultivation for detection of secreted inflammatory mediators....	41
3.2.16	Isolation of leukocytes from colon tissue .....	41
3.2.17	Protein expression in whole colon tissue and colon leukocytes .....	41
3.2.18	Detection of cytokines/ chemokines in different samples.....	42
3.2.19	Data analysis.....	43
4	Results.....	44
4.1	Calcium phosphate nanoparticles for gene silencing of NF- $\kappa$ B and their impact on cellular players of inflammation .....	44
4.1.1	Uptake of nanoparticles in the cellular players of inflammation.....	44
4.1.2	Nanoparticles (undecorated) and their effect on monocytes .....	47
4.1.3	Nanoparticles decorated with cRGD peptide for the targeting of endothelial cells.....	52
4.1.4	Nanoparticles decorated with CD69-IgG for the targeting of B cells.....	53
4.1.5	Nanoparticles decorated with CD69-IgG for the targeting of T cells .....	55
4.2	Therapeutic efficiency of nanoparticles with p65 siRNA to ameliorate inflammation in a murine colitis model .....	59
4.2.1	Optimization of murine colitis model to study therapeutic efficiency of F-NPs	59
4.2.2	Impact of F-NPs on the development of colonic inflammation .....	60
4.2.3	Short-term therapeutic efficiency of F-NPs in colitis (measured 72 h after treatment).....	61
4.2.4	Long-term therapeutic efficiency of F-NPs in colitis.....	65
4.3	Biodistribution of nanoparticles and side effects .....	67
5	Discussion.....	72

## Contents

---

5.1	Nanoparticles with functional siRNA and their impact on the p65 expression and inflammatory process in cellular players of inflammation.....	72
5.1.1	Internalization of nanoparticles in the cellular players of inflammation .....	72
5.1.2	Internalization mechanism of nanoparticles .....	75
5.1.3	Cytoplasmic availability of nanoparticles after internalization.....	77
5.1.4	Efficiency of siRNA-nanoparticles in downregulation of p65 expression.....	78
5.1.5	Impact of siRNA-nanoparticles on inflammatory signaling.....	81
5.2	Therapeutic efficiency of nanoparticles with p65 siRNA in DSS-induced colitis in mice.....	83
5.2.1	Impact of F-NPs on the development of colitis.....	83
5.2.2	Impact of F-NPs on the inflammatory protein expression in the colonic tissue.....	84
5.2.3	Impact of F-NPs on the level of inflammatory mediators in colon and blood plasma.....	86
5.3	Potential off-target effects of the nanoparticles for the treatment of inflammation .	88
5.3.1	Biodistribution of nanoparticles in mice with local inflammation .....	88
5.3.2	Impact of siRNA <i>per se</i> on the inflammation process.....	89
5.3.3	Off-target effects of nanoparticles in healthy mice .....	90
6	Conclusion & Outlook .....	92
	References .....	93
	Appendix .....	104
	List of Figures .....	109
	List of Tables .....	111
	Scientific publications and presentations .....	112
	Ehrenwörtliche Erklärung.....	114

## Abbreviations

<b>(q)PCR</b>	Quantitative polymerase chain reaction
<b>5-ASA</b>	5-aminosalicylic acid
<b>a.u.</b>	Arbitrary unit
<b>AF</b>	Alexa Fluor
<b>APC</b>	Antigen-presenting cell
<b>APC</b>	allophycocyanin
<b>APS</b>	Ammonium persulfate
<b>aqua dest.</b>	<i>aqua destillata</i> , distilled water
<b>Bcl-2</b>	B-cell lymphoma 2
<b>BSA</b>	bovine serum albumin
<b>BW</b>	Body weight
<b>CaP</b>	Calcium phosphate
<b>CaP-NPs</b>	Calcium phosphate nanoparticles
<b>CD</b>	Crohn's disease
<b>cLSM</b>	confocal laser scanning microscopy
<b>CO<sub>2</sub></b>	Carbon dioxide
<b>COX-2</b>	inducible cyclooxygenase 2
<b>DAI</b>	Disease activity index
<b>DAMP</b>	Danger-associated molecular pattern
<b>ddH<sub>2</sub>O</b>	double-deionized water
<b>DLS</b>	Dynamic light scattering
<b>DMEM</b>	Dulbecco's Modified Eagle Medium
<b>DMSO</b>	Dimethyl sulfoxide
<b>DNA</b>	Deoxyribonucleic acid
<b>dsRNA</b>	Double-stranded RNA
<b>EDTA</b>	ethylenediaminetetraacetic acid
<b>ex/em</b>	excitation/ emission
<b>FACS</b>	fluorescence-activated cell sorting
<b>FBS</b>	fetal bovine serum
<b>FDA</b>	Food and drug administration USA
<b>FITC</b>	Fluorescein isothiocyanate
<b>GI</b>	gastrointestinal
<b>GM-CSF</b>	Granulocyte-macrophage colony-stimulating factor
<b>H<sub>2</sub>O</b>	Water
<b>HBSS</b>	Hank's Buffered Saline solution
<b>HCl</b>	Hydrochloric acid
<b>HRP</b>	Horseradish peroxidase
<b>HSP-90</b>	Heat shock protein 90
<b>IBD</b>	Inflammatory bowel disease
<b>IFN</b>	Interferon
<b>IgG</b>	Immunoglobulin G
<b>IHC</b>	Immunohistochemistry
<b>IKK</b>	IκB kinase complex

## Abbreviations

---

<b>IL</b>	interleukin
<b>iNOS</b>	Inducible nitric oxide synthase
<b>I<math>\kappa</math>B</b>	Inhibitor of NF- $\kappa$ B
<b>Lcn-2</b>	Lipocalin-2
<b>MCP-1</b>	Monocyte chemoattractant protein 1 (CCL2)
<b>MHC</b>	Major histocompatibility complex
<b>miRNA</b>	Micro RNA
<b>MLN</b>	Mesenteric lymph nodes
<b>mRNA</b>	Messenger RNA
<b>n.d.</b>	Not determined
<b>NEMO</b>	NF- $\kappa$ B essential modulator
<b>NF-<math>\kappa</math>B</b>	transcription factor nuclear factor- $\kappa$ B
<b>NIK</b>	NF- $\kappa$ B-inducing kinase
<b>NP</b>	Nanoparticle
<b>PAGE</b>	Polyacrylamide gel electrophoresis
<b>PAMP</b>	Pathogen-associated molecular pattern
<b>PBS</b>	phosphate-buffered saline
<b>PD-1</b>	Programmed death 1
<b>PDI</b>	Polydispersity index
<b>PE</b>	Phycoerythrin
<b>PEG</b>	Polyethylene glycol
<b>PEI</b>	polyethyleneimine
<b>PRR</b>	Pattern recognition receptor
<b>rcf</b>	relative centrifugal force
<b>RHD</b>	Rel homology domain
<b>RISC</b>	RNA-induced silencing complex
<b>RNA</b>	Ribonucleic acid
<b>RNAi</b>	RNA interference
<b>ROI</b>	Region of interest
<b>ROS</b>	Reactive oxygen species
<b>RT</b>	room temperature
<b>SDS</b>	sodium dodecyl sulfate
<b>siRNA</b>	Small interfering RNA
<b>TAD</b>	transcription activation domain
<b>TAK1</b>	TGF $\beta$ -activated kinase-1
<b>TCR</b>	T cell receptor
<b>TLR</b>	Toll-like receptor
<b>TNF</b>	Tumor necrosis factor
<b>TNFR</b>	Tumor necrosis factor receptor
<b>UC</b>	Ulcerative colitis
<b>v/v</b>	Volume per volume
<b>w/v</b>	Weight per volume

## Abstract

A dysregulated immune system can cause many different diseases, for example inflammatory bowel diseases like ulcerative colitis. In most of these disorders, the dysregulation of the transcription factor NF- $\kappa$ B as central regulator in inflammation is involved. The treatment options for these diseases, especially for long-time treatment of chronic conditions, are limited and often coupled with severe side effects. In recent years, novel treatments have emerged. Especially the application of nanoparticles as carrier systems for the targeted delivery of drugs is exceedingly studied. Furthermore, the mechanism of RNA interference presents an advantageous new therapeutic platform.

In this study, the biological activity of a novel formulation of calcium phosphate nanoparticles with incorporated p65 siRNA is assessed concerning the ability to silence NF- $\kappa$ B p65 expression and thereby ameliorate inflammatory processes. Data indicate that the nanoparticles are internalized in key cellular players of inflammation, namely monocytes, endothelial cells, B cells and T cells. The specific decoration of the nanoparticles even increased the uptake in some cell types. The internalization process was shown to be mostly energy-dependent, and the cargo of the nanoparticles was localized in the cytoplasm after uptake. Moreover, the p65 siRNA nanoparticles were efficient in downregulating p65 in target cells, where the impact was variably strong for the tested cell types.

Furthermore, investigations concerning the therapeutic efficiency in a murine colitis model revealed a distinct amelioration of the local inflammation after intravenous application of the nanoparticles carrying p65 siRNA. A distinct impact of the nanoparticles on the inflammatory signaling cascade in the colon could be shown. The biodistribution of the nanoparticles was clearly influenced by the colonic inflammation with increased localization in the adjacent lymphoid organs. Nanoparticles carrying non-functional, scrambled siRNA also showed distinct impact on the colonic inflammation, while no notable off-target effects of the nanoparticles were found in the colon of healthy mice.

Summarized, the data presented here demonstrate a versatile novel nanoparticle-based system for the suppression of NF- $\kappa$ B-mediated pro-inflammatory reactions in the main cellular players of inflammation and therefore the amelioration of colonic inflammation in mice. Hence, it offers a promising approach as a treatment of a plethora of different acute and chronic diseases in the future.



## Zusammenfassung

Überschießende oder dysregulierte Reaktionen des Immunsystems sind der Ausgangspunkt vieler verschiedener Krankheiten, zum Beispiel chronisch-entzündlicher Darmerkrankungen, wie Colitis ulcerosa. In viele dieser Erkrankungen ist der Transkriptionsfaktor NF- $\kappa$ B als zentraler Regulator involviert. Die Behandlungsmöglichkeiten, insbesondere für die Langzeitbehandlung chronischer Verläufe, sind limitiert und oftmals verbunden mit starken Nebenwirkungen. In den letzten Jahren wurden viele neuartige Behandlungsmethoden erforscht. Ein Fokus lag dabei auf der Anwendung von Nanopartikeln als Transportsystem für die spezifische lokale Ablieferung von Medikamenten. Außerdem ist die Anwendung der RNA Interferenz als therapeutischer Ansatz vielversprechend.

Im Rahmen dieser Dissertation wurde die biologische Aktivität einer neuartigen Formulierung aus Kalziumphosphat-Nanopartikeln mit eingebauter p65 siRNA untersucht in Bezug auf ihre Fähigkeit, die Expression von NF- $\kappa$ B p65 zu inhibieren und damit die Entzündungsprozesse zu vermindern. Die Ergebnisse zeigen eine Internalisierung der Nanopartikel in zelluläre Schlüsselspieler der Entzündung, hier Monozyten, Endothelzellen, B-Zellen und T-Zellen. Spezifische Dekorierungen der Nanopartikel verstärkten die Aufnahme in einige Zellarten. Es zeigte sich, dass der Aufnahmeprozess der Nanopartikel größtenteils energieabhängig ist und dass nach der Aufnahme die Fracht der Partikel im Zytoplasma zu finden ist. Außerdem waren die Nanopartikel mit p65 siRNA in der Lage, die p65 Expression in den Zielzellen herunterzuregulieren, wobei die Stärke des Effektes abhängig war von der Zellart.

Des Weiteren zeigten die Untersuchungen zur therapeutischen Effizienz der Nanopartikel in einem murinen Kolitis-Modell eine deutliche Verbesserung der lokalen Entzündung nach intravenöser Gabe. Die Nanopartikel schwächten die entzündliche Signalkaskade im Darm deutlich ab. Die lokale Entzündung beeinflusste die Verteilung der Nanopartikel im Organismus deutlich, was sich dadurch zeigte, dass die Partikel verstärkt in benachbarten lymphoiden Organen zu finden waren. Nanopartikel mit nicht-funktionaler siRNA beeinflussten die Entzündung im Darm ebenfalls, wohingegen keine deutlichen lokalen Nebenwirkungen der Nanopartikel im Darm gesunder Tiere sichtbar waren.

Zusammenfassend wird in dieser Arbeit ein vielseitiges Nanopartikel-basiertes System für die Inhibition von NF- $\kappa$ B-gesteuerten entzündlichen Reaktionen in den wichtigsten Zelltypen vorgestellt, was zu einer deutlichen Verbesserung der Kolon-Entzündung in Mäusen führt. Damit eröffnet dieses System zukünftig eine neuartige Behandlungsmöglichkeit für eine Vielzahl verschiedener akuter und chronischer entzündlicher Erkrankungen.

# 1 Introduction

## 1.1 Inflammation

Inflammation is the protective immune mechanism by which the body deals with invading pathogens or tissue injury and the associated challenges to homeostasis. Dysregulated or non-resolving inflammation is associated with many common diseases and disorders, like inflammatory bowel disease (IBD) (Matricon *et al.* 2010), cancer (Diakos *et al.* 2014), sepsis (Taeb *et al.* 2017, Hattori *et al.* 2017), obesity (Zeyda and Stulnig 2009), diabetes (Donath 2014), various cardiovascular diseases, like atherosclerosis and acute myocardial infarction (Ruparelia *et al.* 2017, Tabas *et al.* 2015), as well as Alzheimer disease (Wyss-Coray and Rogers 2012), and other mood disorders (Rosenblat *et al.* 2014). Acute inflammation is characterized by local vasodilation and increased vascular permeability, the migration of neutrophils to the site of inflammation, accumulation of fluid and proteins into interstitial space and the release of inflammatory mediators. This is indicated by the five cardinal signs of inflammation: *rubor* (redness), *calor* (heat), *tumor* (swelling), *dolor* (pain), and *functio laesa* (loss of function). The highly organized process of inflammation can be generally structured into four main stages. First, the initial insult of pathogens is recognized by the binding of pathogen-associated or danger-associated molecular patterns (PAMPs and DAMPs) by innate pattern recognition receptors (PRRs) on tissue macrophages or mast cells. Second, this capturing leads to a transduction of the initial signal via different cascades, resulting in the transcriptional activation and secretion of pro-inflammatory mediators, like cytokines and chemokines. Afterwards, these molecules mediate the exacerbation of pro-inflammatory signals and the progression of inflammation via the recruitment and activation of additional immune cells. Third, recruited and activated immune cells eliminate invading pathogens by secretion of additional signaling molecules, degranulation, and the generation of reactive oxygen species (ROS). Oxidative stress triggered by redox reactions is critical in the pathophysiology of inflammation. The ideal outcome of inflammation is the resolution, the fourth step, which is classically defined as the time between peak inflammatory cell influx and the restoration of functional homeostasis (Fullerton and Gilroy 2016). This last stage of inflammation is initiated as a negative feedback launched partly by the host response during the inflammatory phase and is governed by a complex balance between pro- and anti-inflammatory events (Headland and Norling 2015, Serhan 2009, Sugimoto *et al.* 2016, Buckley *et al.* 2014). In analogy to the cardinal signs of inflammation also five characteristics can be defined for the resolution phase: the removal of microbes and dead cells, the restoration of vascular integrity, the

regeneration of tissue, the remission of fever, and the relief of pain (Basil and Levy 2016). Key mechanisms are therefore the induction of apoptosis in spent neutrophils, the termination of the synthesis of pro-inflammatory mediators, the transformation of classically activated to alternatively activated macrophages, and the cessation of neutrophil tissue infiltration (Headland and Norling 2015, Fullerton and Gilroy 2016).

As mentioned above, inflammatory bowel diseases (IBD) are one of the common conditions resulting from dysregulated or non-resolving inflammation. Common characteristics of IBD are severe inflammation of the colon and/or the small intestine resulting in frequent diarrhea and abdominal pain (Matricon *et al.* 2010). The two most common subtypes of IBD are Crohn disease (CD) (Torres *et al.* 2017) and ulcerative colitis (UC) (Ungaro *et al.* 2017), which show distinctive inflammation patterns with histological alterations in the intestinal wall of the entire gastrointestinal (GI) tract (CD), or only in the colon and caecum (UC) (Matricon *et al.* 2010). Many factors influence the development of UC, like diet, microbiota and genetic predisposition (Hmar *et al.* 2021). Furthermore, patients with UC have an increased risk for development of colorectal cancer compared to the general population (Jess *et al.* 2012). Recent statistics set the incidence of UC in Europe to 2.4 to 44.0 per 100,000 person-years, which has risen markedly in the last years (Zhao *et al.* 2021).

Treatment options for UC are dependent on the severity of the disease and are primarily aimed to induce and maintain remission to resolve the clinical symptoms and prevent colectomy and colorectal cancer (Ungaro *et al.* 2017). For mild colitis, 5-aminosalicylic acid (5-ASA) drugs are commonly used and often administered via suppositories to directly reach the site of inflammation. In case this treatment option does not render an amelioration of symptoms, corticosteroids can be used alone or in combination with 5-ASA. Due to their substantial adverse side effects, including increased risk for infection, hypertension, decreased wound healing, edema, peptic ulcers, and psychoses, corticosteroids are in general only used in severe inflammation disorders where other anti-inflammatory drugs have not been efficient (Brenner and Krakauer 2003). Moderate to severe UC can be treated using thiopurines (azathioprine or 6-mercaptopurine), anti-TNF- $\alpha$  drugs (like infliximab, adalimumab, golimumab) or the combination of both (Hmar *et al.* 2021). Patients with severe acute UC are treated with intravenous corticosteroids, but ultimately colectomy is indicated in case the drug treatment fails (Ungaro *et al.* 2017, Hmar *et al.* 2021). Besides drug treatments, the transplantation of healthy fecal microbiota is also discussed as a treatment option for UC and has shown promising results (Hmar *et al.* 2021).

Recently, new treatment options based on nanotechnology have emerged. For example, synthesized nanoparticles were used to transport (plant-derived) drugs to the inflammation site to overcome unfavorable properties, like low bioavailability, of the already well

characterized drugs (Conte *et al.* 2017, Szelenyi 2012). Another study to treat colonic inflammation tested selenium nanoparticles coupled with a polysaccharide, which was proven to have promising immunomodulatory effects for the treatment of IBD (Zhu *et al.* 2017). Moreover, another group of researchers developed self-derived nanovesicles consisting of phospholipids and cholesterol enriched with leukocyte membrane proteins, that were extracted from primary immune cells to treat colitis in mice (Corbo *et al.* 2017). But despite these recent advances in treatment, especially for acute severe inflammation, the treatment options are still limited and further research for novel, safe, and well-tolerated drugs with increased efficiency for maintaining long-term remission of UC is needed.

In this context, animal models are needed to mirror the human disease and study the efficiency of novel therapeutics. Many different mouse models for IBD were established, which can be classified as chemically induced models, cell-transfer-models, spontaneous models, and genetically engineered models (Mizoguchi 2012). Due to their simple induction mechanisms, and their controllable immediate onset, duration and severity of inflammation, chemically induced models are most commonly used (Perše and Cerar 2012). Among these, the induction of colitis by administration of dextran sulfate sodium (DSS) via the drinking water is most frequently used (Chassaing *et al.* 2014, Manicassamy and Manoharan 2014, Mizoguchi 2012, Whitem *et al.* 2010). The clinical and histopathological features of this model reflect those of human IBD (Perše and Cerar 2012). The oral administration of DSS with a molecular weight of about 40 kDa was shown to develop diffuse colitis in middle and distal third of the large bowel compared to lower or higher molecular weights (Kitajima *et al.* 2000). Early changes in the colonic region during DSS colitis involve mucin depletion, epithelial degeneration, and necrosis leading to disappearance of epithelial cells. In the advanced phase neutrophil infiltration in the lamina propria and submucosa, cryptitis, crypt abscesses and phlegmonous inflammation in mucosa and submucosa are visible (Perše and Cerar 2012).

## 1.2 NF- $\kappa$ B

Among the many signaling pathways, that mediate the second step during the inflammatory process by potentiating the initial signal, the NF- $\kappa$ B pathway is one of the most important ones. The transcription factor nuclear factor- $\kappa$ B (NF- $\kappa$ B) acts as central mediator of pro-inflammatory gene induction and functions in both innate and adaptive immune cells. It plays a most important and evolutionary conserved role in the immune response, but also impacts the cell survival, differentiation, and proliferation (Hayden and Ghosh 2008).

Remarkably, a plethora of stimuli, including endogenous and exogenous ligands as well as a diversity of physical and chemical stresses may lead to the activation of the NF- $\kappa$ B

pathway. Furthermore, many important inflammatory genes are directly transcriptionally regulated by NF- $\kappa$ B, including cytokines and chemokines (e.g., interleukins IL-1 or IL-6, tumor necrosis factor  $\alpha$  (TNF- $\alpha$ )), immunoreceptors (e.g., toll-like receptors (TLRs)), major histocompatibility complexes (MHC)), regulators of apoptosis (e.g., B-cell lymphoma 2 (Bcl-2)), growth factors (e.g., Granulocyte-macrophage colony-stimulating factor (GM-CSF)), different enzymes (e.g., Inducible nitric oxide synthase (iNOS), inducible cyclooxygenase-2 (COX-2)) as well as NF- $\kappa$ B itself and its regulators (Gilmore-Lab Boston University).

The NF- $\kappa$ B family of transcription factors is composed of five structurally related members (p50, p52, p65/ RelA, c-Rel, and RelB), that all share an N-terminal Rel homology domain (RHD) (Chen *et al.* 2001). This domain is responsible for the homo- or heterodimerization of the NF- $\kappa$ B proteins, as well as the binding of these dimers to the DNA at a specific element, the  $\kappa$ B enhancer (Liu *et al.* 2017). Among the NF- $\kappa$ B members, only p65, c-Rel and RelB possess the transcription activation domain (TAD), which is necessary for the positive regulation of gene expression (Xiao 2004). Out of these subunits, p65 was found to be the most important player in managing inflammatory responses, since it controls the transcriptional regulation of many key inflammatory mediators (Schmitz and Baeuerle 1991). The other members, p50 and p52 may repress the transcription as homodimers bound to DNA, unless they form heterodimers with TAD-containing subunits (Hayden and Ghosh 2008).

In general, the NF- $\kappa$ B pathway can be divided into the canonical and the noncanonical signaling route, which are both important for the regulation of immune and inflammatory responses despite regulating different distinct sets of target genes (Hayden and Ghosh 2008, Liu *et al.* 2017). The canonical pathway is connected to all mechanisms of immune response, while the noncanonical route is mainly a supplementary signaling axis, that participates in the regulation of specific functions of the adaptive immune system (Liu *et al.* 2017).

A basic scheme of the canonical signaling is shown in Figure 1. Inactive NF- $\kappa$ B dimers are bound to its inhibitor I $\kappa$ B and are localized in the cytoplasm. The I $\kappa$ B family of inhibitors consists of different members, all characterized by multiple ankyrin repeat domains, with I $\kappa$ B $\alpha$ , I $\kappa$ B $\beta$ , or I $\kappa$ B $\epsilon$  as typical subunits (Yates and Gorecki 2006). The presence of inactive NF- $\kappa$ B dimers, that can be inducibly and rapidly activated is crucial for the signal responsiveness of this pathway (Hayden and Ghosh 2008). The NF- $\kappa$ B signaling is based on a series of positive and negative regulatory elements. Inducing stimuli for the canonical pathway include ligands of various cytokine receptors, PRRs, TNF receptor (TNFR) superfamily members, as well as T cell- and B cell-receptors (Liu *et al.* 2017). These stimuli activate the I $\kappa$ B kinase complex (IKK) through several kinases, especially the

TGF $\beta$ -activated kinase-1 (TAK1) (Sato *et al.* 2005), which leads to phosphorylation of I $\kappa$ B proteins bound to NF- $\kappa$ B dimers (Xiao 2004). The IKK complex consists of two highly homologous catalytic kinase subunits IKK $\alpha$  and IKK $\beta$  and a regulatory subunit NEMO (NF- $\kappa$ B essential modulator)/IKK $\gamma$  (Hayden and Ghosh 2008). In the canonical signaling both of the mentioned kinase subunits can mediate phosphorylation of I $\kappa$ B proteins. The phosphorylation occurs at two N-terminal serins, which triggers the ubiquitin-dependent degradation of I $\kappa$ B in the proteasome (Liu *et al.* 2017). The release of the NF- $\kappa$ B dimers from the inhibitor, which masks the nuclear localization sequence, subsequently leads to rapid and transient nuclear translocation, binding to  $\kappa$ B sites with the consensus sequences 5' GGGRNWWYYCC 3' (N: any base, R: purine; W: adenine or thymine; Y: pyrimidine) (Hoffmann *et al.* 2006) in the promoter/ enhancer regions of target genes and finally to the regulation of their transcription (Xiao 2004). The transcription of target genes can be further regulated by posttranscriptional modifications of NF- $\kappa$ B, that affect the capacity to interact with transcriptional coactivators (Hayden and Ghosh 2008). The signaling cascade is regulated by a negative feedback loop, in which the NF- $\kappa$ B dimers activate the transcription of their own inhibitors I $\kappa$ B, resulting in the termination of the response (Hayden and Ghosh 2008).

In contrast, the noncanonical / alternative pathway is regulated through inducible proteasomal processing of p100, the precursor of p52 and also through the C-terminal I $\kappa$ B-like RelB-specific inhibitor (Sun 2011). The processing generates mature p52 dimers, that can translocate to the nucleus and activate expression of target genes (Liu *et al.* 2017). Induction of the noncanonical signaling is mediated by a subset of TNFR superfamily members, such as LT $\beta$ R, BAFFR, CD40 and RANK (Sun 2011). As a central and required signaling molecule, the NF- $\kappa$ B-inducing kinase (NIK) activates and functionally cooperates with IKK $\alpha$  to facilitate the p100 phosphorylation and subsequent processing (Liu *et al.* 2017). Indeed, NIK was found to be required for the noncanonical NF- $\kappa$ B signaling (Senftleben *et al.* 2001).

As a central mediator of inducing pro-inflammatory gene expression, the NF- $\kappa$ B signaling has important, distinct functions both in innate and adaptive immune cells.

Innate immune cells, like macrophages, dendritic cells, and neutrophils, are essential for the innate immune response during inflammation. All these cells express PRRs, that recognize PAMPs and DAMPs and activate the NF- $\kappa$ B pathway for subsequent expression of many pro-inflammatory mediators (Newton and Dixit 2012). Some of these induced mediators, in turn, may activate the differentiation of T cells or other inflammatory cells (Liu *et al.* 2017). For macrophages in detail, the activation of NF- $\kappa$ B signaling in tissue-resident cells acts as the first line of immunological defense against infections. Activated M1 macrophages

express a large number of inflammatory mediators, like TNF- $\alpha$ , IL-1 $\beta$ , IL-6, IL-12p40 and COX-2, that are controlled by the key transcription factor NF- $\kappa$ B (Liu *et al.* 2017).

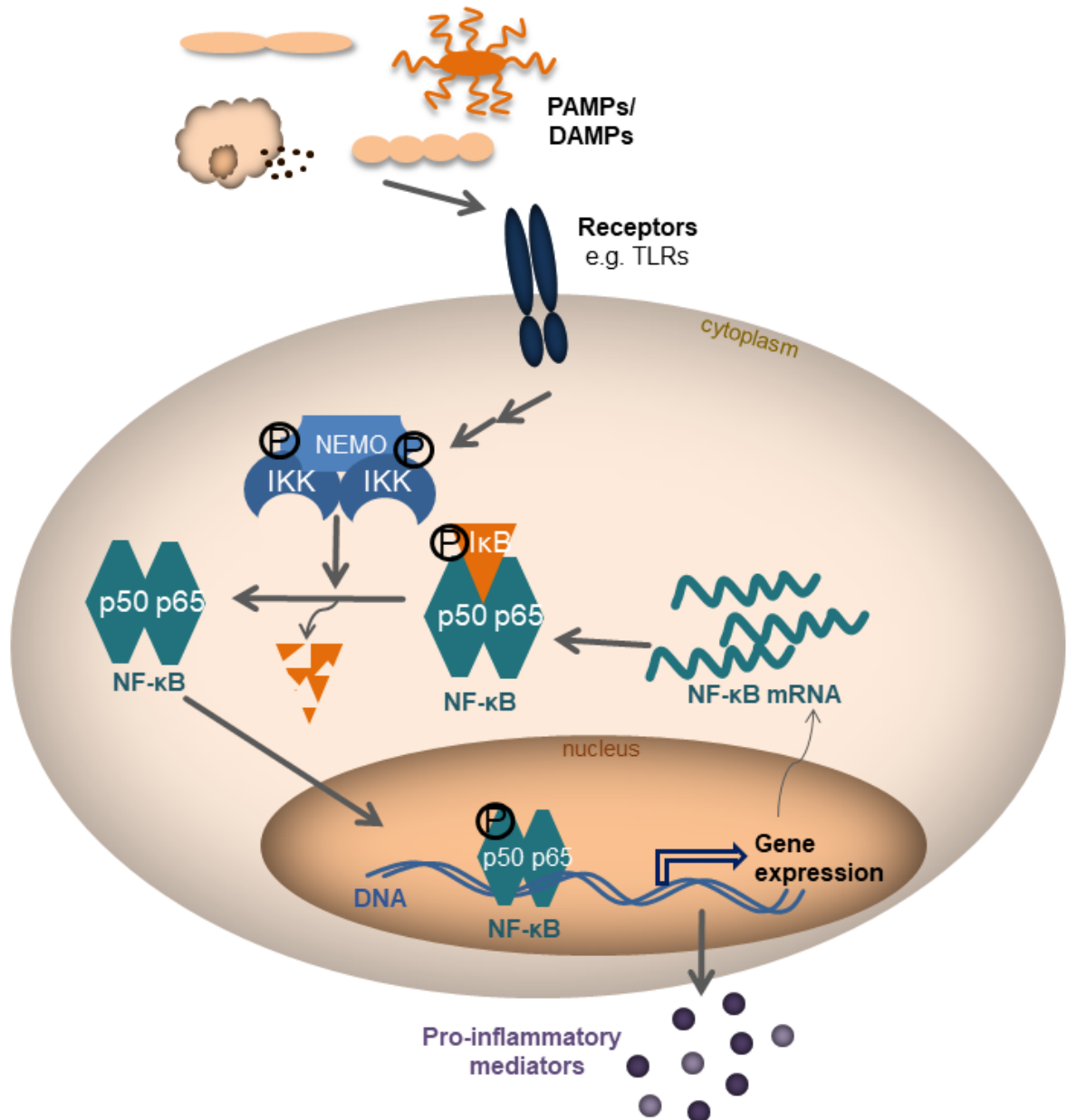


Figure 1: **Scheme of the canonical NF- $\kappa$ B signaling pathway** (own figure). PAMPs/ DAMPs: pattern-/ danger-associated molecular patterns; TLR: toll-like receptor; NEMO: NF- $\kappa$ B essential modulator; IKK: I $\kappa$ B kinase complex; P: phosphorylation; I $\kappa$ B: inhibitor of NF- $\kappa$ B; mRNA: messenger RNA.

As part of the adaptive immune system, T cells, particularly CD4<sup>+</sup> helper cells, also play an essential role in the inflammatory response. Naïve T cells are activated upon stimulation of the T cell receptor (TCR) by specific antigen presentation of antigen-presenting cells (APCs). Signaling downstream of the TCR is strongly dependent on the NF- $\kappa$ B pathway (Liu *et al.* 2017). Furthermore, this pathway is involved in the development, differentiation, activation, and survival of T cells, and both the canonical and the noncanonical pathway seem to play important, but distinct roles (Oh and Ghosh 2013).

In B cells, the NF- $\kappa$ B signaling is involved in the formation and maturation of marginal zone and follicular mature B cells (Gerondakis and Siebenlist 2010). Again, both NF- $\kappa$ B pathways are important for the activation of B cells, as well as the maintenance and general functions (Kaileh and Sen 2012).

Besides immune cells, the NF- $\kappa$ B signaling also has distinct key roles in the pro-inflammatory responses of endothelial cells, including the activation of a pro-adhesive phenotype and the reduction of barrier functions (Mussbacher *et al.* 2019).

In many diseases that are associated with inflammatory reactions, the dysregulation of the NF- $\kappa$ B signaling pathway has been implicated (Hayden and Ghosh 2008). In detail, NF- $\kappa$ B was shown to be involved in the pathogenesis of rheumatoid arthritis, multiple sclerosis, atherosclerosis, type I diabetes, asthma, and inflammatory bowel diseases, to name a few (Liu *et al.* 2017, Pai and Thomas 2008). Recently, targeting the NF- $\kappa$ B pathway was also suggested for the treatment of critically ill COVID-19 patients (Kircheis *et al.* 2020).

In IBD patients, a constitutive activation of NF- $\kappa$ B was found in the inflamed colonic tissue (Schreiber *et al.* 1998) and genetic mutations in the NF- $\kappa$ B-stimulating immune receptors and NF- $\kappa$ B target genes, like IL-12 and IL-23, were also associated with human IBD (Abraham and Cho 2009). Since NF- $\kappa$ B is important for maintaining the epithelial integrity and intestinal immune homeostasis in intestinal epithelial cells, the abnormal activation of NF- $\kappa$ B or genetic mutations may contribute to the pathogenesis of IBD (Liu *et al.* 2017).

Due to this involvement of NF- $\kappa$ B in the development of colonic inflammation, targeting this signaling pathway suggests an attractive approach for a therapeutic intervention. Indeed, several categories of inhibitors of the NF- $\kappa$ B pathway have been developed, such as IKK inhibitors (e.g., sc-514), proteasome inhibitors (e.g., Bortezomib), or blockers of the nuclear translocation of NF- $\kappa$ B (e.g., Selinexor) (Liu *et al.* 2017, Sehnert *et al.* 2020, Ramadass *et al.* 2020). Furthermore, drugs targeting the TLR4 signaling or the TNF- $\alpha$  signaling were shown to be effective in IBD, due to indirectly inhibiting the NF- $\kappa$ B pathway (Dejban *et al.* 2021, Gareb *et al.* 2020). Another approach would be to directly inhibit the NF- $\kappa$ B molecules or even target their expression. Also, some well-established drugs have been shown to inhibit the NF- $\kappa$ B pathway by acting on key players in the signaling cascade, like sodium salicylate, which was shown to block the degradation of I $\kappa$ B $\alpha$  (Kopp and Ghosh 1994). Despite the benefits of these treatments to inhibit NF- $\kappa$ B signaling, there are distinct obstacles for their application regarding the balance between efficacy and safety, since the NF- $\kappa$ B signaling is essential for normal cellular function in the whole organism.



### 1.3 RNA interference

The discovery of the RNA interference (RNAi) process not only revolutionized the understanding of gene regulation (Carthew and Sontheimer 2009, Wilson and Doudna 2013), but also revealed a novel mechanism to selectively inhibit the expression of specific target proteins as a therapeutic approach (Kim and Rossi 2007). Initially discovered as single microRNA (miRNA) in the *Caenorhabditis elegans* genome (Lee *et al.* 1993, Fire *et al.* 1998), in the meantime it has been identified as a natural process in both plants and animals to control the expression of genetic information (Shabalina and Koonin 2008).

The endogenous process of RNAi controls many vital mechanisms such as cell growth, tissue differentiation, heterochromatin formation and cell proliferation (Lu *et al.* 2008, Wilson and Doudna 2013). Indeed, about 5% of the human genome was proven to encode for micro RNAs (miRNAs), that regulate at least 30% of all genes by RNAi (Jinek and Doudna 2009, MacFarlane and Murphy 2010, Wilson and Doudna 2013).

The mechanism of RNAi, as depicted in Figure 2, is generally based on the direct inhibition of target genes using complementary short RNA strands. Here, a discrimination can be made between the endogenous microRNAs (miRNAs) and small interfering RNAs (siRNAs), that are typically exogenous and of synthetic or viral origin (Wilson and Doudna 2013). Both types of RNA share a common mode of action. These RNAi precursors are trimmed down to a double-stranded (ds)RNA duplex of appropriate size, typically by the Dicer enzyme (Shabalina and Koonin 2008). The resulting dsRNA consists of a duplex of 21 to 25 nucleotides, with a two nucleotide-overhang at each 3' terminus and a phosphate group at each recessed 5' terminus (Schwarz *et al.* 2003). Binding of an Argonaute family protein to this effector RNA forms the RNA-induced silencing complex (RISC) (Wilson and Doudna 2013). During this process, the dsRNA is divided into single strands, with the guide/antisense strand being bound to the RISC and the passenger/ sense strand being discarded (Zhang *et al.* 2021). Complementary binding of the guide strand to its target mRNA sequence finally triggers the cleavage of the mRNA by the Argonaute endonucleases inside the RISC (Wilson and Doudna 2013). The efficiency of the gene silencing elicited by RNAi is dependent on many crucial factors, like the dynamics of gene expression and the applied dosage of RNA (Raab and Stephanopoulos 2004).

RNAi as a therapeutic approach offers key advantages since the efficiency of siRNA is mostly dependent on the exact base pairing with the target mRNA, compared to small molecular inhibitors or mononuclear antibodies, which have to recognize the complicated spatial conformation of the target proteins with high affinity and specificity (Hu *et al.* 2020). Therefore, siRNA therapeutics potentially offer reduced research and development times together with more possible therapeutic applications, compared to other inhibitors.

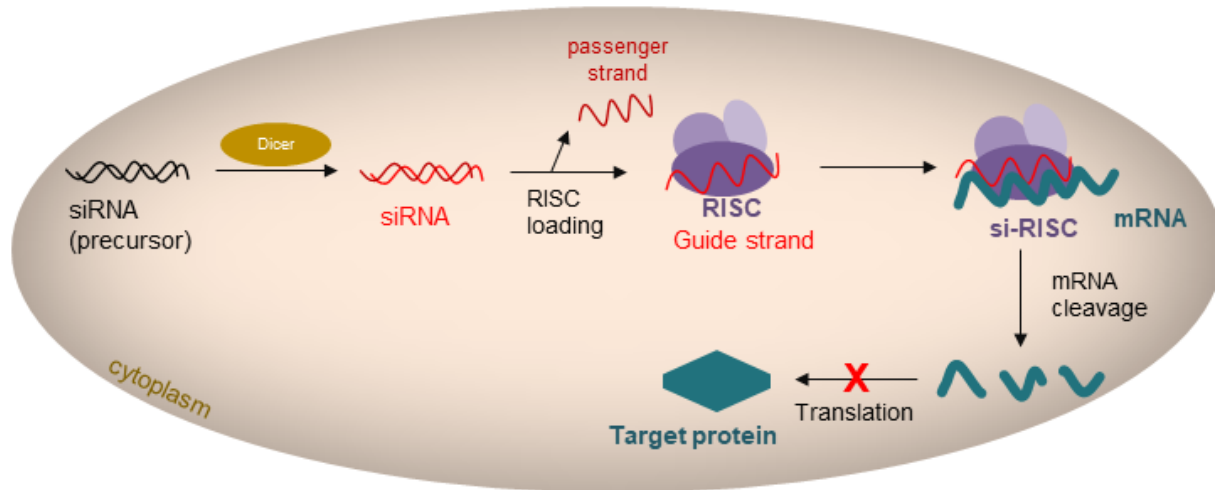


Figure 2: **Schematic depiction of the process of RNA interference (RNAi)** (own figure). siRNA: small interfering RNA, RISC: RNA-induced silencing complex; si-RISC: RISC-siRNA complex; mRNA: messenger RNA.

Recent studies investigated the application of siRNA against different targets involved in inflammation and other diseases, like IKK $\beta$  (Lee *et al.* 2021b), TNF- $\alpha$  (Gurcan *et al.* 2021, Tenkumo *et al.* 2020), programmed death 1 (PD-1) (Gao *et al.* 2021), heat shock protein 90 (Hsp-90) (Yang *et al.* 2020), as well as NF- $\kappa$ B (Rauch *et al.* 2021, Wang *et al.* 2020). In 2018, the first RNAi-based drug, named Patisiran, was approved by the FDA (Food and Drug Administration USA) for the treatment of hereditary transthyretin amyloidosis in the liver by targeting the protein transthyretin, whose mutations cause the disease (Setten *et al.* 2019, Zhang *et al.* 2021). To date, three further siRNA-based agents were approved by the FDA, seven drugs undergo phase 3 clinical trials, and several others are in advanced stages of the drug development pipeline (Zhang *et al.* 2021). The drug candidates are tested for the treatment of many different diseases, including cancer, neurodegenerative diseases, ocular diseases, and viral diseases (Kim and Rossi 2007).

Despite the obvious advantages, there are some barriers for the therapeutic application of RNAi and disadvantages to be considered. Systemic application of naked siRNA will directly result in the degradation by endonucleases and exonucleases, which prevents the active therapeutic siRNA from reaching the intended tissue, resulting in poor stability and pharmacokinetic behavior (Hu *et al.* 2020, Setten *et al.* 2019).

Furthermore, the siRNA may trigger unwanted side effects, like activation of TLR3 or silencing of other genes by mismatched pairing (Hu *et al.* 2020, Setten *et al.* 2019). To circumvent most of the unwanted effects in off-target tissues, the specific accumulation of the siRNA in the target tissue is an important consideration to be made for the application as therapeutic agents.

Moreover, due to their large molecular weight and substantial negative charge, siRNA molecules cannot easily diffuse through cellular membranes, as is possible for small molecule drugs (Akhtar and Benter 2007). Therefore, the effective trafficking across cellular lipid bilayer membranes is an extensive obstacle to be considered for the application of siRNA as therapeutic agents. Having overcome this barrier, the next obstacle is the cytoplasmic location of the siRNA needed for efficient gene silencing. Uptake of siRNA molecules by endocytic processes will lead to endolysosomal location of the siRNA, where the siRNA would eventually be degraded due to acidic conditions (Martens *et al.* 2014). An escape from the entrapment in the endolysosomes is therefore another important step for the effective application of siRNA drugs.

Recent studies suggest different approaches to overcome the barriers and disadvantages of siRNA as therapeutic agents. On the one hand, chemical modifications of siRNA molecules (phosphonate, ribose, or base modifications) can enhance the efficiency, specificity and stability of the siRNA, while reducing the toxicity and immunogenicity (Hu *et al.* 2020, Setten *et al.* 2019, Zhang *et al.* 2021). On the other hand, incorporation of the siRNA into carriers renders protection from endonucleases, while allowing for specific targeting of tissues and cells, and especially facilitating the transmembrane trafficking and endolysosomal escape (Hu *et al.* 2020, Setten *et al.* 2019, Dowdy 2017, Wang *et al.* 2010). Generally, viral carriers can be effectively used to transport siRNA due to their intrinsic mechanism for gene transduction, like Retroviruses, Lentiviruses, Adenoviruses, Adeno-Associated Viruses, and Baculoviruses (Li *et al.* 2006). Besides the viral delivery, non-viral carriers present another option to transport and protect the siRNA in the organism, including cationic liposomes, polymers, and inorganic nanoparticles (Liu *et al.* 2018, Tatiparti *et al.* 2017, Akhtar and Benter 2007, Guo *et al.* 2010). An important advantage of the application of nanoparticles is the possibility of coupling different moieties on the surface of the nanoparticles, like specific antibodies, for the targeting of different cell types or tissues (Notabi *et al.* 2021, Lee *et al.* 2021a, Yang *et al.* 2019).

### **1.4 Calcium phosphate nanoparticles as transfection agents**

As mentioned above, the specific delivery of siRNA to the target tissue and inside the cytoplasm and the protection from degradation is still an obstacle for the application as therapeutic treatment. Such a delivery vehicle should be biocompatible, easy to produce, and should protect the siRNA from enzymatic degradation and rapid clearance. Furthermore, a targeted delivery to the tissue of interest where the cargo siRNA can be released accurately is desired (Xu *et al.* 2016). One possible delivery method is to

incorporate the siRNA molecules into nanoparticles. For nanoparticle-based delivery of siRNA, various materials, like lipids, polymers and inorganic nanomaterials, have been used (Zu and Gao 2021). Decoration of the nanoparticles with special targeted moieties assists in accurate targeted delivery (Layek and Singh 2019, Tian *et al.* 2020)

Among the inorganic materials, calcium phosphate (CaP) is very promising due to its inherent biocompatibility and biodegradability (Xu *et al.* 2016). Since it is a natural component of human hard tissue, for example bone and teeth, the general cytotoxicity is negligible (Epple *et al.* 2010). Another advantage of CaP nanoparticles (CaP-NPs) for the delivery of siRNA is the possibility to easily introduce functional moieties on the nanoparticles' surface for the targeting of specific tissues or cell types. Furthermore, fluorescent dyes can be introduced into or onto the nanoparticles for tracking purposes.

Notably, calcium phosphate-based delivery vehicles for DNA were already developed 40 years ago, while applications for siRNA followed shortly after the discovery of the RNAi mechanism (Xu *et al.* 2016). Since then, they have been used as carriers for siRNA or DNA for many different applications, including the targeted delivery to tumors for cancer treatment (Zhang *et al.* 2020a, Huang *et al.* 2020, Li *et al.* 2019), gene silencing of TNF- $\alpha$  (Tenkumo *et al.* 2020), or bone regeneration (Levingstone *et al.* 2019).

As already discussed above, the cytoplasmic location is important for the efficient delivery of siRNA into the cells. CaP-NPs support the delivery by being internalized into the cells via the endocytosis route (Epple 2018). CaP in the endolysosomes will be dissolved by the acidic conditions, which increases the osmotic pressure inside the endolysosomes. Ultimately this leads to rupture of the lysosomes, facilitating the release of the nanoparticle components into the cytoplasm (endolysosomal escape) (Martens *et al.* 2014, Epple 2018). Some adaptations in the nanoparticle composition can enhance the rupture efficiency, for example the addition of positively charged moieties (like polyethyleneimine (PEI), poly-L-lysine, or imidazole-containing polymers) (Martens *et al.* 2014, Nimesh *et al.* 2011).

Despite the good internalization capabilities of CaP-NPs, still a main problem is the physical instability and low transfection efficiency of those nanoparticles that limits their therapeutic application (Xu *et al.* 2016). Different strategies for the stabilization of CaP-NPs have been proposed, among them coating with polyethylene glycol (PEG), liposomes, or silica (Xu *et al.* 2016). Indeed, CaP-NPs coated with a silica shell with incorporated siRNA were shown to have excellent transfection capability and good stability, and provide the possibility of adding targeting moieties, like antibodies (Kozlova *et al.* 2012).

Figure 3 schematically summarizes the above-mentioned steps in the application of CaP-NPs with incorporated siRNA from internalization in the cells via endocytosis, to lysosomal escape up to gene silencing in the cytoplasm via RNAi. Addition of PEI and silica to the

nanoparticles enhances the stability and transfection efficiency, while addition of a fluorescent dye is utilized to visualize the nanoparticles.

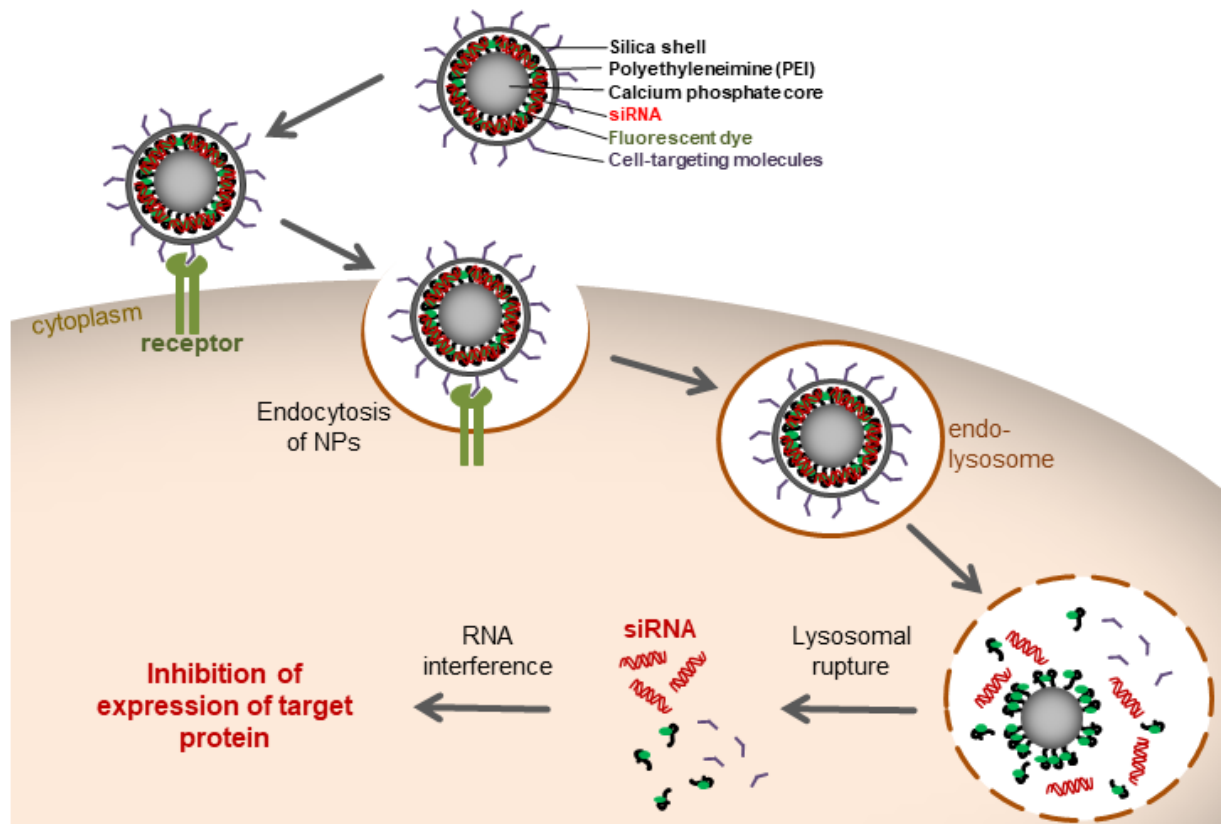


Figure 3: Scheme for the application of calcium phosphate nanoparticles as transfection agents for siRNA against NF- $\kappa$ B p65 (own figure). siRNA: small interfering RNA; PEI: polyethyleneimine.

## 2 Aims of the study

In this study, the biological activity of a novel formulation of calcium phosphate nanoparticles (CaP-NPs) with incorporated p65 siRNA is tested concerning the ability to silence NF- $\kappa$ B p65 expression and thereby ameliorate inflammatory processes.

First, the impact of these nanoparticles in the main cellular players of inflammation is analyzed to elucidate the mechanism of action. Second, the therapeutic efficiency of this nanoparticle formulation in the inflammatory disease colitis is investigated *in vivo*.

In particular, the following main questions are addressed in this study:

- 1. Are CaP-NPs with incorporated functional siRNA able to impact the p65 expression and thereby the inflammatory process in cellular key players of inflammation?**

For answering this question, we modeled the key cellular players of inflammation *in vitro* by choosing four cell lines, namely monocytes, endothelial cells, T cells, and B cells. To enhance the uptake of the nanoparticles into the cells, decoration with the RGD-peptide for endothelial cells and CD69 antibody for B cells and T cells is used.

Since one of the most important requirements for their therapeutic efficiency is the cytoplasmic location of the siRNA, the nanoparticles with incorporated siRNA need to be taken up into the cells and located in the cytoplasm. In this context, first, the uptake and cytotoxicity of the nanoparticles in these key players of inflammation is analyzed. Furthermore, for monocytes as the main target of the nanoparticles, the uptake mechanism and the location inside the cells is further studied.

As potential treatment of inflammation-associated diseases, nanoparticles with incorporated functional p65 siRNA should impact the NF- $\kappa$ B expression in inflamed cellular key players. The efficiency of nanoparticles with functional p65 siRNA (F-NPs) is investigated by measuring the p65 protein expression after incubation with the nanoparticles and specific stimulation of the cells to induce inflamed status. For monocytes as main target, also the changes in gene expression and cytokine secretion are studied. Since the monocytes take up nanoparticles regardless of surface decoration, the undecorated nanoparticles are used, while for the other cell types the respectively decorated nanoparticles are used. As control for the p65 siRNA, a scrambled, non-functional siRNA is incorporated into the nanoparticles (S-NPs). Also, nanoparticles without siRNA (NPs) are used to study the impact of the other nanoparticles' components on the inflammatory signaling. Furthermore, the transfection of "free" functional or scrambled siRNA with the classical transfection reagent

“Lipofectamine™” into the cells is used as further control for the transfection capability of the nanoparticles.

## **2. Do nanoparticles with functional siRNA have therapeutic efficiency in DSS-induced colitis in mice?**

As a preclinical study, the therapeutic efficiency of p65 siRNA-nanoparticles is investigated in a murine model for inflammatory disease. In this study, DSS (dextran sulfate sodium)-induced colitis is used as a model for inflammatory bowel diseases.

The effect of DSS on the development of colitis is dependent on many factors. For the optimal induction of colitis in mice, the DSS dosage therefore cannot easily be transferred directly from literature. Here, the optimal dosage of DSS is determined by observing the development of colitis using an adapted clinical score (disease activity index, DAI) and the concentration of the proinflammatory marker lipocalin-2 (Lcn-2) in the feces. There are no previous *in vivo* studies using the identical siRNA-NP-composition with intravenous application, therefore the dosage needs to be optimized. Here, the optimal siRNA-nanoparticle dosage is tested according to publications using similar NP-formulations in mice with DSS-induced colitis (using the experimental parameters selected before), and the impact on the inflammation is determined as described above.

To assess the therapeutic efficiency of p65 siRNA-nanoparticles on the development of colitis, mice with DSS-induced colitis are intravenously injected with nanoparticles carrying functional p65 siRNA (group F, F-NPs). To determine the effect of F-NPs on the colitis development, untreated colitis-bearing mice (C) were used. As control for the non-inflamed level, healthy and untreated mice (H) are used. The development of colitis is observed by the disease activity index and the fecal Lcn-2 level. Furthermore, shortening of the colon as a sign of inflammation is measured and changes in the histopathologic features of colitis upon nanoparticle-treatment are analyzed.

Moreover, the investigation of inflammatory protein expression in the colonic tissue and the secretion of inflammation mediators in colon and plasma are used to further elucidate the short-term and long-term efficiency of the siRNA-nanoparticles. In this context, proteins associated with the NF- $\kappa$ B signaling pathway are analyzed in colonic leukocytes to visualize the primary impact of the F-NPs in inflammatory cells as a direct target of the nanoparticles. Further investigation of these proteins in the whole colon tissue can elucidate the secondary, indirect effects of the NP-treatment in the inflammatory region. Additionally, the cytokine levels in the whole colon tissue are investigated as a measure of the impact of NP-treatment on the total expression of inflammatory mediators at the site of inflammation. Furthermore, the amount of secreted cytokines from the colon is used to elucidate the effect on the transmission of the inflammatory signal between the cells. Finally, the cytokine

concentration in the blood plasma serves as an indicator for the systemic reaction to the treatment.

**3. Are there potential off-target effects when siRNA-nanoparticles are applied to treat inflammation?**

Inflammation, anywhere in the body, affects the composition of immune cells in the whole body. Therefore, it is possible that the presence of inflammation also affects the distribution of intravenously applied nanoparticles, which might impact the therapeutic efficiency. Here, we compare the distribution of nanoparticles in relevant organs in mice with colonic inflammation to healthy mice. Since the siRNA incorporated inside the nanoparticles will likely not affect the biodistribution, nanoparticles without siRNA are used in this experiment. The biodistribution of the fluorescently labeled nanoparticles (Dy-734) is analyzed *ex vivo* in the organs using fluorescent imaging.

Furthermore, the presence of siRNA in the nanoparticles might lead to side-effects concerning the inflammatory response. To this end, nanoparticles carrying scrambled siRNA are used to study the impact of siRNA *per se* on the development of colitis compared to the functional p65 siRNA.

Finally, an important prerequisite for the clinical application of this nanoparticle formulation is a good biocompatibility. Therefore, potential off-target effects of the nanoparticles with incorporated functional p65 siRNA are tested in healthy mice. Special attention is placed on the impact upon the inflammatory signaling in the colon.



## 3 Materials & Methods

### 3.1 Materials

#### 3.1.1 Nanoparticles

All nanoparticles used in this study were synthesized and characterized by cooperation partners at the university Duisburg-Essen, as described previously (Białas *et al.* 2021).

The synthesis was performed by wet-chemical precipitation using aqueous solutions of calcium lactate pentahydrate (18 mM), diammonium hydrogen phosphate (10.8 mM) and PEI-Cy5/Dy734 (2 mg/mL) at a volume ratio of 5:5:7 mL. After stirring, siRNA (0.36 mg/mL) was added. For dual-NPs, instead of siRNA the TAMRA-labeled peptide (VELPPP)<sub>3</sub> was incorporated. For protection of the biomolecules against enzymatic degradation, a silica shell (SiO<sub>2</sub>) was added. For further specific targeting, silica-coated nanoparticles were functionalized by silanization with thiol groups (-SH) to enable covalent decoration of nanoparticles with ligands (cRGDfK peptide or CD69-IgGh).

The obtained nanoparticles were freeze-dried with D-(+)-trehalose dihydrate solution as cryoprotective agent. The Ca<sup>2+</sup> concentration was measured by AAS (atomic absorption spectroscopy), the size, polydispersity index (PDI) and zeta potential were measured by DLS (dynamic light scattering). The concentration of nanoparticles (NP/mL) is calculated using the calcium content in the nanoparticles and the nanoparticle radius. The concentration of PEI-Cy5 and TAMRA-peptide was measured by UV/Vis spectrophotometry, whereas the concentration of PEI-Dy734 was analyzed by fluorescence spectroscopy. The siRNA concentration in the nanoparticles as well as the concentration of surface decoration (peptide or antibody) was also measured by UV/Vis spectrophotometry.

For *in vitro* studies, the nanoparticles were fluorescently labeled with Cy5 covalently bound to PEI. Undecorated NPs (CaP/PEI-Cy5/SiO<sub>2</sub>) were used for different uptake studies and as control for decorated nanoparticles for targeting. Dual-NPs additionally carry fluorescently labeled negatively charged cell-penetrating peptide (VELPPP)<sub>3</sub>, with properties showing good simulation of the siRNA (Martín *et al.* 2011), to study the fate of the nanoparticle-cargo inside the cells. F-NPs carrying functional p65 siRNA were used for testing the efficiency in silencing NF-κB p65 expression in monocytes, with S-NPs (carrying scrambled, unfunctional siRNA) as control (Table 1).

To specifically target endothelial cells, nanoparticles were decorated with cRGDfK-peptide (RGD-NPs). As control, SH-NPs were used as intermediate synthesis product. RGD/F-NPs

carrying functional p65 siRNA were used for testing the gene silencing efficiency with RGD/S-NPs as control with scrambled siRNA (Table 2).

For targeting of B cells and T cells, CD69-NPs were decorated with CD69-antibody (host species Armenian hamster), with nanoparticles decorated with unspecific antibodies from the same host species as control (IgGh-NPs). Nanoparticles decorated with murine unspecific antibodies (IgGm-NPs) were further used to study impact of host species on the uptake of the nanoparticles (Table 3). For investigation of gene silencing efficiency, nanoparticles decorated with CD69-antibodies or control antibodies carrying either functional p65 siRNA (CD69/F-NPs, IgGh/F-NPs) or scrambled siRNA (CD69/S-NPs, IgGh/S-NPs) were used (Table 4).

For all *in vivo* studies, the nanoparticles were fluorescently labeled with Dy734 covalently bound to PEI, since dyes in the near-infrared region are better suited for *in vivo* studies due to the low absorption of biological molecules in this wavelength region (Zhang *et al.* 2012). F-NPs carrying functional p65 siRNA were used to study the therapeutic efficiency as well as potential side-effects in healthy mice. S-NPs carrying scrambled siRNA were further used to investigate the impact of the siRNA present in the nanoparticles on colitis-bearing mice. The biodistribution was studied using nanoparticles without siRNA (NPs) (Table 5).

**Table 1: Characteristics of nanoparticles for *in vitro* studies without decoration and with or without siRNA/ cargo peptide.**

	(undecorated) NPs	dual-NPs	F-NPs	S-NPs
<b>application</b>	Uptake, control for targeting	Uptake mechanism	Efficiency p65 silencing	Efficiency p65 silencing
<b>composition</b>	CaP/PEI-Cy5/SiO <sub>2</sub>	CaP/PEI-Cy5/TAMRA-pep/SiO <sub>2</sub>	CaP/PEI-Cy5/siRNAf/SiO <sub>2</sub>	CaP/PEI-Cy5/siRNAs/SiO <sub>2</sub>
<b>Size (DLS) [nm]</b>	146.3 ± 6.4	121.0 ± 7.0	272.9 ± 1.8	249.7 ± 4.1
<b>Pdl</b>	0.27 ± 0.06	0.25 ± 0.03	0.26 ± 0.04	0.25 ± 0.01
<b>ζ potential [mV]</b>	25.7 ± 0.8	25.0 ± 1.0	24.7 ± 0.2	26.6 ± 0.5
<b>Ca<sup>2+</sup> content [μg/mL]</b>	51.8	24.2	39.6	36.6
<b>siRNA/peptide concentration [μg/mL]</b>	/	25.5	36.4	35.4
<b>PEI content [μg/mL]</b>	64.7	180.0	61.8	92.8
<b>Endotoxin content [EU/mL]</b>	< 0.1	< 0.1	< 0.1	< 0.1
<b>Concentration [NP/mL]</b>	3.4·10 <sup>11</sup>	1.3·10 <sup>11</sup>	4.0·10 <sup>11</sup>	4.0·10 <sup>11</sup>

Table 2: Characteristics of nanoparticles for *in vitro* studies with cRGDfK peptide decoration and with or without siRNA to target endothelial cells.

	<b>RGD-NPs</b>	<b>SH-NPs</b>	<b>RGD/F-NPs</b>	<b>RGD/S-NPs</b>
<b>application</b>	Specific targeting of ECs	Specific targeting of ECs	p65 silencing ECs	p65 silencing ECs
<b>composition</b>	CaP/PEI-Cy5/SiO <sub>2</sub> /SH/cRGDfK	CaP/PEI-Cy5/SiO <sub>2</sub> /SH	CaP/PEI-Cy5/siRNAf/SiO <sub>2</sub> /SH/cRGDfK	CaP/PEI-Cy5/siRNAs/SiO <sub>2</sub> /SH/cRGDfK
<b>Size (DLS) [nm]</b>	212.1 ± 3.0	210.7 ± 3.2	230.3 ± 4.4	325.4 ± 24.5
<b>Pdl</b>	0.20 ± 0.03	0.23 ± 0.01	0.24 ± 0.04	0.35 ± 0.04
<b>ζ potential [mV]</b>	30.5 ± 1.5	28.7 ± 1.4	41.1 ± 0.4	39.3 ± 1.1
<b>Ca<sup>2+</sup> content [μg/mL]</b>	19.2	41.1	< 7.0	< 7.0
<b>siRNA concentration [μg/mL]</b>	/	/	32.7	20.4
<b>cRGDfK concentration [μg/mL]</b>	92.1	/	95.4	100
<b>PEI content [μg/mL]</b>	101.8	125.5	145.5	173.9
<b>Endotoxin content [EU/mL]</b>	< 0.1	< 0.1	< 0.1	< 0.1
<b>Concentration [NP/mL]</b>	2.5·10 <sup>11</sup>	1.0·10 <sup>12</sup>	< 5.1·10 <sup>10</sup>	< 3.6·10 <sup>10</sup>

Table 3: Characteristics of nanoparticles for *in vitro* studies with IgG decoration and without siRNA to target B cells and T cells.

	<b>CD69-NPs</b>	<b>IgGh-NPs</b>	<b>IgGm-NPs</b>
<b>application</b>	Specific targeting B-, T cells	Specific targeting B-, T cells	Specific targeting
<b>composition</b>	CaP/PEI-Cy5/SiO <sub>2</sub> /SH/IgG-CD69	CaP/PEI-Cy5/SiO <sub>2</sub> /SH/IgG-Iso	CaP/PEI-Cy5/SiO <sub>2</sub> /SH/IgG-IC-model
<b>Size (DLS) [nm]</b>	211.5 ± 3.8	205.7 ± 6.0	145.0 ± 4.0
<b>Pdl</b>	0.28 ± 0.03	0.27 ± 0.04	0.25 ± 0.02
<b>ζ potential [mV]</b>	31.4 ± 1.5	42.7 ± 0.8	34.0 ± 4.0
<b>Ca<sup>2+</sup> content [μg/mL]</b>	13.1	< 7.0	13.2
<b>IgG concentration [μg/mL]</b>	120.0	121.0	153.0
<b>PEI content [μg/mL]</b>	126.6	145.6	138.0
<b>Endotoxin content [EU/mL]</b>	< 0.1	< 0.1	< 0.1
<b>Concentration [NP/mL]</b>	4.4·10 <sup>11</sup>	< 1.3·10 <sup>11</sup>	4.3·10 <sup>12</sup>

Table 4: Characteristics of nanoparticles for *in vitro* studies with IgG decoration and with siRNA to target B cells and T cells.

	CD69/F-NPs	IgGh/F-NPs	CD69/S-NPs	IgGh/S-NPs
<b>application</b>	p65 silencing B- and T cells	p65 silencing B- and T cells	p65 silencing B- and T cells	p65 silencing B- and T cells
<b>composition</b>	CaP/PEI-Cy5/siRNAf/SiO <sub>2</sub> /SH/CD69	CaP/PEI-Cy5/siRNAf/SiO <sub>2</sub> /SH/IgG-Iso	CaP/PEI-Cy5/siRNAs/SiO <sub>2</sub> /SH/CD69	CaP/PEI-Cy5/siRNAs/SiO <sub>2</sub> /SH/IgG-Iso
<b>Size (DLS) [nm]</b>	189.0 ± 7.2	224.2 ± 11.1	205.1 ± 7.0	217.5 ± 1.0
<b>Pdl</b>	0.26 ± 0.06	0.33 ± 0.06	0.20 ± 0.04	0.28 ± 0.02
<b>ζ potential [mV]</b>	37.2 ± 3.9	31.7 ± 1.2	29.0 ± 1.2	26.8 ± 1.2
<b>Ca<sup>2+</sup> content [μg/mL]</b>	13.3	19.5	34.1	16.1
<b>siRNA concentration [μg/mL]</b>	32.7	29.3	28.9	29.1
<b>IgG concentration [μg/mL]</b>	136.9	159.7	267.3	243.2
<b>PEI content [μg/mL]</b>	110.7	175.7	140.6	158.4
<b>Endotoxin content [EU/mL]</b>	< 0.1	< 0.1	< 0.1	< 0.1
<b>Concentration [NP/mL]</b>	3.7·10 <sup>11</sup>	6.4·10 <sup>11</sup>	4.2·10 <sup>11</sup>	1.0·10 <sup>11</sup>

 Table 5: Characteristics of nanoparticles for *in vivo* studies without decoration and with or without siRNA.

	F-NPs	S-NPs	NPs
<b>application</b>	<i>In vivo</i> therapeutic efficiency	Side effects siRNA	biodistribution
<b>composition</b>	CaP/PEI-Dy734/siRNAf/SiO <sub>2</sub>	CaP/PEI-Dy734/siRNAs/SiO <sub>2</sub>	CaP/PEI-Dy734/SiO <sub>2</sub>
<b>Size (DLS) [nm]</b>	253.0 ± 3.0	190.0 ± 2.0	143.0 ± 2.0
<b>Pdl</b>	0.177 ± 0.02	0.176 ± 0.02	0.20 ± 0.04
<b>ζ potential [mV]</b>	22.0 ± 1.0	25.0 ± 1.0	20.0 ± 2.0
<b>Ca<sup>2+</sup> content [μg/mL]</b>	46.0	55.0	133
<b>siRNA concentration [μg/mL]</b>	36.0	26.6	/
<b>PEI content [μg/mL]</b>	240.0	240.0	266.0
<b>Endotoxin content [EU/mL]</b>	< 0.1	< 0.1	< 0.1
<b>Concentration [NP/mL]</b>	3.9·10 <sup>10</sup>	3.3·10 <sup>10</sup>	1.1·10 <sup>12</sup>

### 3.1.2 Cell lines

The different cell lines used for *in vitro* experiments are listed in Table 6.

Table 6: **Used cell lines with origin and supplier.**

CELL LINE	ORIGIN	SUPPLIER
J774A.1	Murine Hematopoiesis Macrophage, monocytic cell line (BALB/c)	CLS Cell Lines Service GmbH, Eppelheim, DE
MOPC-315	Murine B lymphocyte cell line from MOPC 315 plasmacytoma (BALB/c)	American Type Culture Collection, ATCC, 141 CCL81, Rockville, MD, US
SVEC4-10	Murine endothelial cell line derived by SV40 (strain 4A) transformation of endothelial cells from axillary lymph node vessels (C3H/HeJ)	American Type Culture Collection, ATCC, 141 CCL81, Rockville, MD, US
TK-1	Murine T-cell lymphoma cell line from spontaneous thymic lymphoma/leukemia (AKR/Cum)	American Type Culture Collection, ATCC, 141 CCL81, Rockville, MD, US

### 3.1.3 Animals

For *in vivo* experiments the mouse strain BALB/cJrj from Janvier Labs (CS 4105 Le Genest St Isle, 53941 St Berthevin Cedex, France) was used. All mice were about 8 weeks old at the beginning of experiments. Only female mice were used for the experiments.

### 3.1.4 Used equipment and devices

All described experiments were performed using the equipment listed in Table 7.

Table 7: **List of used equipment with supplier.**

EQUIPMENT	SUPPLIER
Automatic tissue processor Leica TP1020	Leica Biosystems Nussloch GmbH, Nussloch, DE
Balance Kern 440-33	Kern & Sohn GmbH, Albstadt, DE
Balance La 230P	Sartorius AG, Göttingen, DE
BD Accuri™ C6 Plus Flow Cytometer	BD Biosciences, San José, US
Blotting apparatus Mini Protean Tetra Cell®	Bio-Rad Laboratories GmbH, München, DE
Camera Canon Eos 650D	Canon Inc., Tokio, JP
Cell counter CASY® Model TT	Roche Applied Science, Penzberg, DE
Centrifuge Biofuge primo	Heraeus Instruments GmbH, Osterode, DE
Centrifuge Eppendorf 5417 R	Eppendorf AG, Hamburg, DE
Centrifuge Universal 320R	Hettich GMBH&Co KG, Tuttlingen, DE
Cryotom CM 3050 S	Leica Microsystems, Wetzlar, DE
Cycler peqLAB 96 Universal Gradient	VWR International GmbH, Darmstadt, DE
Electrophoresis Power-Pac™ Basic	Bio-Rad Laboratories GmbH, München, DE
FUSION FX7 Edge	VILBER LOURMAT Deutschland GmbH, Eberhardzell,

GentleMACS	DE
Haematology analyzer XT-1800i	Miltenyi Biotec B.V. & Co. KG, Bergisch Gladbach, DE
ImageQuant LAS 4000	Sysmex Deutschland GmbH, Norderstedt, DE
Incubator HERACELL 150i	GE Healthcare Europe GmbH, Freiburg, DE
Isoflurane Vaporizer Ohmeda Isotec 4	Thermo Fischer Scientific Germany BV & Co. KG, Braunschweig, DE
IVIS Spectrum CT	GE Healthcare, München, DE
Leica EG1160 embedding center	PerkinElmer LAS (Germany) GmbH, Rodgau-Jügesheim, DE
Leica RM 2165 automated rotary microtome	Leica Biosystems Nussloch GmbH, Nussloch, DE
LSM 900	Leica Biosystems Nussloch GmbH, Nussloch, DE
LSM Meta 510	Carl Zeiss GmbH, Jena, DE
MACS Separator	Carl Zeiss GmbH, Jena, DE
Microscope CK40	Miltenyi Biotec B.V. & Co. KG, Bergisch Gladbach, DE
Microscope Olympus BX 50	Olympus Europa Holding GmbH, Hamburg, DE
pH-Meter pH 330i	Olympus Deutschland GmbH, Hamburg, DE
Pipet Boy®	WTW, Weilheim, DE
Pipettes	Lab-Laborfachhandel, München, DE
Rotary shaker Heidolph Polymax 2040	Eppendorf AG, Hamburg, DE
RotorGene Q	Heidolph Instruments GmbH & Co. KG, Schwabach, DE
Spectrophotometer NanoDrop 2000C	Qiagen GmbH, Hilden, DE
TECAN Sunrise Plate Reader	Fisher Scientific GmbH, Schwerte, DE
UV2 Sterilizing PCR Workstation	Tecan Group Ltd., Männedorf, CH
Vortexer	UVP
Work bench	IKA®-Werke GmbH & Co. KG, Staufen, DE
	Hera Safe, Heraeus Instruments GmbH, Bad Grund (Harz), DE

### 3.1.5 Consumption items

The consumption items used for all experiments described herein are listed in Table 8.

Table 8: **List of consumption items with supplier.**

CONSUMPTION ITEM	SUPPLIER
96 well plate, transparent or black	Greiner-bio-one GmbH, Frickenhausen, DE
C tubes gentleMACS	Miltenyi Biotec B.V. & Co. KG, Bergisch Gladbach, DE
Capillaries for blood draw	VWR International GmbH, Darmstadt, DE
CASY®Cups	Roche Innovatis AG, Reutlingen, DE
Cell culture flasks (25, 75, 175 cm <sup>2</sup> )	Greiner Bio-One GmbH, Frickenhausen, DE
Cell scraper	Greiner Bio-One GmbH, Frickenhausen, DE
CellStar 6/ 12/ 24 well plate	Greiner-bio-one GmbH, Frickenhausen, DE
Chamber Slide 16 well, LAB-Tek w/ cover	Thermo Fischer Scientific Germany BV & Co. KG, Braunschweig, DE
Cover slips 24x24/ 24x50 / Ø12mm	Menzel GmbH & Co KG, Braunschweig, DE
DAKO PEN	AKO Denmark A/S, Glostrup, DK
Embedding cassettes	Carl Roth GmbH + Co. KG, 76185 Karlsruhe, DE

FACS tubes	Corning Incorporated Life Sciences, Durham, US
Falcon tubes	Greiner-bio-one GmbH, Frickenhausen, DE
Filtered tips	Greiner-bio-one GmbH, Frickenhausen, DE
M tubes gentleMACS	Miltenyi Biotec B.V. & Co. KG, Bergisch Gladbach, DE
MACS Separation Columns LS	Miltenyi Biotec B.V. & Co. KG, Bergisch Gladbach, DE
Object slides Superfrost®Plus	Menzel GmbH & Co KG, Braunschweig, DE
Omnican50, U-100, 0.5 mL	B. Braun Melsungen AG, Melsungen, DE
PCR tubes 0,2 mL	Eppendorf AG, Hamburg, DE
Pipet tips	Brand GmbH + Co KG, Wertheim, DE
Protein LoBind tubes; 0.5; 1.5; 2.0 mL	Eppendorf AG, Hamburg, DE
PVDF-membrane	Merck Millipore KGaA, Darmstadt, DE
SafeLock Tubes 0.5; 1.5; 2.0 mL	Eppendorf AG, Hamburg, DE
Serum collection tubes (GK 150 Li 200µL Gel)	KABE Labortechnik GmbH, Nümbrecht, DE
Strip Tubes and Caps 0.1 mL	Qiagen GmbH, Hilden, DE
Tissue Tek Cryomold Intermediate Disposable Vinyl Specimen Molds (15mm x 15mm x 15mm)	Weckert Labor-, Röntgen- und Medizintechnik, Kitzingen, DE
Tissues Meliseptol HBV	B. Braun Melsungen AG, Melsungen, DE
V-bottom Plate for LEGENDplex™ Assay	Biolegend, San Diego, California, US
Whatman® cellulose chromatography papers	Sigma Aldrich Chemie GmbH, Steinheim, DE

### 3.1.6 Chemicals

The chemicals used in this study are specified in Table 9.

Table 9: **List of chemicals with supplier.**

CHEMICALS	SUPPLIER
2-Mercaptoethanol	Serva Electrophoresis GmbH, Heidelberg, DE
2-Mercaptoethanol (50 mM)	Thermo Fischer Scientific Germany BV & Co. KG, Braunschweig, DE
2x Laemmli Sample Buffer	BioRad Laboratories GmbH, München, DE
Acetic acid	Sigma Aldrich Chemie GmbH, Steinheim, DE
Agarose NEEO	Carl Roth GmbH & Co. KG, Karlsruhe, DE
Alamar Blue	Invitrogen GmbH, Karlsruhe, DE
APS	BioRad Laboratories GmbH, München, DE
Biotin Blocking System	Biolegend, San Diego, California, US
Bromphenol blue	Serva Electrophoresis GmbH, Heidelberg, DE
BSA (Fraction V)	Carl Roth GmbH & Co. KG, Karlsruhe, DE
Casy®-ton	Roche Diagnostics Deutschland GmbH, Mannheim, DE
CD45 Microbeads (mouse)	Miltenyi Biotec B.V. & Co. KG, Bergisch Gladbach, DE
CD8a (Ly-2) MicroBeads mouse	Miltenyi Biotec B.V. & Co. KG, Bergisch Gladbach, DE
Chloroform	Carl Roth GmbH & Co. KG, Karlsruhe, DE
Chloroquine	Thermo Fischer Scientific Germany BV & Co. KG, Braunschweig, DE

## Materials & Methods

---

Chlorpromazine	Thermo Fischer Scientific Germany BV & Co. KG, Braunschweig, DE
Citric acid monohydrate	AppliChem Inc., Maryland Heights, US
Clarity™ Western ECL Substrate	BioRad Laboratories GmbH, München, DE
cOmplete Tablets EDTA-free, EASY pack	Roche Diagnostics GmbH, Mannheim, DE
Coomassie Brilliant Blue G-250	Merck KGaA, Darmstadt, DE
cRGDFK (Cyclo(-Arg-Gly-Asp-D-Phe-Lys) trifluoroacetate salt)	Bachem Holding AG, Bubendorf, CH
Cytochalasin D	Thermo Fischer Scientific Germany BV & Co. KG, Braunschweig, DE
Dako REAL™ Antibody Diluent	Dako, Agilent Technologies, Carpinteria, US
DMEM, high glucose, GlutaMAX™ Supplement, pyruvate	Thermo Fischer Scientific Germany BV & Co. KG, Braunschweig, DE
DMSO	Merck Millipore KGaA, Darmstadt, DE
DNA Ladder 50 bp	Jena Bioscience GmbH, Jena, DE
Dry milk	Carl Roth GmbH & Co. KG, Karlsruhe, DE
DSS (dextran sulfate sodium) colitis grade MW 36000-50000	MP Biomedicals Germany GmbH, Eschwege, DE
DTT	pjk GmbH, Kleinbittersdorf, DE
EDTA (-Na <sub>2</sub> )	Thermo Fischer Scientific Germany BV & Co. KG, Braunschweig, DE
Eosin B	Sigma Aldrich Chemie GmbH, Steinheim, DE
Ethanol 100%	Merck Millipore KGaA, Darmstadt, DE
Ethanol 96% (v/v), denat.	Nordbrand Nordhausen GmbH, Nordhausen, DE
Faramount Aqueous Mounting Medium	Dako, Agilent Technologies, Carpinteria, US
FCS	Gibco von Invitrogen GmbH, Darmstadt, DE
Formaldehyde solution 5%	Otto Fischer GmbH & Co KG, Saarbrücken, DE
Formaldehyde, 37%	Carl Roth GmbH & Co. KG, Karlsruhe, DE
Glycine	BioRad Laboratories GmbH, München, DE
Guanidin hydrochloride	Sigma Aldrich Chemie GmbH, Steinheim, DE
H <sub>3</sub> PO <sub>4</sub>	Carl Roth GmbH & Co. KG, Karlsruhe, DE
Hematoxylin solution, Mayer's	Merck Millipore KGaA, Darmstadt, DE
Histosec pastilles (paraffin)	Merck Millipore KGaA, Darmstadt, DE
Hoechst 33258	AppliChem Inc., Maryland Heights, US
IL-4	Miltenyi Biotec B.V. & Co. KG, Bergisch Gladbach, DE
Immobilon® Western	Merck Millipore KGaA, Darmstadt, DE
Chemiluminescence HRP Substrate	
Invitrogen™ Platinum™II Hot-Start Green PCR MasterMix 2x	Thermo Fischer Scientific Germany BV & Co. KG, Braunschweig, DE
Isoflurane	Aktavis Deutschland GmbH & Co. KG, Langenfeld, DE
Isopropanol	Carl Roth GmbH & Co. KG, Karlsruhe, DE
KCl	Fluka Chemie GmbH, 9471 Buchs, CH
KH <sub>2</sub> PO <sub>4</sub>	Sigma Aldrich Chemie GmbH, Steinheim, DE
KHCO <sub>3</sub>	Sigma Aldrich Chemie GmbH, Steinheim, DE
Levamisole	Dako, Agilent Technologies, Carpinteria, US
Lipofectamine™-2000	Invitrogen GmbH, Karlsruhe, DE



## Materials & Methods

---

LPS (E. coli Serotype O26:B6)	Sigma Aldrich Chemie GmbH, Steinheim, DE
LysoTracker Green DND-26	Thermo Fischer Scientific Germany BV & Co. KG, Braunschweig, DE
MEM Non-Essential Amino Acids Solution (100X)	Thermo Fischer Scientific Germany BV & Co. KG, Braunschweig, DE
Methanol	Carl Roth GmbH & Co. KG, Karlsruhe, DE
Na <sub>2</sub> HPO <sub>4</sub>	Sigma Aldrich Chemie GmbH, Steinheim, DE
Na <sub>3</sub> VO <sub>4</sub>	Sigma Aldrich Chemie GmbH, Steinheim, DE
NaCl	Carl Roth GmbH & Co. KG, Karlsruhe, DE
Nail polish	Cosnova, Frankfurt, DE
NH <sub>4</sub> Cl	Sigma Aldrich Chemie GmbH, Steinheim, DE
Nuclease-free water (cell culture)	Ambion/ Thermo Fischer Scientific Germany BV & Co. KG, Braunschweig, DE
ODN-2006	Miltenyi Biotec B.V. & Co. KG, Bergisch Gladbach, DE
PageRuler™, prestained protein ladder	Thermo Fischer Scientific Germany BV & Co. KG, Braunschweig, DE
Penicillin/ Streptomycin (10.000 U/mL)	Thermo Fischer Scientific Germany BV & Co. KG, Braunschweig, DE
peqGOLD TriFast™	VWR International GmbH, Darmstadt, DE
Permafluor Mounting Medium	Thermo Fischer Scientific Germany BV & Co. KG, Braunschweig, DE
PERTEX® mounting medium	VWR International GmbH, Darmstadt, DE
Phalloidin-AlexaFluor 488	Thermo Fischer Scientific Germany BV & Co. KG, Braunschweig, DE
Phosphoric acid 85%	Carl Roth GmbH & Co. KG, Karlsruhe, DE
PhosSTOP Phosphatase Inhibitor	Roche Diagnostics GmbH, Mannheim, DE
Pierce® ECL Western Blotting Substrate	Thermo Fischer Scientific Germany BV & Co. KG, Braunschweig, DE
PMSF	Carl Roth GmbH & Co. KG, Karlsruhe, DE
Poly-L-Lysine	Sigma Aldrich Chemie GmbH, Steinheim, DE
Purelock™ Blocking Buffer	VILBER LOURMAT Deutschland GmbH, Eberhardzell, DE
Recombinant mouse Interleukin-2 (IL-2)	Gibco von Invitrogen GmbH, Darmstadt, DE
RNase-free water	1017979; Qiagen GmbH, Hilden, DE
Rotiphorese® Gel30 (Acrylamide 30%)	Carl Roth GmbH & Co. KG, Karlsruhe, DE
RPMI 1640 Medium (ATCC modification), 500 mL	Thermo Fischer Scientific Germany BV & Co. KG, Braunschweig, DE
scrambled siRNA sc-37007	SantaCruz Biotechnology Inc., Heidelberg, DE
SDS	Carl Roth GmbH & Co. KG, Karlsruhe, DE
siRNA p65 sc-29411	SantaCruz Biotechnology Inc., Heidelberg, DE
Sodium desoxycholate	Carl Roth GmbH & Co. KG, Karlsruhe, DE
Streptavidin-AP (alkalic phosphatase)	Southern Biotech, Birmingham, US
TaqMan™ Fast Advanced Master Mix	Thermo Fischer Scientific Germany BV & Co. KG, Braunschweig, DE
TaqMan™ Gene Expression Assay Actb Mm01205647_g1	Thermo Fischer Scientific Germany BV & Co. KG, Braunschweig, DE
TaqMan™ Gene Expression Assay Rela Mm00501346_m1	Thermo Fischer Scientific Germany BV & Co. KG, Braunschweig, DE

TEMED	Carl Roth GmbH & Co. KG, Karlsruhe, DE
TexMACS Medium	Miltenyi Biotec B.V. & Co. KG, Bergisch Gladbach, DE
Tissue Tek O.C.T.TM Component	Sakura, 4583; Sakura, 2408 AV Alphen aan den Rijn, NL
TNF- $\alpha$	PeproTech Rocky Hill, NJ, US
Tramadol	ALIUD PHARMA GmbH, Laichingen, DE
Tris-Base	Carl Roth GmbH & Co. KG, Karlsruhe, DE
Tris-HCl	Carl Roth GmbH & Co. KG, Karlsruhe, DE
TritonX-100	Sigma Aldrich Chemie GmbH, Steinheim, DE
TrypLE™ Express Enzyme (1X), phenol red	Thermo Fischer Scientific Germany BV & Co. KG, Braunschweig, DE
Tween 20	Sigma Aldrich Chemie GmbH, Steinheim, DE
Vitamycin eye ointment	CP-Pharma Handelsgesellschaft mbH, Burgdorf, DE
Wortmannin	Thermo Fischer Scientific Germany BV & Co. KG, Braunschweig, DE
Xylene	Carl Roth GmbH & Co. KG, Karlsruhe, DE
DMEM/Ham's F12 (1:1)	Gibco von Invitrogen GmbH, Darmstadt, DE
1x Hanks BSS pH 7,0 - 7,5	PAA Laboratories GmbH, Cölbe, DE

### 3.1.7 Antibodies

The antibodies used for Western Blot analyses, immunostainings, flow cytometric analyses, and other experiments are listed in Table 10.

Table 10: **Antibodies for Western Blot analyses, immunostainings, flow cytometric analyses, and other experiments with subtype/ clone, item number, LOT, and supplier.**

ANTIBODY	SUBTYPE/ CLONE	ITEM NO	LOT	SUPPLIER
Anti-beta Actin antibody-HRP (mouse anti-mouse)	IgG1 mAbcam 8226	ab20272	GR143514-1	abcam; Cambridge, GB
Anti-CD45R - PE-Vio® 770 (human anti-mouse)	IgG1 REA755	130-110- 848	5190904336	Miltenyi Biotec B.V. & Co. KG, Bergisch Gladbach, DE
Anti-CD51 - PE (rat anti-mouse)	IgG1, $\kappa$ RMV-7	104105	B282870	Biolegend, San Diego, California, US
Anti-CD69 (Armenian hamster anti-mouse)	IgG H1.2F3	104502	B262609	Biolegend, San Diego, California, US
Anti-CD8a - PE-Vio® 770 (human anti-mouse)	IgG1 REA601	130-119- 123	5190904429	Miltenyi Biotec B.V. & Co. KG, Bergisch Gladbach, DE
Anti-COX2 / Cyclooxygenase 2 antibody (rabbit anti mouse)	IgG EPR12012	ab179800	GR222252- 27	abcam; Cambridge, GB
Anti-IkBalphalpha antibody (rabbit monoclonal)	IgG E130	ab32518	GR275907- 35	abcam; Cambridge, GB
Anti-iNOS antibody [EPR16635] (rabbit monoclonal)	IgG EPR16635	ab178945	GR3240243- 6	abcam; Cambridge, GB

## Materials & Methods

APC anti-mouse CD134 (OX-40) Antibody (rat anti-mouse)	IgG1, $\kappa$ OX-40	119413	B262060	Biolegend, San Diego, California, US
APC Rat IgG1, $\kappa$ Isotype Ctrl Antibody	IgG1 $\kappa$ RTK2071	400411	B268024	Biolegend, San Diego, California, US
Armenian Hamster Isotype-ctrl	IgG HTK888	400902	B291754	Biolegend, San Diego, California, US
Bcl-2 (50E3) Rabbit mAB (rabbit anti-mouse)	IgG 50E3	#2870	0005	Cell Signaling Technology; Frankfurt am Main, DE
CD28-Antibody functional grade (hamster anti-mouse)	IgG2 $\lambda$ 37.51	130-093-182	5190813163	Miltenyi Biotec B.V. & Co. KG, Bergisch Gladbach, DE
CD3 $\epsilon$ -Biotin-Antibody functional grade (hamster anti-mouse)	IgG1 145-2C11	130-093-179	5190813162	Miltenyi Biotec B.V. & Co. KG, Bergisch Gladbach, DE
CD45 (D3F8Q) Rabbit mAb (rabbit anti-mouse)	IgG D3F8Q	#70257	00002	Cell Signaling Technology; Frankfurt am Main, DE
FITC anti-mouse CD25 Antibody (rat anti-mouse)	IgG2b, $\kappa$ 3C7	101907	B276319	Biolegend, San Diego, California, US
FITC Rat IgG2b, $\kappa$ Isotype Ctrl Antibody	IgG2b, $\kappa$ RTK4530	400633	B265823	Biolegend, San Diego, California, US
Goat IgG anti-Rabbit IgG (H+L)-Biotin	IgG	#111-065-144	104826	Dianova GmbH, Hamburg, DE
NF- $\kappa$ B p65 (D14E12) XP® Rabbit mAb (rabbit anti-mouse)	D14E12	#8242	0016	Cell Signaling Technology; Frankfurt am Main, DE
NF- $\kappa$ B p65-HRP (mouse anti-mouse)	IgG1, $\kappa$ light chain	sc-8008	J0417	SantaCruz Biotechnology Inc., Heidelberg, DE
PE anti-mouse CD69 Antibody (Armenian hamster anti-mouse)	IgG H1.2F3	104507	B273267	Biolegend, San Diego, California, US
PE Armenian Hamster IgG Isotype Ctrl Antibody	IgG HTK888	400907	B266722	Biolegend, San Diego, California, US
Peroxidase-AffiniPure Mouse Anti-Rabbit IgG (H+L)	IgG	211-035-109	147512	Dianova GmbH, Hamburg, DE
Rat IgG1, $\kappa$ Isotype ctrl – PE	IgG1 $\kappa$ RTK2071	400407	B279417	Biolegend, San Diego, California, US

### 3.1.8 Kits

Kits utilized in this study are listed in Table 11.

Table 11: **List of kits with supplier.**

<b>KIT</b>	<b>SUPPLIER</b>
Annexin-V-FLUOS Staining Kit	Roche Diagnostics Deutschland GmbH, Mannheim, DE
B Cell Isolation Kit (mouse)	Miltenyi Biotec B.V. & Co. KG, Bergisch Gladbach, DE
Dako Liquid Permanent Red	Dako, Agilent Technologies, Carpinteria, US
DuoSet Ancillary Kit 2	R&D Systems, BioTechne GmbH, Wiesbaden, DE
High Capacity cDNA Reverse Transcription Kit	Thermo Fischer Scientific Germany BV & Co. KG, Braunschweig, DE
Lamina Propria Dissociation Kit (mouse)	Miltenyi Biotec B.V. & Co. KG, Bergisch Gladbach, DE
LEGENDplex™ Mouse Inflammation Panel (13-plex)	Biolegend, San Diego, California, US
Mouse Lipocalin-2/NGAL DuoSet ELISA	R&D Systems, BioTechne GmbH, Wiesbaden, DE
Mouse TNF $\alpha$ Uncoated ELISA-Kit	Thermo Fischer Scientific Germany BV & Co. KG, Braunschweig, DE
Spleen Dissociation Kit (mouse)	Miltenyi Biotec B.V. & Co. KG, Bergisch Gladbach, DE

### 3.1.9 Buffer and solutions

The utilized buffers are listed in Table 12. If not indicated otherwise, buffers were prepared with ddH<sub>2</sub>O.

Table 12: **List of buffers and solutions with composition and ingredients.**

<b>BUFFER</b>	<b>INGREDIENTS</b>
Blocking buffer (dry milk)	5% (w/v) dry milk, 0.1% (v/v) Tween20 in TBS buffer
Bradford reagent	0.01% (w/v) Coomassie brilliant blue R-250 5% (v/v) Ethanol 96% (v/v) 5% (v/v) Phosphoric acid 85% (v/v)
Citrate buffer pH 6.0 (10x)	100 mM Citric acid monohydrate
Electrophoresis buffer (10x)	1.92 M Glycine; 0.25 M Tris-base
PBS pH 7.4 (10x)	81 mM Disodium hydrogen orthophosphate 26.8 mM Potassium chloride 1370 mM Sodium chloride 14.7 mM Potassium dihydrogen phosphate

## Materials & Methods

RIPA buffer	50 mM Tris-HCl (pH 8.0) 150 mM Sodium chloride 1% (v/v) Triton-X 100 0.5% (w/v) Sodium deoxycholate 0.1% (w/v) SDS 0.1% (v/v) Sodium orthovanadate (100 mM) 0.1% (v/v) PMSF (400 mM) Protease- + Phosphatase inhibitor cocktail
Running buffer	1x Electrophoresis buffer; 2% (v/v) SDS (10% (w/v))
Separation gel (10%)	5.6 mM Tris-Base (pH 8.8) 1% (v/v) SDS (10% (w/v)) 32.9% (v/v) Rotiphorese® Gel30 (Acrylamide 30%) 0.3% (v/v) Ammonium persulfate (20% (w/v)) 0.1% (v/v) TEMED
Stacking gel (4.5%)	3.3 mM Tris-Base (pH 6.8) 1% (v/v) SDS (10% (w/v)) 16.4% (v/v) Rotiphorese® Gel30 (Acrylamide 30%) 1% (v/v) Ammonium persulfate (20% (w/v)) 0.1% (v/v) TEMED
Stripping buffer	62.5 mM Tris-hydrochloride pH 6.8 100 mM β-Mercaptoethanol 20% (v/v) SDS (10% (w/v))
TBS pH 7.5 (10x)	1.502 M Sodium chloride 0.074 M Tris-Base 0.435 M Tris-hydrochloride
TBS-T (0.1%)	1x TBS buffer; 0.1% (v/v) Tween20
Transfer buffer	10% (v/v) Electrophoresis buffer (10x); 30% (v/v) Methanol

### 3.1.10 Software

Special software employed during this study are specified in Table 13.

Table 13: **Special software with supplier.**

SOFTWARE	SUPPLIER
BD Accuri™ C6 Plus	BD Biosciences, San José, US
Bio-1D Analysis software	VILBER LOURMAT Deutschland GmbH, Eberhardzell, DE
GraphPad PRISM 9	GraphPad Software, San Diego, US
Image Quant™ LAS4000	GE Healthcare Europe GmbH, Freiburg, DE
ImageJ	NIH, Bethesda, MD, US
LEGENDplex™ Data Analysis Software (Version 8)	Biolegend, San Diego, US
Living Image 4.7.3	PerkinElmer LAS (Germany) GmbH, Rodgau-Jügesheim, DE
Rotorgene Q	Qiagen GmbH, Hilden, DE
SPSS Statistics	IBM Corporation, Armonk, NY, US
Tecan i-Control	Tecan Deutschland GmbH, Crailsheim, DE

## 3.2 Methods

### 3.2.1 Cell lines and culture conditions

The murine monocyte cell line J774A.1 cultured in DMEM/F-12 (1:1) (+)-L-glutamine supplemented with 10% (v/v) fetal calf serum (FCS). Cells were harvested by scraping after reaching about 80% confluence. The murine endothelial cell line SVEC4-10 was cultured in DMEM (1x) + GlutaMAX™-I supplemented with 10% (v/v) heat-inactivated FCS. Cells were enzymatically harvested by TrypLE™ Express at about 80% confluence. The murine T-lymphocyte (lymphoma) cell line TK-1 was cultured in RPMI 1640 medium supplemented with 10% (v/v) FCS, 0.1 mM non-essential amino acids and 0.05 mM 2-mercaptoethanol. The murine B lymphocyte (myeloma) cell line MOPC-315 was cultured in DMEM supplemented with 10% (v/v) FCS. Suspension cells were maintained between  $1\text{-}2\cdot 10^6$  cells/mL. All cells were cultured at 37 °C in 5% CO<sub>2</sub> atmosphere.

### 3.2.2 Nanoparticle uptake and cell viability

Cells (J774A.1, SVEC4-10, TK-1 and MOPC-315) were seeded in 24-well cell culture plates at a density of  $(0.8\text{ to }2.5)\cdot 10^4$  cells/cm<sup>2</sup> and pre-incubated for 24 h. Fluorescently labeled undecorated NPs or decorated nanoparticles (RGD-NPs, CD69-NPs, IgGh-NPs, IgGm-NPs) were added at indicated Ca<sup>2+</sup> concentrations (0.0125-1.0 mg/L), and the cells were incubated for another 24 h. SH-NPs were used as control for decoration since they represent an intermediate product during synthesis. Afterwards, the cells were enzymatically harvested, centrifuged (200 rcf, 5 min, 4°C) and washed with PBS. To investigate the cytotoxic effect of the nanoparticles, cells were incubated with a 1:75 dilution of Annexin-V-FLUOS in PBS for 10 to 15 min at RT in the dark. Samples were diluted 1:5 with PBS prior to measurement with an Accuri C6 flow cytometer. For each sample, a minimum of 20,000 events was analyzed in the channels FL1 (Laser 488 nm, emission filter 530/30 nm) for Annexin-V-FLUOS and FL3 (Laser 488 nm, emission filter 670LP) for nanoparticles. Data were analyzed using the BD Accuri™ C6 Plus software with respect to fraction of annexin-negative cells, nanoparticle-positive cells in the whole population and mean fluorescence intensities (MFI) of nanoparticles. The fraction of nanoparticle-positive cells is used as a measure of the total population uptake capability of the nanoparticles, while the MFI represents the single cell uptake capacity.

### 3.2.3 Characterization of targets on immune cells for decorated nanoparticles and their specific uptake in these cells

To investigate the expression of integrin  $\alpha_v\beta_3$  on SVEC4-10 cells, untreated cells were enzymatically harvested, centrifuged (200 rcf, 5 min, 4°C) and washed with PBS/ 1% (w/v) BSA. Cells were stained with PE-anti-mouse CD51 antibody (0.01  $\mu\text{g}/\mu\text{L}$ ) and the corresponding Rat IgG1,  $\kappa$  Isotype ctrl – PE (0.01  $\mu\text{g}/\mu\text{L}$ ) for 30 min on ice in the dark. Cells were washed once and resuspended in PBS/ 1% (w/v) BSA prior to measurement with an Accuri C6 flow cytometer. Samples were measured in triplicates with 10,000 - 20,000 events each.

For B cells and T cells, the expression of the activation marker CD69 was investigated by harvesting, centrifuging (200 rcf, 5 min, 4°C) and washing cells with PBS/ 1% (w/v) BSA. Cells were stained with PE anti-mouse CD69 (0.0025  $\mu\text{g}/\mu\text{L}$ ) as well as its corresponding isotype control in the same concentration for 30 min on ice in the dark. Expression of activation markers on the cell surface was analyzed as described above

To investigate the specificity of uptake of decorated nanoparticles, binding competition experiments were performed. SVEC4-10 cells ( $3.5 \cdot 10^5$  cells/mL) were incubated with RDG-NPs (0.25; 0.5  $\mu\text{g}/\text{mL}$  RGD-peptide) and an 100x excess of free RGD-peptide in 1.5 mL-tubes. TK-1 and MOPC-315 cells ( $4.0 \cdot 10^5$  cells/mL) were incubated with CD69-NPs or IgGh-NPs (0.5 or 1.8  $\mu\text{g}/\text{mL}$  IgG) and an 100x excess of free IgG in 1.5 mL-tubes. Incubation was carried on for 3 h at 37°C with vortexing the cells suspensions every 30 min. Cells were washed once in PBS before NP-uptake was measured using flow cytometry as described in section 3.2.2.

### 3.2.4 Intracellular localization of nanoparticles after cellular uptake

The localization of nanoparticles was analyzed in monocytes using confocal laser scanning microscopy. J774A.1 monocytes were seeded onto untreated glass cover slides ( $\varnothing$  12 mm) in 24 well plates and pre-incubated for 24 h. Afterwards, cells were exposed to dual-NPs (labeled with PEI-Cy5 and TAMRA-peptide), or NPs (only labeled with PEI-Cy5) ( $0.5 \text{ mg}/\text{L Ca}^{2+}$ ) for the indicated time points. Subsequently, the nanoparticle-containing medium was replaced with culture medium containing 400 nM LysoTracker® Green DND-26 for 1.5 h. For the last 15 min of the staining, 1  $\mu\text{g}/\text{mL}$  Hoechst-33258 was added to the medium. Directly after staining, the fluorescence of cells was analyzed by confocal laser scanning microscopy without fixation. The fluorescence parameters were red for nanoparticles (Cy5 fluorescence,  $\lambda_{\text{ex}}$  633 nm,  $\lambda_{\text{em}}$  673 nm), orange for cargo (TAMRA fluorescence,  $\lambda_{\text{ex}}$  546 nm,  $\lambda_{\text{em}}$  579 nm), blue for cell nuclei (Hoechst fluorescence,  $\lambda_{\text{ex}}$  405 nm,  $\lambda_{\text{em}}$  450 nm), and green for endolysosomes (LysoTracker® Green DND-26

fluorescence,  $\lambda_{\text{ex}}$  504 nm;  $\lambda_{\text{em}}$  511 nm). For each time point, four to six images were semi-quantitatively analyzed by counting cells with a colocalization of nanoparticles and endolysosomes, normalized to all nanoparticle-positive cells.

### 3.2.5 Inhibition of nanoparticle uptake pathways in monocytes

J774A.1 monocytes were seeded in 24 well plates or 16 well chamber slides at a density of  $5 \cdot 10^4$  cells/cm<sup>2</sup> and pre-incubated for 24 h. Afterwards, cells were pre-treated with 5  $\mu$ g/mL chlorpromazine, cytochalasin, or wortmannin, respectively, for 1 h at 37 °C. The cells were also incubated at 4 °C for 1 h to inhibit all energy-dependent processes. Finally, the cells were exposed to fluorescently labeled NPs (0.5 mg/L Ca<sup>2+</sup>, 3 h).

For flow cytometric analysis, the cells were harvested, washed with PBS, and finally the nanoparticle fluorescence (PEI-Cy5) in the cell suspensions was measured with an Accuri C6 flow cytometer. Data were analyzed by the BD Accuri C6 Plus software. As a measure of the nanoparticle uptake capacity of the whole cell population, fractions of nanoparticle-positive and nanoparticle-negative subpopulations were determined with reference to the whole cell population number. Additionally, the mean fluorescence intensity of the fractions of fluorescent and non-fluorescent cells was quantified as a measure of the single cell uptake capacity.

For microscopic analysis, cells were washed with PBS, fixed with 3.7% (w/v) formaldehyde for 20 min at 37 °C and afterwards permeabilized using 0.1% (v/v) Triton X-100 for 5 min at RT. After washing the cells with PBS, the cytoskeleton was stained with Phalloidin-AlexaFluor-488 (1:150 in PBS) for 30 min at 37°C. After another washing step, cells were embedded in mounting medium containing approx. 3  $\mu$ g/mL Hoechst-33258 to stain the cell nuclei. Finally, the uptake of the fluorescently labeled nanoparticles into the cells was analyzed by confocal laser scanning microscopy. The fluorescence parameters were red for nanoparticles (Cy5 fluorescence,  $\lambda_{\text{ex}}$  633 nm,  $\lambda_{\text{em}}$  673 nm), green for cytoskeleton (AlexaFluor-488 fluorescence,  $\lambda_{\text{ex}}$  488 nm;  $\lambda_{\text{em}}$  525 nm), and blue for cell nuclei (Hoechst fluorescence,  $\lambda_{\text{ex}}$  405 nm,  $\lambda_{\text{em}}$  450 nm).

### 3.2.6 Incubation of inflamed cells with siRNA-loaded nanoparticles

Cells (J774A.1, SVEC4-10, TK-1 and MOPC-315) were seeded in 12 well plates and incubated with decorated or undecorated nanoparticles carrying functional p65 siRNA (F-NPs, RGD/F-NPs, CD69/F-NPs, IgGh/F-NPs) or scrambled control siRNA (S-NPs, RGD/S-NPs, CD69/S-NPs, IgGh/S-NPs) with a concentration of 1  $\mu$ g siRNA/mL for 72 h. As control, cells were also treated with decorated or undecorated nanoparticles without siRNA



(RGD-NPs, CD69-NPs, IgGh-NPs, SH-NPs) as well as with free siRNAf or siRNAs transfected with Lipofectamine™ for 72 h.

Prior to analysis, cells were stimulated to induce an inflammation status (termed inflamed cells): 1) J774A.1 cells were stimulated with 1 µg/mL LPS for 4 h; 2) SVEC4-10 were treated with 10 µg/mL LPS for 6 h (Mohamadzadeh *et al.* 1998); 3) TK-1 cells were co-stimulated with 5 µg/mL CD3ε-Biotin antibody and 2 µg/mL CD28 antibody for 6 h (Levine *et al.* 1996); and 4) MOPC-315 cells were treated with 0.5 µM ODN-2006 and 75 ng/mL IL-4 for 3 h (Van Belle *et al.* 2016). Unstimulated cells represented the non-inflammatory condition.

After incubation, cells were harvested. J774A.1 cells were lysed for RNA and protein isolation with a peqGOLD TriFast™ reagent according to the manufacturer's protocol (with starting volume 500 µL of the TriFast™ reagent and adaption of all reagent volumes accordingly) and cell supernatants were collected for further analysis of cytokine expression. SVEC4-10, TK-1 and MOPC-315 cells were lysed for protein isolation with 50 – 100 µL RIPA buffer on ice for 45 min. Residual cell debris was removed by centrifugation for 15 min at 12,000 rcf and 4°C and lysates were stored at -80°C.

### **3.2.7 p65 gene expression after incubation with siRNA-loaded nanoparticles**

Inflamed monocytes were incubated with nanoparticles, and the total RNA was isolated as described in section 3.2.6. RNA concentration was spectrometrically determined. The High Capacity cDNA Reverse Transcription Kit was used to synthesize cDNA according to the manufacturer's protocol with an initial input of 2 µg total RNA.

For quantitative real-time PCR (qRT-PCR) analysis of NF-κB p65 gene expression, the TaqMan™ Gene Expression Assays for NF-κB p65 (Mm00501346\_m1) and β-actin (Mm01205647\_g1) together with the TaqMan™ Fast Advanced Master Mix were used. The experiment was performed according to the manufacturer's protocol for 96-well Fast Plate. Analysis was performed using the RotorGene Q qPCR instrument with setup according to the protocol.

For the calculation of the relative gene expression, the  $\Delta\Delta CT$  method was used (Pfaffl 2001). The data were normalized to LPS-primed but non-nanoparticle treated cells as control. The change of gene expression termed as "regulation of p65 gene expression" was calculated with reference to the control (set to zero).

### **3.2.8 p65 protein expression after incubation with siRNA-loaded nanoparticles**

Inflamed cells (J774A.1, SVEC4-10, TK-1 and MOPC-315) were incubated with the nanoparticles, and proteins were isolated as described in section 3.2.6. Total protein concentration in all cell lysates was measured with the Bradford assay. Samples were pre-diluted 1:100 in MilliQ and diluted 1:10 with Bradford reagent in a 96 well plate prior to measurement of the absorption at 595 nm using a plate reader. Samples were measured in triplicates and concentration was calculated using a BSA calibration curve (0 – 20 µg/mL) obtained in parallel with the samples.

Proteins were separated using an SDS-PAGE (20 µg total protein per lane, 110 V for 10 min following 140 V for approx. 55 min), then transferred to an Immobilon-P membrane (assembly of blot according to manufacturer's user manual, 275 mA for 60 min on ice).

All following washing steps were performed for 10 min with PBS-T at RT and all washing and incubation steps were performed on a rotary shaker. Membranes were washed thrice before blocking of unspecific binding sites using 5% (w/v) dry milk in PBS-T for 1 h at RT. For immunodetection, membranes were incubated with HRP-conjugated NF-κB p65 antibody (1:200 in 5% (w/v) dry milk) overnight at 4°C. Membranes were washed three times before detection. Chemiluminescent signals were detected after incubation with Clarity™ Western ECL Substrate using the Imaging systems LAS-4000 or Fusion FX7 Edge. For normalization, the membranes were washed again and incubated with HRP-coupled β-actin antibody (1:5000 in 5% (w/v) dry milk) for 1 h at RT. Chemiluminescence signals were detected again as described above.

Semi-quantitative densitometric analysis was performed using the software ImageJ. Signals from p65 were normalized to corresponding β-actin signals for each sample, then data were normalized to inflamed but non-nanoparticle treated cells. Furthermore, the regulation of p65 protein expression (up- or downregulation) was calculated with respect to the control (inflamed cells only, set to zero).

### **3.2.9 Cytokine secretion after incubation with siRNA-loaded nanoparticles**

LPS-primed monocytes were incubated with the nanoparticles, and the cell supernatant was collected as described in section 3.2.6. To assess the impact of the nanoparticles on the secretion of inflammatory mediators, the supernatants of monocytes after nanoparticle exposure were analyzed by a LEGENDplex™ Mouse Inflammation Panel (13-plex) according to the manufacturer's protocol, but the volume of all reagents and the sample was reduced from 25 µL to 10 µL. Analysis is performed by flow cytometry according to the setup protocol and data were evaluated using the LEGENDplex™ Data Analysis Software.

For further quantification of TNF- $\alpha$ , the mouse TNF- $\alpha$  ELISA Kit was used according to the manufacturer's protocol.

### 3.2.10 Induction of colitis in mice and treatment with nanoparticles

All experiments were approved by the regional animal care committee (UKJ-19-027) and were performed in accordance with international guidelines on the ethical use of animals. For the necessary procedures, the animals were anesthetized with isoflurane (2.0% (v/v)) by inhalation.

In this study, the model of DSS-induced colitis is used to investigate the therapeutic efficiency of p65 siRNA-nanoparticles (without specific decorations). To set up the colitis model in mice, two preliminary examinations were conducted:

- a) To find the optimal DSS dosage to induce colitis in mice, dosages from the recommended range of 2.5 to 5.0% (w/v) in water were tested. Therefore, three different DSS dosages (2.5, 3.75, and 5.0% (w/v)) were administered to each group, consisting of 5 mice each. Colitis severity was assessed until day 12 as described in 3.2.12 and 3.2.13. From this experiment, the optimal DSS dosage, as well as the optimal day for NP-application and the observation time was determined.
- b) The optimal nanoparticle dosage was tested in a range according to publications using similar NP-formulations (Kim *et al.* 2010, Huang *et al.* 2018, Dong *et al.* 2018). Three different siRNA concentrations (1.5; 2.0; 2.5 mg siRNA/ kg body weight in NaCl) were administered to 2 mice each by intravenous injection in the tail vein four days after the start of DSS administration (day 3). Colitis severity was assessed until day 9 as described in section 3.2.12 and 3.2.13.

For the investigation of the therapeutic effect of siRNA-nanoparticles, animals were randomly divided into four experimental groups à 10 mice each. The experimental group F consisted of mice with colitis treated with nanoparticles carrying functional siRNA (F-NPs). As control groups, untreated mice with colitis (group C) or healthy, untreated mice (group H) were used to assess the impact of F-NPs. For groups F and C, 3.75% (w/v) DSS were administered via the drinking water for six days (day 0 – 5). On day 3, respective nanoparticles (2.0 mg siRNA/ kg body weight in NaCl) were injected into mice from group F. Colitis severity was assessed until day 6 (72 h after NP-application) or day 9 (72 h later) as described in section 3.2.12 and 3.2.13. A timeline for the animal experiments is shown in Figure 4.

Further experiments involved the study of side effects of the administered nanoparticles. In this context, 10 mice with colitis received intravenous nanoparticles with scrambled siRNA

(S-NPs, group S) on day 3 (2.0 mg siRNA/ kg body weight in NaCl i.v. in the tail vein) to assess the impact of the siRNA *per se* on the inflammation. Colitis severity was compared to group F until day 9, as described in section 3.2.12. To study possible side effects of the p65 siRNA-nanoparticles in the healthy organism, 10 healthy mice received the F-NPs on day 3. The impact of these nanoparticles on the inflammatory system was observed until day 9, as described in section 3.2.12.

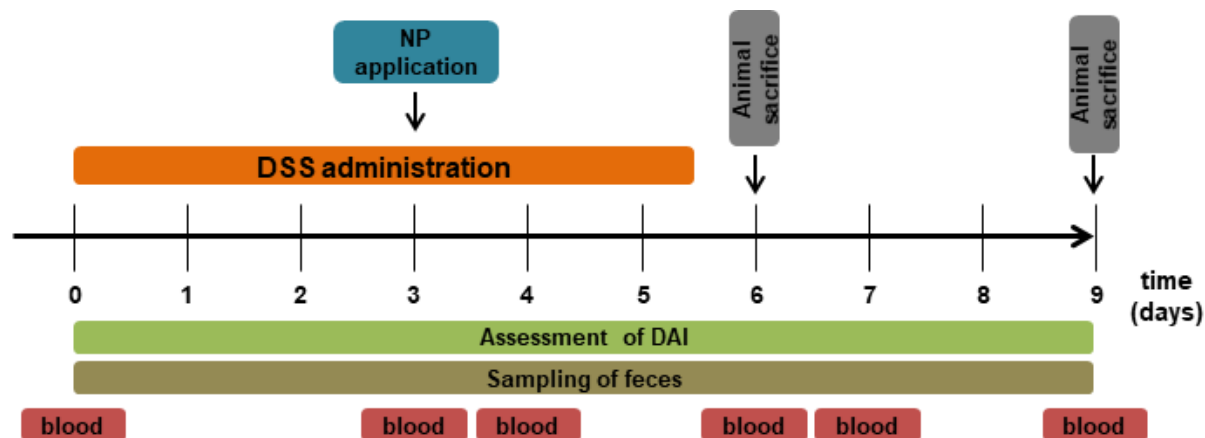


Figure 4: **Timeline of the procedure for *in vivo* experiments.** NP: nanoparticle; DSS: dextran sulfate sodium; DAI: disease activity index; blood: blood draw for hemogram or plasma.

At the end of the observation period, mice were euthanized using an overdose of CO<sub>2</sub> according to the guidelines for ethical use of animals. Serum samples were obtained immediately after death and stored at -80°C until further analysis. Moreover, the colon was resected. After flushing with HBSS (supplemented with 1% (v/v) penicillin/streptomycin), the weight and length of the colon from the ileocecal junction to the distal end at the rectum were determined for each animal. To perform further analyses the colon was cut into three equal-sized pieces: 1) The proximal third was used to determine secreted inflammatory mediators *ex vivo* (see section 3.2.15); 2) The middle part was either directly used for the isolation of leukocytes (see section 3.2.16) or shock-frozen in liquid nitrogen and stored at -80°C for protein analysis (see section 3.2.17); 3) The rectal third was prepared for histologic analysis (see section 3.2.14).

### 3.2.11 Biodistribution of nanoparticles

The biodistribution of the nanoparticles was investigated in healthy mice compared to mice with colitis. In this context, 10 mice per group received either 3.75% (w/v) DSS in the drinking water or normal drinking water over the period of four days. On day 3, nanoparticles (without siRNA) were injected intravenously at a concentration of 2.6 mg Ca<sup>2+</sup>/ kg body weight. This dosage corresponds to the calcium concentration of administered siRNA-nanoparticles with a dose of 2.0 mg siRNA/ kg body weight (see

section 3.2.10). Three hours afterwards, mice were sacrificed and defined organs and tissues (spleen, liver, mesenteric lymph nodes, colon, heart, muscle, skin, bladder, kidneys, lung, ovaries, uterine tubes, uterus, stomach, brain, appendix, and small intestine) were resected. Organs were analyzed for the fluorescence intensity of DY-734 using the IVIS Spectrum CT system. A sequence of images with different combinations of excitation and emission filters (Range: ex: 640 – 745 nm; em: 680 – 840 nm) was acquired (setup using imaging wizard). For all analysis steps the Living Image Software was used. Spectral unmixing of the DY-734-NP spectrum and tissue autofluorescence were carried out according to the device's manual. For quantitative analysis, ROIs were placed in each organ/ tissue covering the whole organ to acquire the Average Radiant Efficiency ( $[\text{p/s/cm}^2/\text{sr}]/[\mu\text{W/cm}^2]$ ). The change of the average radiant efficiency of organs from mice with colitis was calculated with respect to healthy mice (set to zero).

### 3.2.12 Assessment of colitis severity by clinical disease parameters

The colitis severity during the experiments was assessed every day by scoring feces consistency, rectal bleeding and weight loss adapted from a classical clinical scoring system (disease activity index, DAI) described previously (Cooper *et al.* 1993, Kim *et al.* 2020) (Table 14).

To further characterize the severity of colitis, feces samples were collected every day using a forceps, then were weighted, and stored at  $-80^\circ\text{C}$  for further analysis (see 3.2.13).

Blood samples (10  $\mu\text{L}$ ) were obtained at indicated days (Figure 4) by puncture of the *vena facialis*. The samples were diluted 1:12 in NaCl prior to generating a differential hemogram using a Hematology analyzer.

Table 14: **Score parameters for the assessment of colitis.** Sum of scores represents the disease activity index (DAI). For feces consistency and rectal bleeding only the scores 0, 2 or 4 were assigned.

SCORE	WEIGHT LOSS	FECES CONSISTENCY	RECTAL BLEEDING
0	no weight loss	normal	no bleeding
1	1 - 5% weight loss	/	/
2	5 - 10% weight loss	loose feces	blood visible
3	10 - 15% weight loss	/	/
4	16 - 20% weight loss	diarrhea	strong rectal bleeding

### 3.2.13 Detection of inflammation marker Lipocalin-2 in feces

For further investigating the severity of inflammation, the concentration of the inflammation marker Lipocalin-2 (Lcn-2) was determined in the feces every day. This biomarker is already established for the sensitive and non-invasive detection of intestinal inflammation

(Chassaing *et al.* 2012). Therefore, the feces was collected as described in 3.2.12. Frozen feces samples were reconstituted in PBS containing 0.1% (v/v) Tween 20 to a final concentration of 100 mg feces/mL. Samples were homogenized in M tubes using the gentleMACS with the program “Protein\_01\_01”. Afterwards, the samples were centrifuged for 10 min at 16,000 rcf and 4°C. Supernatants were collected and stored at -80°C for further analysis. Lcn-2 levels were determined using the Mouse Lipocalin-2/NGAL DuoSet ELISA and the DuoSet Ancillary Kit 2 according to the manufacturer’s protocol. Samples were diluted 1:20 to 1:4000 depending on the concentration of the analyte and measured in duplicates.

### 3.2.14 Preparation of tissue sections and immunostaining

For histological staining of the colon tissue, Swiss rolls were prepared from the rectal third of the resected colon. Pieces were cut open longitudinally and wrapped around a glass capillary starting from the rectal end with the lumen on the outside (Moolenbeek and Ruitenbergh 1981). Colon rolls were placed in embedding cassettes and stabilized with a pin. Tissue samples were fixed in 5% (v/v) formaldehyde solution for 24 h. After washing with PBS for 24 h or with flowing tap water for 2 h, the tissue samples were dehydrated using an automatic tissue processor (see Table 15). Immediately afterwards, the Swiss rolls were embedded in paraffin. Sections of 3 µm were generated from the pre-cooled paraffin blocks using an automated rotary microtome, applied to microscopic slides, and dried over night at 37°C. Before staining, the cross sections were deparaffined and hydrated using xylene and subsequent decreasing alcoholic series (Table 16).

Table 15: **Dehydration steps using an automated tissue processor.**

REAGENTS	CONDITIONS
2x 70% (v/v) EtOH	1 h, RT
2x 96% (v/v) EtOH	1 h, RT
3x 100% EtOH	1 h, RT
1x 100% EtOH:100% Xylene (1:2)	1 h, RT
2x 100% Xylene	1 h, RT
2x paraffin	1 h, 70°C

Table 16: **Decreasing/ ascending alcoholic series:** Steps from Xylene to Aqua dest. used as decreasing series for deparaffination and rehydration of cross sections; Steps from Aqua dest. to xylene used as ascending series for dehydration prior to embedding.

REAGENTS	CONDITIONS
100% xylene	2x 5 min
96% (v/v) EtOH	1x 5 min
70% (v/v) EtOH	1x 5 min
50% (v/v) EtOH	1x 5 min
Aqua dest.	1x 5 min

For the hematoxylin & eosin (H&E) staining, slides were incubated in hematoxylin solution (Mayer's) for 5 min, and then washed twice in Aqua dest., and incubated in warm water for 2 min. Afterwards, cross sections were incubated in freshly prepared 0.1% (w/v) eosin B solution for 3 min. Before embedding the cross sections with PERTEX mounting medium, the slides were dehydrated using the ascending alcoholic series (Table 16). Stained slides were scored for extent of colonic inflammation according to the histopathologic score listed in Table 17. For each experimental group, cross sections of 3 to 5 animals were scored by four blinded researchers and these scores were summarized for each animal.

Table 17: **Histopathological scoring of H&E sections calculated by adding the scores of the listed parameters.**

<b>SCORE</b>	<b>EXTENT OF INFLAMMATION</b>	<b>EXTENT OF CRYPT DAMAGE</b>	<b>EXTENT OF CRYPT DAMAGE IN THE WHOLE SECTION</b>
0	none	none	none
1	mucosa only	basal 1/3	25% of section
2	mucosa and submucosa	basal 2/3	50% of section
3	transmural	crypt loss	75% of section
4	/	/	100% of section

For immunohistologic stainings, as a first step antigen retrieval was performed by incubating the slides in boiling citrate buffer for 25 min (in a microwave). After cooling down and removal of the buffer, cross sections were encircled with a PAP-Pen and shortly rinsed in 0.1% (v/v) TBST. Subsequently, biotin blocking was performed using the Biotin Blocking System (Bio Legend) according to the manufacturer's protocol. Afterwards, cross sections were incubated with 100 µL of the corresponding primary antibodies dilution in Antibody Diluent for 40 to 80 min at RT. In detail, primary rabbit monoclonal antibodies against p65 (1:1,000-2,000), IκB (1:100-300), COX-2 (1:100-400) and CD45 (1:250) were used. After washing the slides three times in 0.1% (v/v) TBST, cross sections were incubated with 150 µL of the biotinylated goat anti-rabbit secondary antibody diluted in Antibody Diluent (1:2250) for 30 to 45 min at RT. Subsequently, after three additional washings steps in 0.1% (v/v) TBST, cross sections were incubated with 100 µL of a 1:75 dilution of Streptavidin-AP in Antibody Diluent for 30 to 45 min at RT. Chromogen staining was performed using the Dako Liquid Permanent Red Kit according to the manufacturer's protocol. In short, cross sections were incubated in 100 µL chromogen solution (500 µL Substrate Buffer, 1 µL Levamisole, 1.65 µL chromogen) for 20 min at RT. After a washing step in Aqua dest., the slides were counterstained with a hematoxylin solution (Mayer) for 5 min and washed again twice in Aqua dest.. After incubation in warm water for 5 min, the cross sections were embedded with Faramount Mounting Medium and sealed with nail polish.

### **3.2.15 *Ex vivo* colon cultivation for detection of secreted inflammatory mediators**

To determine the amount of secreted inflammatory mediators from colon tissue, the proximal part of the colon (resection see 3.2.12) was weighted, and then cut open longitudinally. The colon pieces were washed three times serially in HBSS (supplemented with 1% (v/v) penicillin/streptomycin) prior to incubation in 1 mL RPMI medium supplemented with 1% (v/v) penicillin/streptomycin in a 24 well plate at 37°C with 5% CO<sub>2</sub> for 24 h. Supernatants were subsequently collected and stored at -80°C for further analyses, which are described in section 3.2.18. The procedure was adapted from a previously described method (Chassaing *et al.* 2014).

### **3.2.16 Isolation of leukocytes from colon tissue**

Since it can be expected that the intravenously injected nanoparticles are taken up directly by immune cells in the blood stream and transported to the inflamed bowel tissue, leukocytes were isolated from the middle third of the colon (resection see 3.2.12). Therefore, the colon piece was cut open longitudinally and divided into parts about 0.5 cm in length. For the dissociation of the colon tissue the Lamina Propria Dissociation Kit (mouse) was used according to the manufacturer's protocol. The isolated colon cells were counted using a cell counter. For each mouse,  $(1.0 \text{ to } 1.5) \cdot 10^7$  cells were used for the subsequent separation, which was performed using CD45 Microbeads according to the protocol provided by the supplier. Afterwards the amount of CD45-positive cells was determined. These CD45-positive cells were washed with HBSS, centrifuged and cell pellets were stored at -80°C until further analysis.

### **3.2.17 Protein expression in whole colon tissue and colon leukocytes**

Proteins were extracted from the middle part of the colon tissue (resection see 3.2.12) or from isolated colon leukocytes (see 3.2.16) for Western blot analyses to investigate the direct effects of F-NPs after internalization in leukocytes (so called "primary effects" of F-NPs) as well as the indirect effects of these nanoparticles in colon lysates due to signaling between cells (so called "secondary effects").

Regarding the whole colon tissue, pieces of 9 to 50 µg tissue were transferred into M tubes containing 1.5 mL RIPA buffer and lysed using the gentleMACS (program "Protein\_01\_01"). Lysates were centrifuged for 10 min at 10,000 rcf and 4°C to remove tissue debris and stored at -80°C for further analysis. In case of colon leukocytes, obtained cell pellets (see



3.2.16) were lysed in 50 – 100  $\mu$ L RIPA buffer on ice for 45 min. Residual cell debris was removed by centrifugation for 15 min at 14,400 rcf and 4°C and stored at -80°C.

The protein concentration of all lysates was determined using the Bradford protein assay as described in section 3.2.8. To facilitate the simultaneous detection of 6 different proteins, multi-strip Western blotting was performed (Aksamitiene *et al.* 2007). Therefore, proteins from up to 52 samples were separated using four SDS gels simultaneously, as described in section 3.2.8. Afterwards, gels were cut with a scalpel into strips from about 180 to 95 kDa, from 95 to 55 kDa, from 55 to 30 kDa and from 30 to 20 kDa using the prestained protein ladder as orientation. The corresponding strips from each gel were combined in a transfer cassette for blotting as described in section 3.2.8.

All following washing steps were performed for 10 min with PBS-T at RT and all washing and incubation steps were performed on a rotary shaker. Membranes were washed thrice before blocking with Purelock™ Blocking Buffer for 1 h at RT. Membranes were then probed with the corresponding primary antibodies diluted in Purelock™ Blocking Buffer according to the size-range of the strips. Primary antibodies against p65 (1:1,000), I $\kappa$ B (1:6,000), INOS (1:1,000), COX-2 (1:1,000) and Bcl-2 (1:1,000) were incubated at 4°C overnight. After washing thrice, membranes were incubated with the respective HRP-coupled secondary antibody (1:10,000) or HRP-conjugated  $\beta$ -actin antibody (1:7,500) as loading control for 1 h at RT. Chemiluminescence signals were detected as described in section 3.2.8. In case two or more proteins had to be detected on one strip because of similar size, the membrane was stripped by incubation with stripping buffer at 55°C for 30 min and subsequent washing steps in Aqua dest. and re-blocking with Purelock™ Blocking Buffer.

To quantify the expression of p65 in the different treatment groups, a densitometric analysis of Western Blot bands was performed with the software Bio1D. Data were normalized to group H (no nanoparticles, healthy).

### **3.2.18 Detection of cytokines/ chemokines in different samples**

To determine the amount of proinflammatory mediators in different samples, the LEGENDplex™ Mouse Inflammation Panel (13-plex) was used according to the kit's protocol. Whole colon protein lysates (see section 3.2.17) were used to determine total concentrations of cytokines in the colon as general indicators of the local inflammation, while the supernatant of *ex vivo* cultivated colon pieces (see section 3.2.15) was analyzed for the secreted inflammatory mediators as a measure for the transmission of the inflammatory signal between cells. Plasma samples acquired after euthanasia were used to measure systemic inflammation markers as indicators for systemic reaction to the treatment. Samples were diluted 1:2 in Matrix C according to the protocol were measured in

duplicates. For data analysis the recommended LEGENDplex™ Data Analysis Software (Version 8) was used. Concentration of measured cytokines for the colon and the *ex vivo* cultivated colon were normalized to the weight of the used colon piece for each sample.

### **3.2.19 Data analysis**

Data obtained from independent experiments are represented as mean ± standard error of the mean SEM (if not indicated otherwise). For statistical analyses of *in vitro* data, the software PRISM 6 (GraphPad software, La Jolla, USA) with a Student's *t*-test or a two-way ANOVA (analysis of variance) with Tukey's post hoc test was used. Furthermore, the software SPSS with an ANOVA and Dunnett-T (2-sided) post hoc test or a generalized linear model with Wald-Chi-Quadrat pairwise comparisons was used for *in vivo* data. Differences with *p*-values of 0.05 or less were considered as statistically significant.

## **4 Results**

### **4.1 Calcium phosphate nanoparticles for gene silencing of NF- $\kappa$ B and their impact on cellular players of inflammation**

The internalization of undecorated calcium phosphate nanoparticles (NPs) was shown to be dependent on the investigated cell type. The uptake of nanoparticles was highest in monocytes, while endothelial cells (ECs) and B cells showed intermediate and T cells low uptake capacity. No notable cytotoxicity of the nanoparticles was found in all cell lines. Moreover, the internalization mechanism in monocytes was found to be mostly energy dependent. Visual investigations confirmed the localization of the cargo of the nanoparticles in the cytosol after uptake. Furthermore, by using decorated nanoparticles for specific targeting of ECs, B cells, and T cells enhanced uptake capacity was achieved. Finally, the gene silencing capability of nanoparticles carrying p65 siRNA was also found to be dependent on the target cell type. Moreover, a substantial impact of the nanoparticles itself on the inflammatory signaling was found in all cell types.

#### **4.1.1 Uptake of nanoparticles in the cellular players of inflammation**

The assessment of the internalization of the undecorated calcium phosphate nanoparticles (without cargo siRNA) revealed a readily uptake by monocytes, with almost 100% of total cells being NP-positive (Figure 5). The single cell uptake capacity showed that though almost all cells had taken up the fluorescent nanoparticles (mean fluorescence intensity per cell), the uptake in single cells still increased with rising concentrations. Endothelial cells and B cells showed intermediately strong, concentration-dependent uptake of the nanoparticles. The single cell uptake capacity was lower (approx. one third) as that of monocytes. In contrast, T cells only had a low total uptake capability as well as a low single cell uptake capacity, which was also dependent on the used concentration.

Incubation with the nanoparticles had no impact on the cell viability of monocytes and endothelial cells as shown with the annexin-negative cell population (viability > 80% of total cells). In contrast, some degree of cytotoxicity was shown for B cells and T cells for the higher concentrations used.

Summarized, the calcium phosphate nanoparticles were taken up into cells involved in inflammation depending on the concentration and cell type and were cytocompatible for the concentrations used.

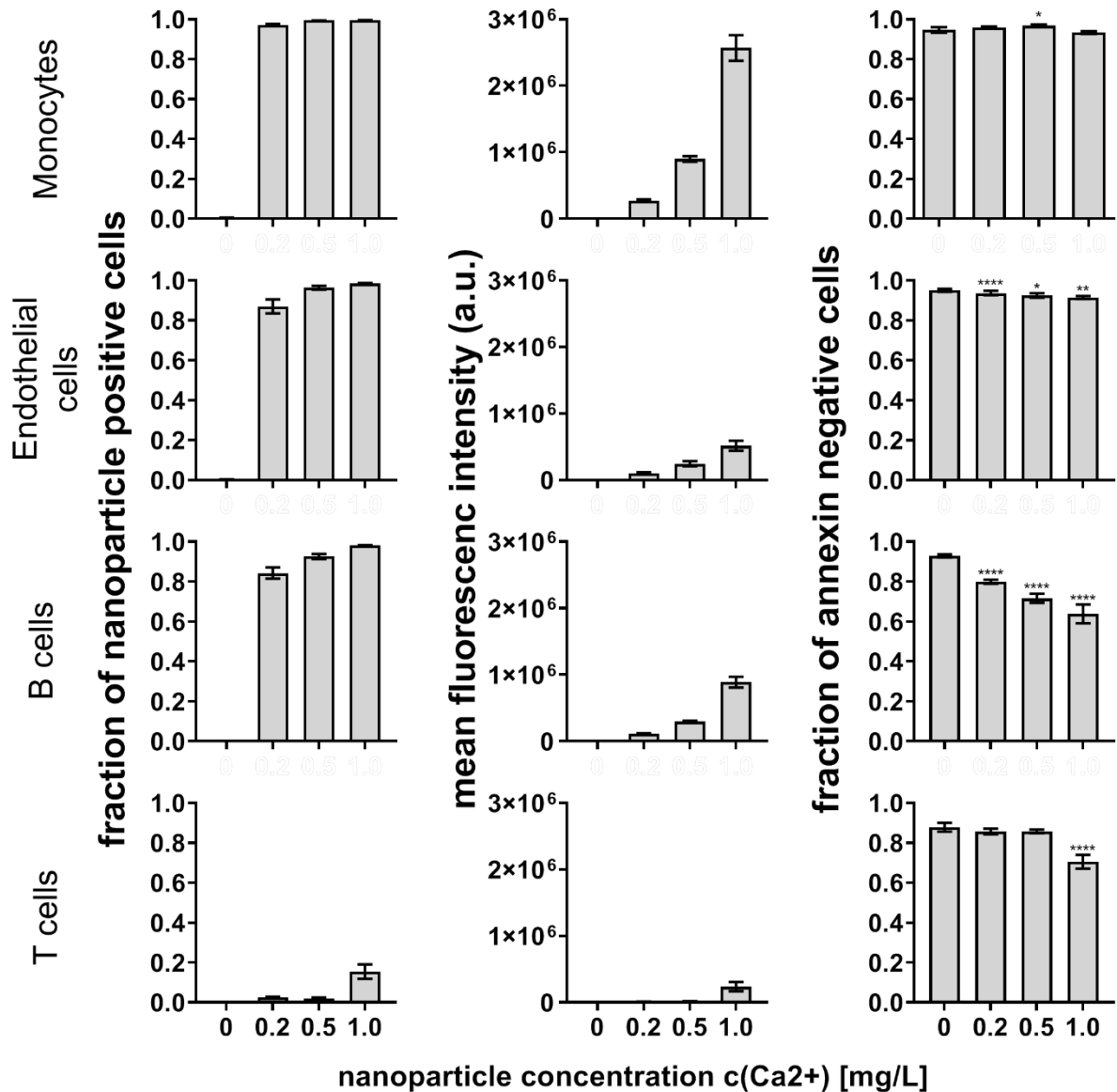


Figure 5: **Calcium phosphate nanoparticles (NPs) were readily taken up by most of the cells from the blood compartment while exhibiting low cytotoxicity effects.** Left: Uptake behavior, middle: mean fluorescence intensity (NPs), right: impact on the cell viability. The cells (monocytes J774A.1, endothelial cells SVEC4-10, B cells MOPC-315, T cells TK-1) were exposed to fluorescently labeled NPs (0 - 1.0 mg/L  $\text{Ca}^{2+}$ ) and incubated for 24 h prior to staining with annexin and flow cytometric analysis. Shown are the mean and SEM for three independent experiments. For fraction of annexin-negative cells: significantly different from non-treated control (0 mg/L  $\text{Ca}^{2+}$ ) with \*  $p < 0.05$ , \*\*  $p < 0.01$ , \*\*\*  $p < 0.001$ , and \*\*\*\*  $p < 0.0001$  tested using a two-way ANOVA (analysis of variance) with Tukey's post hoc test.

Since the uptake of nanoparticles in endothelial cells, B cells and T cells was distinctively lower than in monocytes, decoration of nanoparticles for specific targeting of these cell types was investigated for enhanced uptake.

Investigation of the impact of the host species of antibodies (Armenian hamster vs. murine origin) used for targeting showed, that for all cell types (B cells, endothelial cells, monocytes, and T cells) the uptake of nanoparticles decorated with unspecific antibodies from Armenian hamster (IgGh-NPs) was significantly higher than that of undecorated NPs

## Results

for relevant concentrations (Figure 6). Furthermore, no differences in the cytotoxicity between the nanoparticles were found for all cell lines (Figure A. 1, see appendix on page 104). Interestingly, the uptake of nanoparticles decorated with allogeneic (murine) antibodies (IgGm-NPs) was rather inhibited in B cells and T cells compared to undecorated NPs. Therefore, the uptake of antibody-decorated nanoparticles into the different target cells was highly dependent on the origin of the antibodies without affecting the viability of the cells. For following targeting attempts using antibodies, the ones originated in Armenian hamster were used.

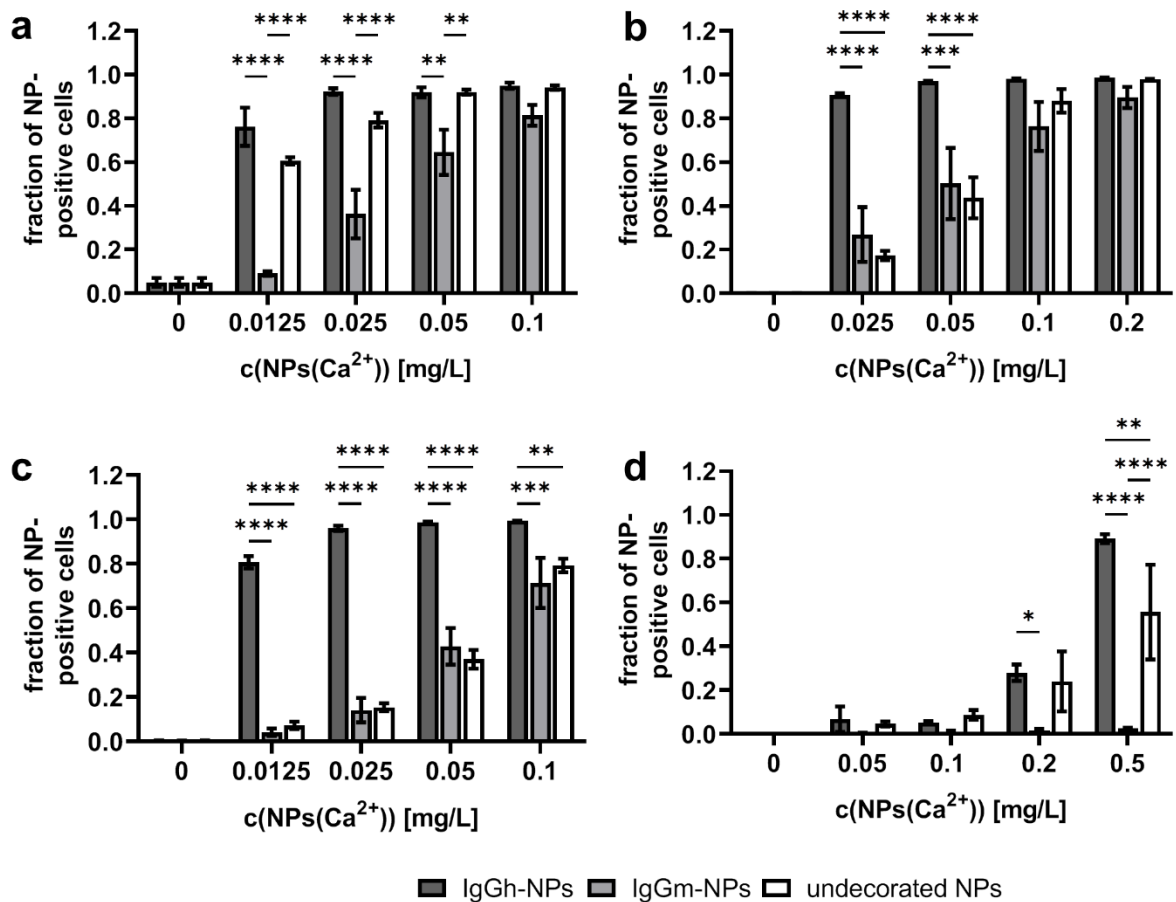


Figure 6: **Uptake of IgG-decorated nanoparticles in target cells is mostly dependent on the IgG-host species.** B cells MOPC-315 (a), endothelial cells SVEC4-10 (b), monocytes J774A.1 (c) and T cells TK-1 (d) were incubated with nanoparticles decorated with unspecific Armenian hamster IgG (IgGh), murine IgG (IgGm) or undecorated NPs for 24 h prior to analysis by flow cytometry. Shown is the fraction of NP-positive cells as the mean and SEM for 3 independent experiments. Differences between indicated groups tested by a two-way ANOVA with Tukey's post hoc test were considered as statistically significant for \*  $p < 0.05$ , \*\*  $p < 0.01$ , \*\*\*  $p < 0.001$ , and \*\*\*\*  $p < 0.0001$ .

#### 4.1.2 Nanoparticles (undecorated) and their effect on monocytes

The investigation of the uptake mechanism of the nanoparticles into monocytes by means of cell incubation at 4°C revealed a reduced nanoparticle-uptake capacity of the whole cell population from more than 90% to less than 50% compared to cells incubated at 37°C (Figure 7). Furthermore, the single cell uptake capacity was slightly decreased by about 0.6 a.u. and fluorescent images clearly show the locations of nanoparticles on the surface of the cells, not in the cytoplasm. This indicates an energy-dependent uptake mechanism for these nanoparticles. By blocking the microtubule rearrangement using cytochalasin D, both the uptake capacity for the whole population and single cells was significantly reduced to 81% and 2.0 a.u. respectively and the nanoparticles interacting with cells were clearly localized on the outer cell surface. Wortmannin was used to inhibit micropinocytosis, and the incubation resulted in only a slight decrease of the whole population uptake capacity but in a significant reduction of the single cell uptake capacity to 2.1 a.u. with nanoparticles being clearly localized outside the cells. The treatment of cells with Chlorpromazine to inhibit clathrin-mediated endocytosis also significantly reduced both whole population and single cell uptake capacity to 80% and 3.5 a.u. respectively. Taken together, the nanoparticles were found to be taken up into monocytes with a high contribution of energy-dependent mechanisms and to a lower extent by processes related to phagocytosis and clathrin-mediated endocytosis.

Furthermore, the assessment of the intracellular localization of the nanoparticles showed that the fraction of cells with colocalization of the nanoparticles and the lysosomes was significantly increased from 59% to 85% for incubation of 1 h to 6 h (Figure 8a, b). After 6 h, the colocalization significantly decreased again to reach the level of 1 h after 24 h again. The decrease of colocalization was found to continue up to 72 h after beginning of incubation, where only 27% of cells still showed a colocalization of nanoparticles with lysosomes.

Moreover, a clear colocalization of the nanoparticle cargo (fluorescently labeled, negatively charged cell-penetrating peptide) with lysosomes could be shown after 24 h (Figure 8c). In contrast, after 72 h the colocalization of cargo with lysosomes markedly decreased and the peptide was found to be more evenly distributed in the cytoplasm. These findings indicate that the nanoparticles are degraded in the lysosomes and that the cargo siRNA can be subsequently released into the cytoplasm to exert its function.

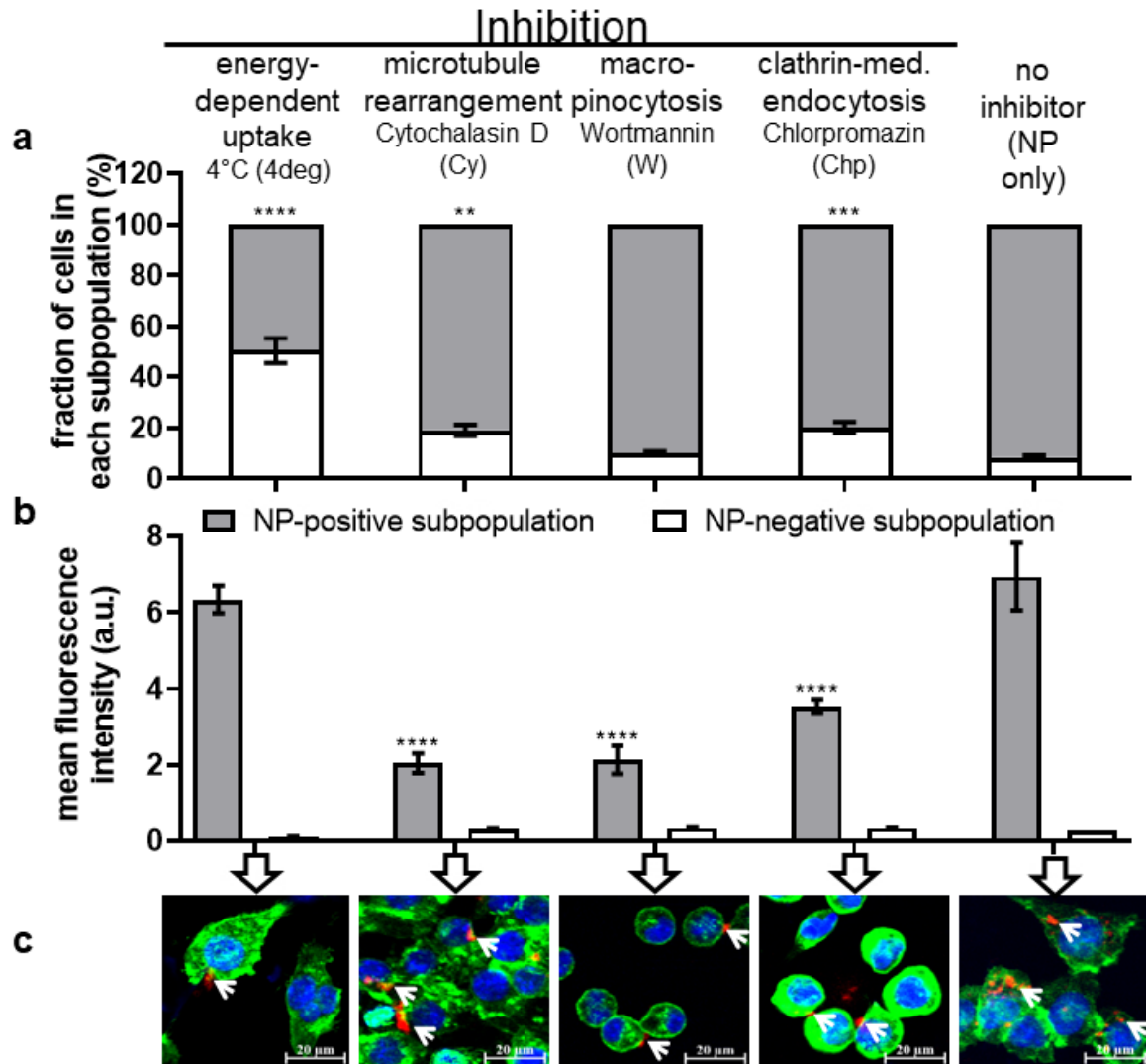


**Figure 7: Monocytes internalize nanoparticles via energy-dependent mechanisms and in parts by interplay of different endocytosis machineries.** J774A.1 cells were pre-incubated with the indicated inhibitors (5 μg/mL) for 1 h prior to addition of fluorescently labeled NPs (0.5 mg/L Ca<sup>2+</sup>) for 3 h and subsequent analysis by flow cytometry. (a) Fractions of NP-positive and negative cells relative to whole cell population showing the nanoparticle uptake capacity. (b) Mean fluorescence intensities (MFI) of Cy-5 (NPs) of these populations representing the single cell uptake capacity. Mean and standard deviation of three measurements. Significant difference from non-treated control (NP-exposed cells without inhibitors incubated at 37°C) with  $p < 0.0001$  (\*\*\*\*),  $p < 0.001$  (\*\*\*), or  $p < 0.01$  (\*\*) tested using a two-way ANOVA with Tukey's post hoc test. (c) Representative images of each experimental group visualizing the uptake of NPs after incubation with inhibitors. Red: Cy5 fluorescence of CaP-NPs (ex: 633 nm, em: 673 nm); blue: DAPI fluorescence (ex: 405 nm; em: 450 nm); green: Phalloidin-AlexaFluor-488 fluorescence (ex: 488 nm; em: 525 nm). Scale bar 20 μm.

## Results

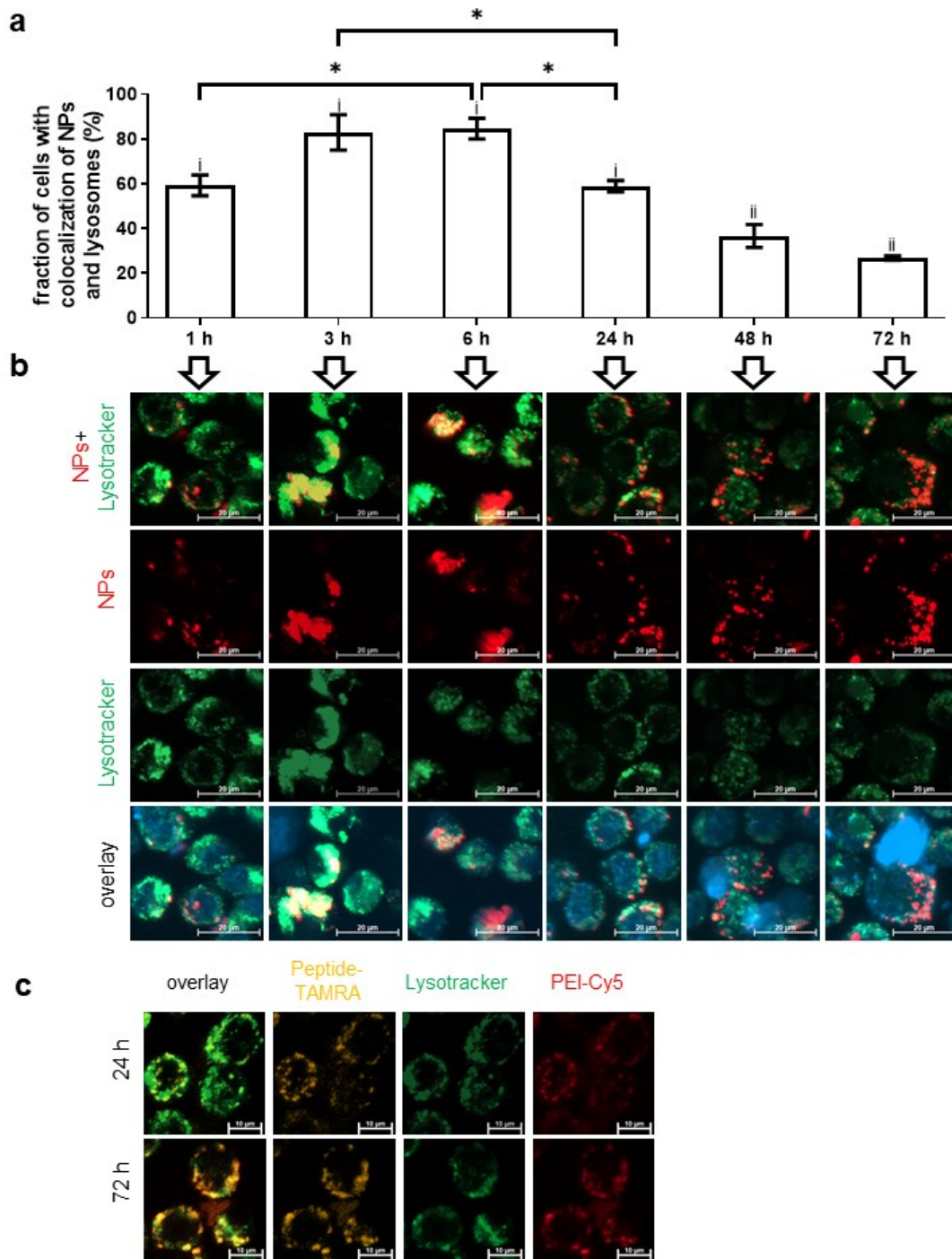


**Figure 8: Nanoparticles are colocalized with lysosomes after internalization in monocytes and the cargo was released into the cytoplasm.** J774A.1 cells were incubated with fluorescently labeled nanoparticles with or without cargo-peptide ( $0.5 \text{ mg/L Ca}^{2+}$ ) for 1 – 72 h. Subsequently, cells were stained with Lyso Tracker<sup>®</sup> Green DND-26 and Hoechst-33258. Living cells were directly analyzed by confocal laser scanning microscopy. (a) Semiquantitative analysis of microscopic images. Shown is the fraction of cells with colocalization of nanoparticles and lysosomes normalized to all NP-positive cells. Mean and SEM for three (i) or two (ii) independent experiments (\* for  $p < 0.05$  using a two-way ANOVA with Tukey's post hoc test). (b) Maximum intensity projection of representative Z-Stacks (see Figure A. 2, appendix on page 105). red: Cy5 fluorescence (ex: 633 nm, em: 673 nm); blue: Hoechst fluorescence (ex: 405 nm; em: 450 nm); and green: Lyso-Tracker<sup>®</sup> Green DND-26 fluorescence (ex: 504 nm; em: 511 nm). Scale bar 20  $\mu\text{m}$ . (c) Colocalization of nanoparticles with cargo-peptide with lysosomes. red: Cy5 fluorescence of nanoparticles (ex: 633 nm, em: 673 nm); orange: TAMRA fluorescence of the cargo peptide (ex: 546 nm; em: 579 nm); and green: Lyso-Tracker<sup>®</sup> Green DND-26 fluorescence (ex: 504 nm; em: 511 nm). Scale bar 10  $\mu\text{m}$ .



The incubation of monocytes with nanoparticles carrying 1.0 µg/mL siRNA for different incubation revealed a significant downregulation of p65 protein expression to a minimum of 55% (compared to non-NP-treated cells) after 72 h, while lesser siRNA concentration did not show sufficient effects on the protein expression (Figure A. 3, see appendix on page 105). Therefore, further gene silencing investigations were performed after NP incubation for 72 h with 1.0 µg/mL siRNA.

Inflamed monocytes treated with nanoparticles carrying functional siRNA (F-NPs) for 72 h clearly exhibited decreased p65 gene expression of about 30% compared to untreated inflamed cells (Figure 9a). Notably, nanoparticles with scrambled siRNA (S-NPs) as control of the specificity of the p65 siRNA even significantly increased the p65 gene expression by 37% beyond the inflamed level. Interestingly, nanoparticles without cargo (as control for impact of NP-components) and Lipofectamine<sup>TM</sup>-transfected p65 siRNA (siRNAf) as control for the transfection efficiency of the nanoparticles exhibited no notable effect on the gene expression of p65.

On protein expression level, the treatment with F-NPs clearly downregulated the p65 expression to 26% in the range of the non-inflammatory condition (Figure 9b). In contrast, treatment with S-NPs, NPs without cargo, or with Lipofectamine<sup>TM</sup>-complexed siRNAf even slightly increased the p65 protein expression compared to the inflammatory level.

To this end, no impact of the different treatments on the morphology of the monocytes was visible (Figure 9c), and the stimulation of cells with LPS to create inflamed monocytes did not impact the cell viability (Figure 9d).

Summarized, nanoparticles with p65 siRNA reverted the p65 expression (gene and protein level) in inflamed monocytes almost to the non-inflammatory, healthy condition without influencing the viability of the cells. In turn, these results present a passive confirmation that siRNA incorporated into the nanoparticles is able to translocate from lysosomes into cytoplasm after internalization in its functional form.

Furthermore, the incubation of inflamed monocytes with F-NPs also had a distinct effect on the secretion of inflammatory mediators (Figure 10). For the secretion of TNF-α, IL-6, and IFN-β, the incubation of cells with F-NPs led to a distinct downregulation towards the non-inflamed level. But remarkably, the incubation with S-NPs (as control of specificity of p65 siRNA) and NPs without cargo exhibited a comparable effect on the secretion of these cytokines, indicating the distinct effect from the nanoparticles' components.

In contrast, the IL-1β secretion was strongly upregulated for all conditions with nanoparticles present, which also indicates that this effect is mediated by components of the nanoparticles itself, not by the siRNA. Intriguingly, the stimulation with LPS itself did not

influence the IL-1 $\beta$  secretion, since no notable difference between the inflamed level and the non-inflamed level was seen in contrast to the other cytokines, where a clear change was seen for the inflamed status. In conclusion, the nanoparticles exhibited a distinct effect on the secretion of pro-inflammatory mediators TNF- $\alpha$ , IL-6, IFN- $\beta$ , and IL-1 $\beta$ .

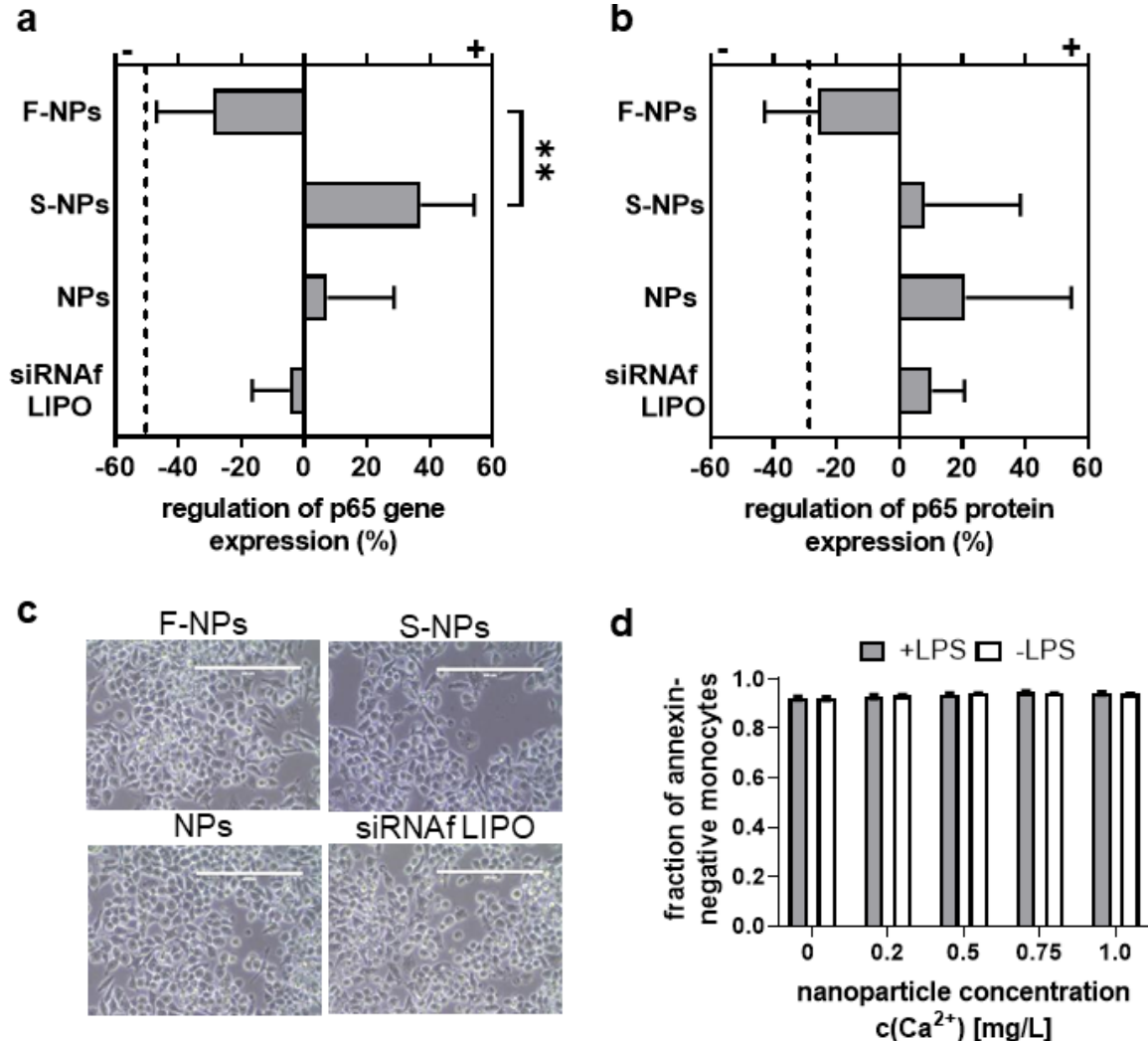


Figure 9: **Efficiency of nanoparticles with incorporated NF- $\kappa$ B p65 siRNA (F-NPs) in reversing p65 gene and protein expression on inflamed J774A.1 monocytes towards the non-inflamed condition.** F-NPs: Nanoparticles carrying functional p65 siRNA; S-NPs: Nanoparticles carrying scrambled siRNA; NPs: Nanoparticles without siRNA; siRNAf LIPO: functional p65 siRNA transfected with Lipofectamine<sup>TM</sup>. (a, b) Regulation of p65 gene (a) and protein (b) expression in LPS-primed monocytes after incubation with nanoparticles for 72 h. The regulation was defined as the ratio of p65 expression with respect to the inflammatory condition (LPS-primed cells without nanoparticles) set to zero. "+": upregulation, "-": downregulation. The dashed lines depict the non-inflammatory condition. Shown is the mean and SEM of 3 independent experiments with statistical differences between indicated groups tested with a two-way ANOVA with Tukey's post hoc test (\*\*  $p < 0.01$ ). (c) Representative microscopic images of cells incubated with nanoparticles. Scale bar 200  $\mu$ m. (d) Viability of LPS-primed and unstimulated monocytes in presence of indicated concentrations of NPs for 72 h measured by annexin-staining and flow cytometry. Mean and SEM of 3 independent experiments.

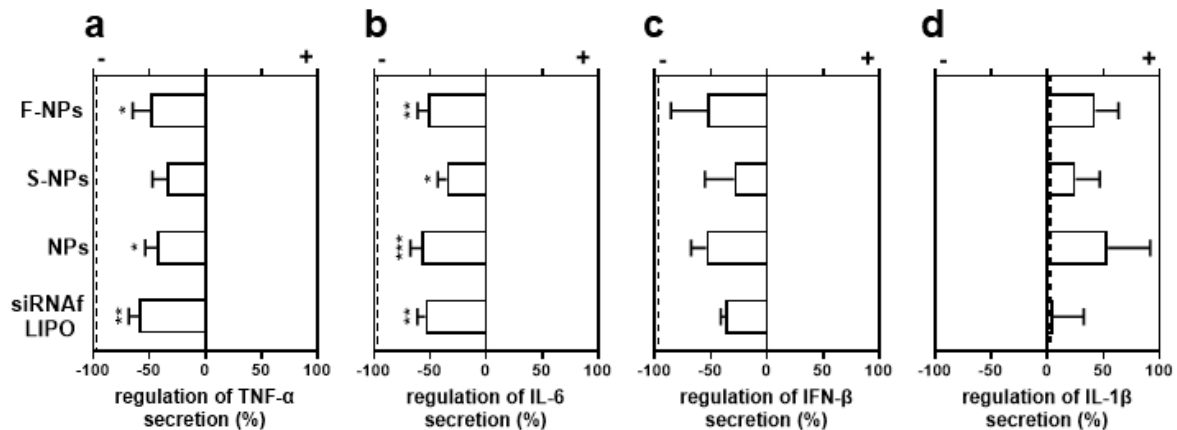


Figure 10: **Impact of the exposure of inflamed monocytes to NF- $\kappa$ B p65 siRNA-nanoparticles (F-NPs) on the secretion of pro- and anti-inflammatory mediators.** Regulation is defined as the ratio of cytokine secretion with respect to the inflammatory condition (LPS-primed cells without nanoparticles) set to zero. “+”: upregulation, “-”: downregulation. The dashed lines depict the non-inflammatory condition. F-NPs: Nanoparticles carrying functional p65 siRNA; S-NPs: Nanoparticles carrying scrambled siRNA; NPs: Nanoparticles without siRNA; siRNAf LIPO: functional p65 siRNA transfected with Lipofectamine™. TNF-alpha (a), IL-6 (b), IFN-beta (c), and IL-1beta (d) were measured in the cell supernatants after incubation with nanoparticles for 72 h. Shown are the means and SEM of 3 independent experiments. Significant differences compared to the inflammatory condition tested with a two-way ANOVA with Tukey's post hoc test are indicated with \* for  $p < 0.05$ , \*\* for  $p < 0.01$ , and \*\*\* for  $p < 0.001$ .

#### 4.1.3 Nanoparticles decorated with cRGD peptide for the targeting of endothelial cells

Considering that the uptake of undecorated NPs in endothelial cells (ECs) was not as high as for monocytes (Figure 5), the specific targeting of these cells was attempted to enhance the uptake. As seen in Figure 11c, the endothelial cell line SVEC4-10 expresses integrin  $\alpha$  (CD51) on the cell surface, which presents a good target for nanoparticles decorated with the peptide cRGDfK (RGD-NPs).

Indeed, the RGD-NPs were taken up into ECs to a higher extent than the undecorated NPs in a concentration-dependent manner (Figure 11a). For higher concentrations, the internalization was saturated, hence no difference between RGD-NPs and undecorated NPs was visible anymore, showing that the positive effect of RGD-decoration on the internalization is only present for low concentrations. Interestingly, SH-NPs, which present an intermediate step during the synthesis of RGD-NPs directly before covalent coupling of the peptide, were internalized into ECs to an even lower extent than the undecorated NPs. For all tested nanoparticles, no cytotoxic effect on the cells could be seen (Figure 11b).

Moreover, the specific binding competition by excess of unbound RGD-peptide resulted in a significant concentration-dependent reduction of the NP-positive population by 10 – 20% compared to the control condition without competition (Figure 11c). Taken this into account,

the enhanced uptake was at least in part due to the specific binding of RGD-NPs and integrin on the surface of ECs.

Furthermore, the incubation of inflamed ECs with RGD-NPs carrying p65 siRNA (RGD/F-NPs) resulted in a marked decrease of the p65 protein expression of 14% (compared to non-NP-treated inflamed cells), that is almost to the non-inflammatory level (Figure 11e). In contrast, RGD-NPs with scrambled siRNA (RGD/S-NPs) as control for the specificity of the siRNA, or RGD-NPs without cargo as control of the impact of the nanoparticles *per se* even increased the p65 expression by 17% and 38%, respectively. The Lipofectamine<sup>TM</sup>-mediated transfection of p65 siRNA as control for the transfection efficiency of the nanoparticles significantly decreased the p65 expression by more than 40%, even beyond the non-inflammatory level. As controls for the Lipofectamine<sup>TM</sup> transfection, the incubation of cells with scrambled siRNA and Lipofectamine<sup>TM</sup> or Lipofectamine<sup>TM</sup> alone even slightly increased the p65 protein expression. Taken together, nanoparticles with p65 siRNA and RGD-peptide were able to downregulate the p65 protein expression in inflamed ECs to the non-inflammatory level.

#### **4.1.4 Nanoparticles decorated with CD69-IgG for the targeting of B cells**

As for ECs, the uptake of undecorated NPs in B cells was distinctively lower than in monocytes (Figure 5), therefore also a specific targeting was attempted to enhance the internalization. The B cell line MOPC-315 was shown to express CD69 on the surface (Figure 12c), which was used as a target for nanoparticles decorated with anti-CD69 IgGh (CD69-NPs).

As anticipated, the uptake of CD69-NPs was even higher than that of SH-NPs (an intermediate product during synthesis before covalent binding of the antibodies) with consideration of the lower concentrations used (Figure 12a). In relation to the higher nanoparticle-concentrations, the internalization was saturated, therefore no difference between the decorated and undecorated NPs was visible. Intriguingly, nanoparticles decorated with unspecific IgGh (isotype control, IgGh-NPs) even exhibited higher internalization than the specific CD69-NPs for the lower concentrations. For all investigated nanoparticle types, no distinctive impact on the cell viability was seen (Figure 12b).

Interestingly, the competition of binding between CD69-antibody on nanoparticles and CD69 on the cell surface using excess unbound antibody resulted in only a small reduction of the NP-positive population of less than 1% compared to control cells without competition (Figure 12d). The same was true for the uptake of IgGh-NPs competed with unbound IgGh. Taking these results into account, the enhanced uptake seen for antibody-decorated nanoparticles in B cells was not due to specific binding of the antibody to CD69.

## Results

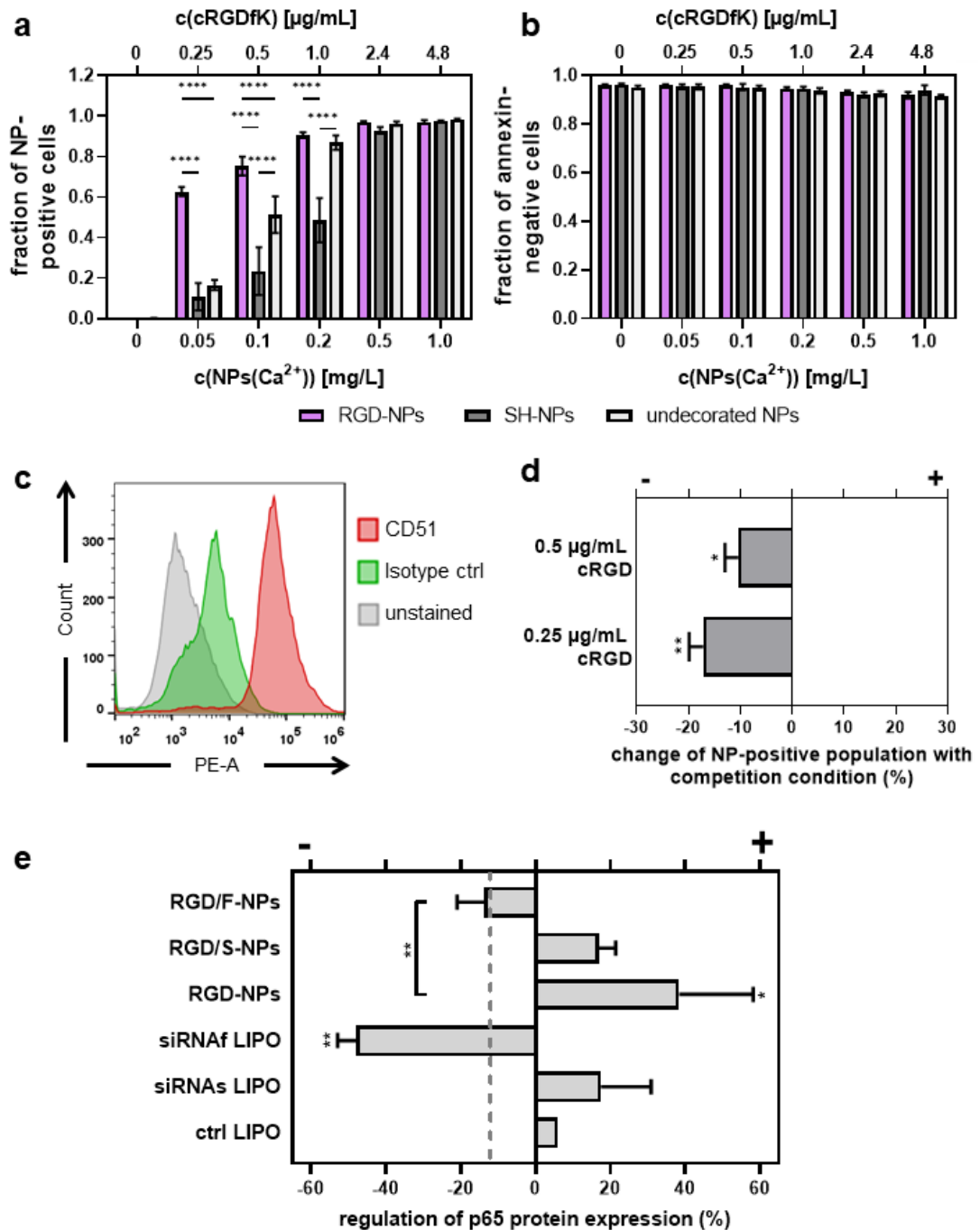


Figure 11: **Target-specific nanoparticles with RGD-peptide (RGD-NPs) in endothelial cells (ECs).** (a, b) Uptake (a) and cytotoxicity (b) of RGD-NPs in endothelial cells. Endothelial cells SVEC4-10 were exposed to fluorescently labelled RGD-NPs, SH-NPs or undecorated NPs and incubated for 24 h prior to staining with annexin and flow cytometric analysis. Shown are the mean and SEM for 3 independent experiments. (c) Expression of CD51/ integrin  $\alpha_v$  on the surface of ECs as target for RGD-decorated nanoparticles. Measurement by flow cytometry with unstained cells and isotype IgG as control. Shown is a representative image of 3 independent measurements. (d) Specific uptake of RGD-NPs measured by binding competition. SVEC4-10 cells were incubated with RGD-NPs and 100x excess of free RGD peptide. Shown is the change of uptake with competition condition with respect to non-competition measured by flow cytometry as mean and SEM from 3 independent experiments. (e) Potential of RGD-NPs with incorporated p65 siRNA to downregulate the p65 protein expression in inflamed ECs (LPS-stimulated). LIPO: Lipofectamine™. The regulation was defined as the ratio of p65 expression with respect to the inflammatory condition (stimulated cells without nanoparticles) set to zero. The dashed line depicts the non-inflammatory condition. Shown is the mean and SEM of 3 independent experiments. Statistical difference between indicated groups or with respect to the control was tested using a two-way ANOVA with Tukey's post hoc test (\*  $p < 0.05$ , \*\*  $p < 0.01$ , \*\*\*\*  $p < 0.0001$ ).

Despite the proven higher internalization of the nanoparticles, the incubation of inflamed B cells with CD69-NPs or IgGh-NPs carrying p65 siRNA (CD69/F-NPs or IgGh/F-NPs) did not result in a downregulation of p65 protein expression compared to untreated inflamed cells (Figure 12e). Further incubation with CD69-NPs or IgGh-NPs carrying scrambled siRNA (CD69/S-NPs or IgGh/S-NPs) to control the impact of the functional siRNA, by tendency, rendered an upregulation of p65 expression of about 15%. The same tendency was observed for SH-NPs without cargo. The Lipofectamine™-mediated transfection of p65 siRNA, as control for the transfection efficiency of the nanoparticles, significantly downregulated the p65 protein expression by 69%, even beyond the non-inflamed level. In contrast, the transfection of scrambled siRNA (to check for the impact of p65 siRNA) even significantly increased the p65 expression by 46%, while the incubation with Lipofectamine™ alone did not have an impact on the p65 level. Summarized, the transfection of B cells with p65 siRNA and the subsequent downregulation of the protein expression is generally effective as seen for the Lipofectamine™-transfection, but the presence of the nanoparticles seems to impede this effect.

#### **4.1.5 Nanoparticles decorated with CD69-IgG for the targeting of T cells**

Since among all the investigated cellular players of inflammation, T cells exhibited the lowest internalization of undecorated NPs (Figure 5), hereto also specific targeting to enhance the uptake was attempted. As already shown for B cells, the used T cell line TK-1 also expressed CD69 on the cell surface, therefore the same antibody-decorated nanoparticles as for B cells were used for the targeting (Figure 13c).

Analogously to B cells, the nanoparticles decorated with anti-CD69 antibodies (CD69-NPs) exerted a higher concentration-dependent uptake capacity than SH-NPs (an intermediate product during synthesis before covalent binding of the antibodies) or undecorated NPs (Figure 13a). In contrast to B cells, this trend was seen for all investigated concentrations, as no uptake saturation was achieved. Interestingly, nanoparticles decorated with unspecific IgGh-antibodies (IgGh-NPs) were even internalized into T cells to a higher extent than CD69-NPs, which is similar to the findings in B cells. For all investigated types of nanoparticles, no significant impact on the cell viability was seen for all concentrations (Figure 13b).

## Results

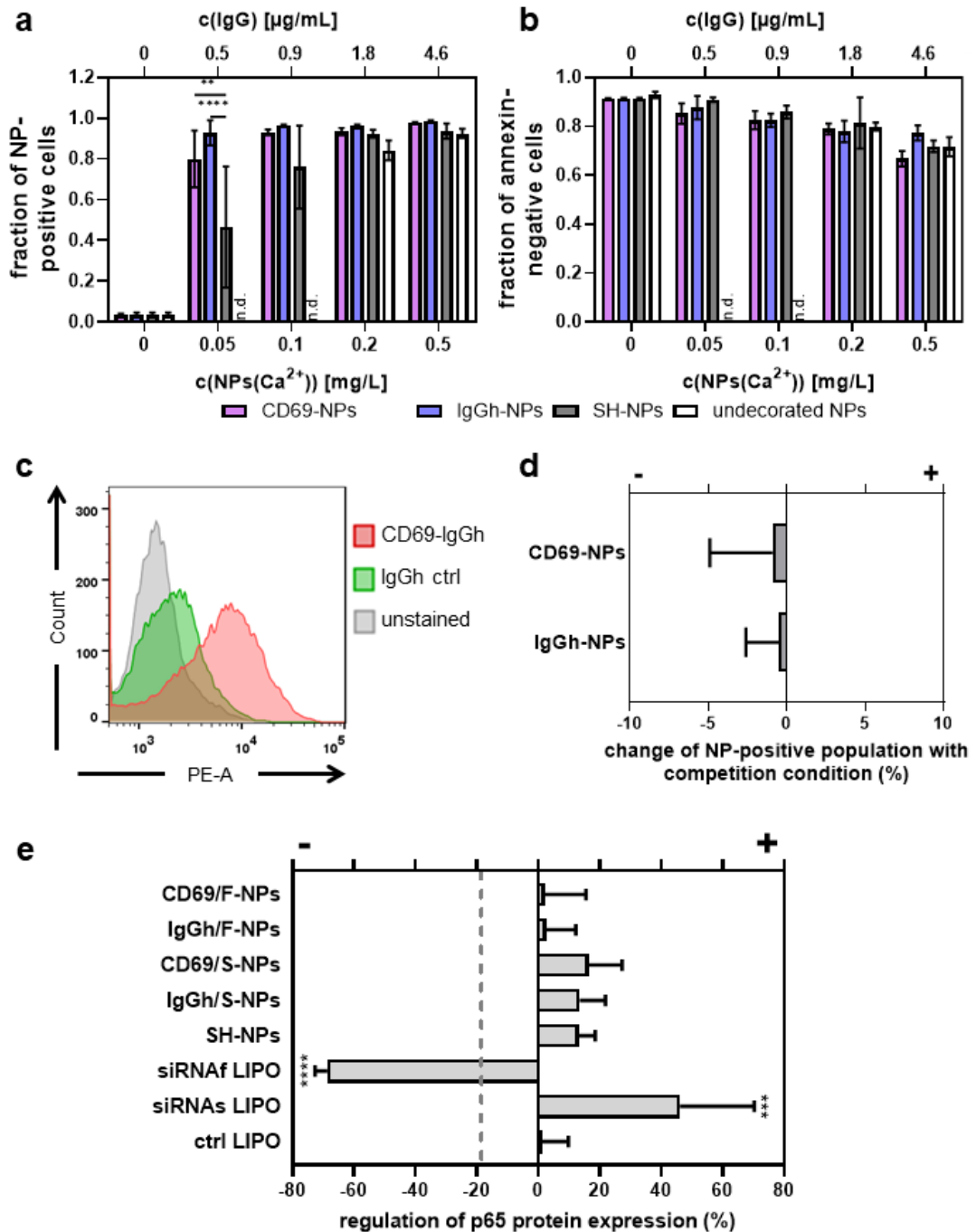


**Figure 12: Target-specific nanoparticles decorated with CD69-IgG (CD69-NPs) and their impact on B cells.** (a, b) Uptake (a) and cytotoxicity (b) of CD69-NPs in B cells. MOPC-315 cells were exposed to fluorescently labelled CD69-NPs, IgGh-NPs, SH-NPs, or undecorated NPs and incubated for 24 h prior to staining with annexin and flow cytometric analysis. Shown are the mean and SEM for 3 independent experiments. n.d.: not determined. (c) Expression of CD69 on the surface of B cells as target for CD69-decorated nanoparticles. Measurement by flow cytometry with unstained cells and isotype IgG as control. Shown is a representative image of 3 independent measurements. (d) Specific uptake of CD69-NPs measured by binding competition. MOPC-315 cells were incubated with IgG-NPs and 100x excess of free IgG. Shown is the change of uptake with competition condition with respect to non-competition measured by flow cytometry as mean and SEM from 3 independent experiments. (e) Potential of CD69-NPs with incorporated p65 siRNA to downregulate the p65 protein expression in inflamed B cells (stimulated with ODN-2006 and IL-4). LIPO: Lipofectamine™. The regulation was defined as the ratio of p65 expression with respect to the inflammatory condition (stimulated cells without nanoparticles) set to zero. The dashed lines depict the non-inflammatory condition. Shown is the mean and SEM of 3 independent experiments. Statistical difference between indicated groups or with respect to the control was tested using a two-way ANOVA with Tukey's post hoc test (\*\*  $p < 0.001$ , \*\*\*  $p < 0.001$ , \*\*\*\*  $p < 0.0001$ ).

Investigations concerning the specificity of uptake of CD69-NPs by creating a competition situation with an excess of unbound CD69-antibodies revealed a notable reduction of nanoparticle-positive population by 23% compared to control cells incubated only with the CD69-NPs (Figure 13d). For incubation with IgGh-NPs in presence of excess of unbound IgGh the reduction was less pronounced with 12%. Together, this proves that the enhanced uptake of antibody-decorated nanoparticles in T cells is at least in part due to specific binding to CD69 on the cell surface, even though binding of unspecific antibodies also had a distinct effect.

Moreover, the incubation of inflamed T cells with CD69-NPs carrying p65 siRNA (CD69/F-NPs) resulted in a small downregulation of the p65 protein expression by 5% with respect to the untreated inflamed condition (Figure 13e). Strikingly, the impact on the p65 expression was somewhat higher for IgGh-NPs carrying p65 siRNA (IgGh/F-NPs) with 12% to about the level of non-inflamed cells. Additionally, an even higher downregulation of 25% was measured after incubation with CD69-NPs carrying scrambled siRNA (CD69/S-NPs) and a small downregulation was also achieved for IgGh/S-NPs. In contrast, the exposure to SH-NPs, as control of the impact of the nanoparticles *per se*, resulted, by tendency, in an upregulation of p65 protein expression by 5%. Remarkably, the Lipofectamine™-mediated transfection with p65 siRNA as control for the transfection efficiency of the nanoparticles even increased the p65 expression by 14%. In contrast, the incubation with Lipofectamine™ and scrambled siRNA or Lipofectamine™ alone even had a negative impact on the p65 protein expression. Taken together, all nanoparticles carrying siRNA (independent of type of decoration or functionality of siRNA) were able to downregulate p65 protein expression to different extent in T cells, while nanoparticles without siRNA and transfection with Lipofectamine™ had no notable effect.



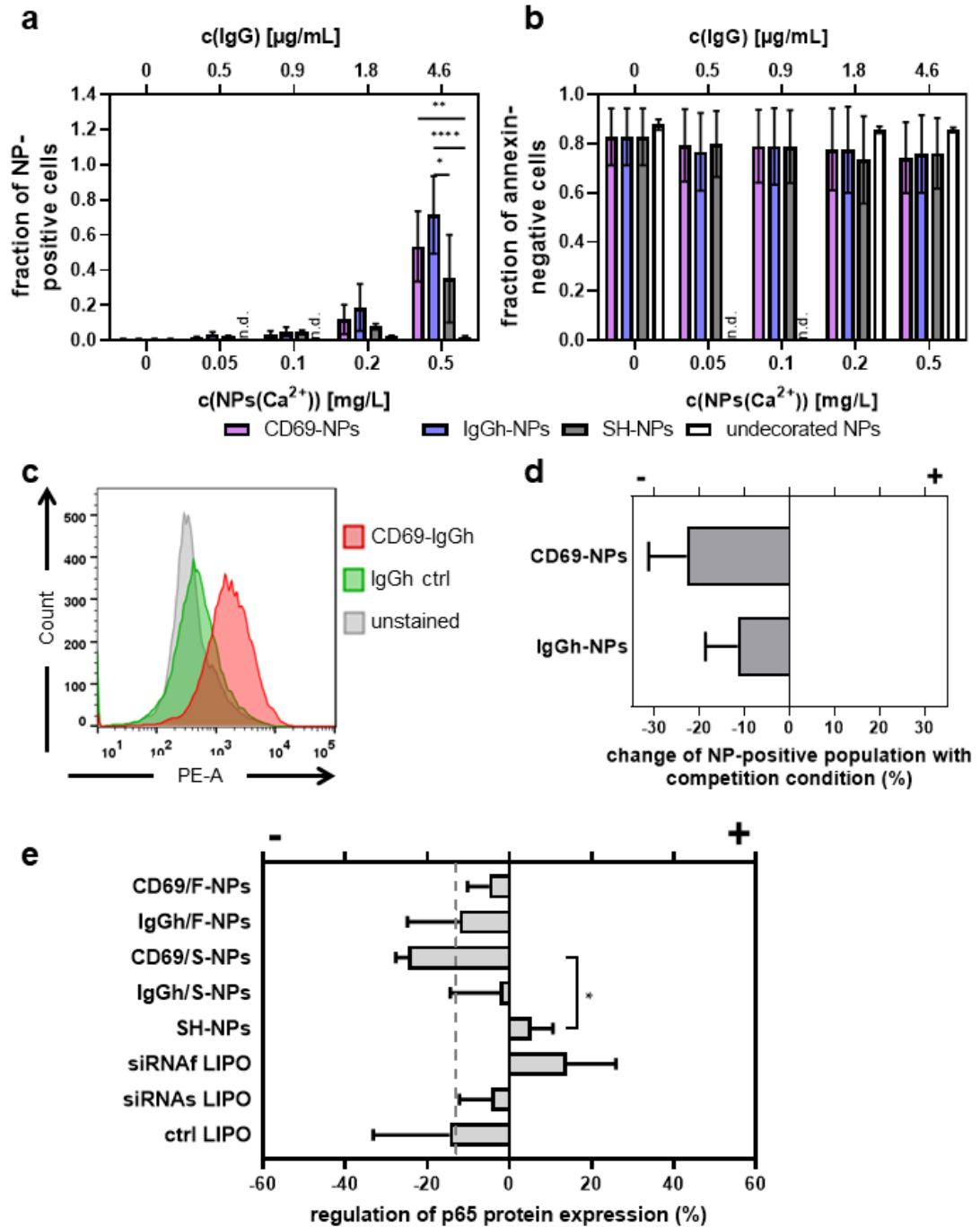


**Figure 13: Target-specific nanoparticles decorated with CD69-IgG (CD69-NPs) and their impact on T cells.** (a, b) Uptake (a) and cytotoxicity (b) of CD69-NPs in T cells. TK-1 cells were exposed to fluorescently labelled CD69-NPs, IgGh-NPs, SH-NPs, or undecorated NPs and incubated for 24 h prior to staining with annexin and flow cytometric analysis. Shown are the mean and SEM for 3 independent experiments. n.d.: not determined. (c) Expression of CD69 on the surface of T cells as target for CD69-decorated nanoparticles. Measurement by flow cytometry with unstained cells and isotype IgG as control. Shown is a representative image of 3 independent measurements. (d) Specific uptake of CD69-NPs measured by binding competition. TK-1 cells were incubated with IgG-NPs and 100x excess of free IgG. Shown is the change of uptake with competition condition with respect to non-competition measured by flow cytometry as mean and SEM from 3 independent experiments. (e) Potential of CD69-NPs with incorporated p65 siRNA to downregulate the p65 protein expression in inflamed T cells (stimulated with CD3 $\epsilon$  and CD28). LIPO: Lipofectamine™. The regulation was defined as the ratio of p65 expression with respect to the inflammatory condition (stimulated cells without nanoparticles) set to zero. The dashed lines depict the non-inflammatory condition. Shown is the mean and SEM of 3 independent experiments. Statistical difference between indicated groups or with respect to the control was tested using a two-way ANOVA with Tukey's post hoc test (\*  $p < 0.05$ , \*\*  $p < 0.001$ , \*\*\*\*  $p < 0.0001$ ).

## **4.2 Therapeutic efficiency of nanoparticles with p65 siRNA to ameliorate inflammation in a murine colitis model**

The preceding optimization of the murine colitis model rendered information about the optimal DSS dosage, the effective siRNA concentration as well as the ideal observation times for the further experiments.

The investigations concerning the therapeutic efficiency of the nanoparticles with functional siRNA (F-NPs) revealed an effective alleviation of the DSS-induced clinical features of colitis in mice. Furthermore, for short-term and long-term investigations (3 or 6 days after nanoparticle administration respectively), distinct effects of the F-NPs were found on the expression of inflammatory proteins in the colon as well as on the expression and secretion of inflammatory mediators in the colon and blood circulation.

### **4.2.1 Optimization of murine colitis model to study therapeutic efficiency of F-NPs**

The investigation for finding the optimal DSS dosage to induce colitis revealed an increased disease activity index (DAI), as a non-invasive measure of colitis severity, for all three DSS dosages up until day 8 (Figure A. 4a, see appendix on page 106). In this context, the dosage of 3.75% (w/v) DSS showed the most consistent development with a gradual steady increase. Furthermore, the measurement of the fecal inflammatory marker Lipocalin-2 (Lcn-2) revealed the most pronounced increase of inflammation for this concentration up to day 8 (Figure A. 4b, see appendix on page 106). Both parameters, DAI and fecal Lcn-2 level, were decreased at observation days 8 to 9, hinting to a naturally decreasing inflammation for longer observation periods after cessation of DSS-administration (day 6).

Taking these results into account, the optimal dosage of DSS to induce stable colitis in further experiments was set to 3.75% (w/v) due to the steadiest increase in inflammation without reaching harmful levels. Furthermore, day 9 was defined as the longest observation point due to the natural decrease of inflammation for longer time periods. Day 6 was specified for short-term investigations, since it represents the time point where the previous *in vitro* studies revealed a substantial impact of nanoparticles with p65 siRNA on the p65 protein expression for the main cellular players of inflammation. Finally, day 3 was determined as the optimal day for intravenous application of the nanoparticles since the DAI reached the value of 2. This value cannot be attributed to only slight weight loss, which can occur naturally during experiments, but is either caused by significant weight loss due to inflammation or signs of colonic inflammation due to loosening of the feces. Therefore, this time point represents the beginning of the severe colonic inflammation.

In the context of finding the optimal siRNA dosage, the most pronounced effect in the development of colitis, as measured using the DAI and fecal Lcn-2 level, was seen for 2.0 mg siRNA/ kg body weight (BW) with an attenuated increase of both parameters and a more pronounced decrease at the end of the observation time compared to the other tested concentrations (Figure A. 4c, d, see appendix on page 106). Therefore, this concentration was used for further investigations of the efficiency of the F-NPs.

### **4.2.2 Impact of F-NPs on the development of colonic inflammation**

Concerning the DAI as a non-invasive measure of colitis development, the treatment with F-NPs (group F) significantly attenuated the effect of DSS compared to the untreated colitis group (group C) (Figure 14). In detail, the DAI index for group C showed a steady escalation from day 3 onward with a maximum score of 6 at day 7, and a plateau after day 6. In contrast, the DAI from group F increased starting from day 3 with a maximal score of 4 at day 7, and afterwards the DAI even decreased to 2 on day 9. In comparison, the DAI of the healthy control group (group H) did not show an increase beyond the value of 1, showing that this index was not influenced by other factors than the colitis during the experiments.

Furthermore, the treatment with F-NPs markedly impacted the single scores of the DAI (Figure 14c, d, e). The weight loss of animals was most prominent for the groups C and F, compared to the healthy group, indicating the impact of colitis. For the feces consistency score as well as the rectal bleeding score, a significant difference between mice treated with F-NPs and untreated colitis animals could be shown. In detail, weak rectal bleeding in mice treated with F-NPs was only seen for 2 days, while for the control group C, stronger occurrence of rectal bleeding lasted for 4 days.

Moreover, the investigation of the fecal inflammation marker Lcn-2 revealed a lesser increase of the concentration for mice treated with F-NPs compared to the colitis group starting from day 4 (Figure 14b). In contrast, almost no Lcn-2 was detected in the healthy mice (group H).

The white blood cell count (WBC) was only slightly influenced by the colonic inflammation, especially on day 6, while the treatment with F-NPs somewhat impeded this effect (Figure A. 5, see appendix on page 107). The amount of lymphocytes and monocytes in the blood increased especially on day 6 for both group C and F compared to the healthy control. In contrast, for the platelet count, no trend could be seen due to the overall high deviations within the groups.

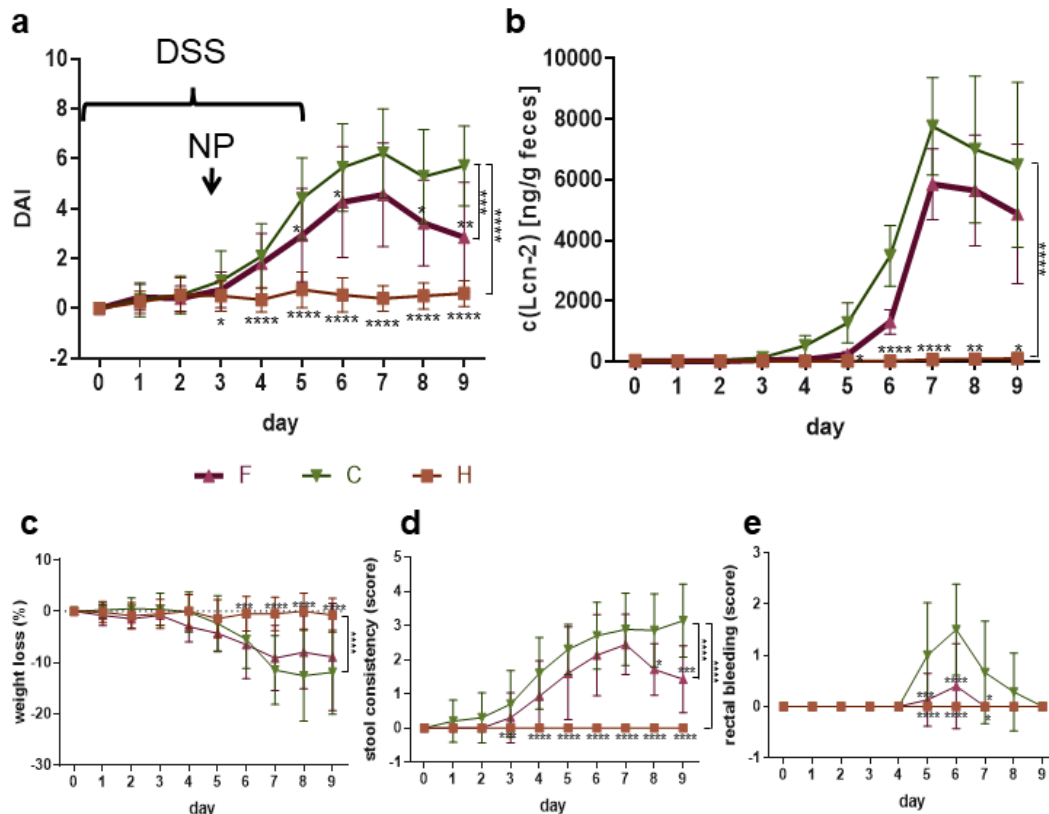


Figure 14: **Effects of siRNA-loaded nanoparticles (F-NPs) on the development of DSS-induced colitis in mice.** Mice were given 3.75% (w/v) DSS in drinking water for 6 days and F-NPs (2.0 mg siRNA/kg BW) were administered intravenously to the respective groups on day 3. F: F-NPs, colitis (n = 8 – 20); C: no nanoparticles, colitis (n = 7 – 20); H: no nanoparticles, healthy (n = 20). For detailed list of mouse counts, see Table A. 1 (appendix on page 107). Effects of NP-treatment on the DAI (a) and Lcn-2 levels in feces (b) were monitored for 9 days. (c - e) Effect of nanoparticle-treatment on the single parameters which form the DAI: (c) relative weight loss compared to initial body weight. (d) Score to quantify the feces consistency and (e) score to analyze the rectal bleeding. Shown is the mean with SD (SEM for (b)) for 7 – 20 mice. Total differences between indicated groups and differences for each day with respect to group C were tested using a generalized linear model with Wald-Chi-Quadrat pairwise comparisons and considered significant for  $p < 0.05$  (\*),  $p < 0.01$  (\*\*),  $p < 0.001$  (\*\*\*), and  $p < 0.0001$  (\*\*\*\*). DSS: dextran sulfate sodium. Lcn-2: Lipocalin-2.

#### 4.2.3 Short-term therapeutic efficiency of F-NPs in colitis (measured 72 h after treatment)

After 72 h (day 6), the treatment with F-NPs significantly ameliorated the inflammatory shortening of the colon to an average of 7.5 cm, compared to untreated mice (group C) with 6.3 cm, towards healthy mice with 8.6 cm (Figure 15a, b). Exemplary macroscopic images also revealed a thickening of the colon for the treatment with DSS.

Furthermore, the treatment with F-NPs significantly lowered the histopathologic changes evoked by the colitis at 72 h after treatment as demonstrated by the decrease in the histologic score from 5.4 for group C to 2.2 for group F (Figure 15c, d). Especially the crypt loss as a marker for colonic inflammation was decreased by the treatment with F-NPs compared to untreated mice as shown by exemplary microscopic images of the colon.

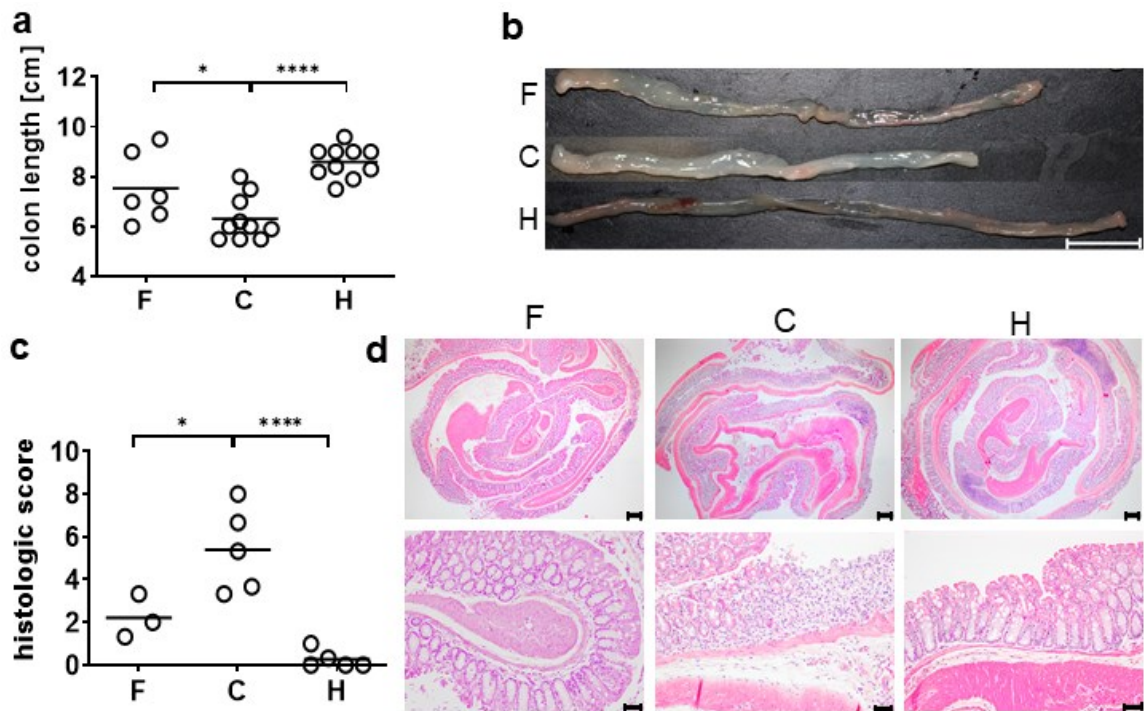


Figure 15: **Short-term changes of macroscopic and histopathologic features of colitis upon treatment with F-NPs.** Mice were given 3.75% (w/v) DSS in drinking water for 6 days and F-NPs (2.0 mg siRNA/kg BW) were administered intravenously to the respective groups on day 3. Investigations were performed 72 h later (day 6). F: F-NPs, colitis; C: no nanoparticles, colitis; H: no nanoparticles, healthy. (a) Colon length of all animals as single values and mean.  $n = 6 - 10$ . (b) representative images of colon length. Scale bar 2 cm. (c) histologic score for all groups. Shown are the single means for each animal scored from four blinded scientists as well as the mean from these means.  $n = 3 - 5$ . (d) representative images of histologic sections used for the scoring. Scale bar 200  $\mu\text{m}$  for upper panels, 50  $\mu\text{m}$  for lower panels. Statistical differences compared to control group C tested with an ANOVA and Dunnett-T (2-sided) post hoc test (\*  $p < 0.05$ ; \*\*\*\*  $p < 0.0001$ ).

Analysis of colonic leukocytes to visualize the direct impact of nanoparticles in inflammatory cells, revealed that treatment with F-NPs attenuated the DSS-mediated decrease of the p65 level, towards the level of healthy mice (Figure 16a). Phosphorylated I $\kappa$ B, as an indicator of the activation of the NF- $\kappa$ B signaling, was downregulated in leukocytes for the treatment with F-NPs compared to the untreated colitis group even beyond the non-inflamed level. For unphosphorylated I $\kappa$ B, which represents the active inhibitor of NF- $\kappa$ B, no change in the expression was found for mice treated with F-NPs compared to untreated mice, while the level of healthy mice was upregulated. In contrast, the level of iNOS, as a direct target of NF- $\kappa$ B-mediated regulation of gene expression and a pro-inflammatory mediator, was found to be upregulated for the treatment with F-NPs compared to the colitis group, while there was no change for healthy mice. Furthermore, COX-2 was investigated as another target of NF- $\kappa$ B transcriptional regulation and an inflammatory mediator, with the levels found to be downregulated both in NP-treated mice and the healthy group compared to mice with colitis. Moreover, the level of Bcl-2, as a major regulator of cell survival and apoptosis and a target of NF- $\kappa$ B, was slightly upregulated in animals treated with F-NPs compared to group C, and this effect was even more pronounced for the healthy control group.

In contrast, in whole colon tissue, as measure of indirect effects of the nanoparticles in the inflammatory region, the level of p65 was slightly upregulated in mice treated with F-NPs compared to untreated mice with colitis, while it was even downregulated in healthy mice (Figure 16b). Furthermore, phosphorylated I $\kappa$ B was severely and significantly upregulated in healthy mice compared to the colitis group, with the F-NP-treatment not having any effect, while the unphosphorylated protein was shown to be regulated reversely. Also, iNOS was found to be downregulated in mice treated with F-NPs and even more significantly for healthy mice compared to the colitis group. Moreover, the COX-2 and Bcl-2 expression was both upregulated in healthy mice compared to animals with colitis, while the treatment with F-NPs did not influence these proteins.

Furthermore, leukocytes were found to be only sparsely distributed in the colonic mucosa of healthy mice, while the induction of colitis substantially increased the amount of CD45-positive cells in the mucosa and submucosa coupled with crypt loss as already mentioned above (Figure 16d). In mice treated with F-NPs, less leukocytes were found in the colonic mucosa compared to the colitis group. The distribution of p65 was mostly limited to the mucosal crypt epithelium for all groups. Furthermore, I $\kappa$ B $\alpha$  was found to be localized primarily on the apical surface of the mucosal epithelium, especially in healthy mice and mice treated with F-NPs. The expression of COX-2 was rather less dominant and mostly located in the mucosa and submucosa.

Additionally, the treatment with F-NPs led to mostly unchanged or only slightly upregulated expression of inflammatory mediators in the whole colon tissue compared to mice with colitis (Figure 16c). In contrast, the expression of most of the mediators was downregulated in healthy mice compared to animals with colitis. Notably, IL-1 $\beta$  was highly and significantly upregulated in the whole colon for the treatment with F-NPs compared to the untreated group. Also, IFN- $\beta$  was only expressed in the healthy colon tissue, while the expression was depleted in mice with colitis independent of the treatment.

The secretion of cytokines from the colon tissue was predominantly negatively regulated or unchanged in F-NP-treated mice as well as healthy animals compared to the colitis group. Simultaneously, circulating cytokines in the blood plasma were mostly downregulated for the treatment with F-NPs compared to untreated mice, except for the level of IL-6, which was slightly upregulated. Accordingly, the cytokine expression in the blood plasma from healthy mice was downregulated, by tendency, compared to the colitis group.

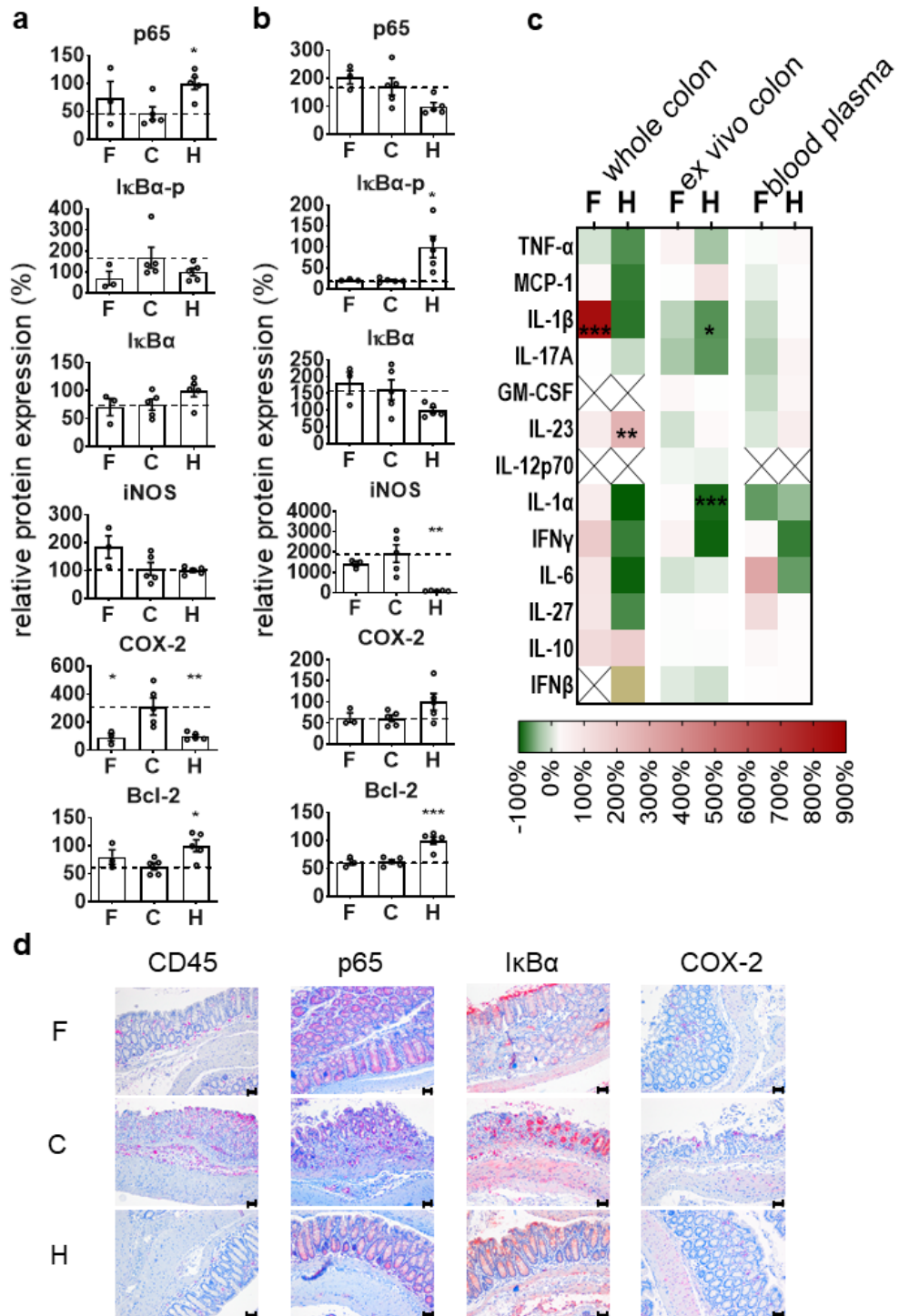


**Figure 16: Short-term impact of F-NPs on p65 NF-κB and related inflammatory mediators during colitis.** Mice were given 3.75% (w/v) DSS in drinking water for 6 days and F-NPs (2.0 mg siRNA/kg BW) were administered intravenously to the respective groups on day 3. Mice were sacrificed on day 6. F: F-NPs, colitis; C: no nanoparticles, colitis; H: no nanoparticles, healthy. (a, b) Protein expression in colonic leukocytes (CD45<sup>+</sup> cells) (a) and whole colon tissue (b). Protein expression was related to group H. Shown is the mean with values for each individual (n = 3 – 5). (c) Expression of inflammatory mediators in whole colon tissue, ex vivo cultivated colon tissue and blood plasma. Heat map showing the relative expression compared to mice with colitis (C). Red (scale): upregulation; green (scale): downregulation; X: cytokine level below detection threshold; brown: new expression. Mean of the groups with n = 3 – 10. (d) Representative images of colonic tissue slides stained for p65, IκB, INOS, COX-2 and Bcl-2. Scale bar 50 μm. Statistical differences compared to control group C tested with an ANOVA and Dunnett-T (2-sided) post hoc test (\* p < 0.05; \*\* p < 0.01, \*\*\* p < 0.001).

#### 4.2.4 Long-term therapeutic efficiency of F-NPs in colitis

The investigation of the long-term efficiency of F-NPs revealed a recovery of the colon length for mice treated with F-NPs compared to untreated mice, with an average of 7.3 cm compared to 6.8 cm (Figure 17a, b). The images of representative colon pieces for each group again revealed a thickening of the colon after treatment with DSS to induce colitis.

Moreover, treating the mice with F-NPs also reduced the histopathologic changes evoked by the colonic inflammation, by decreasing the histologic score from 7.1 to 5.4 (Figure 17c, d). Again, the main impact of the treatment with F-NPs was visible for the total crypt loss, as shown in the representative histological cross sections.

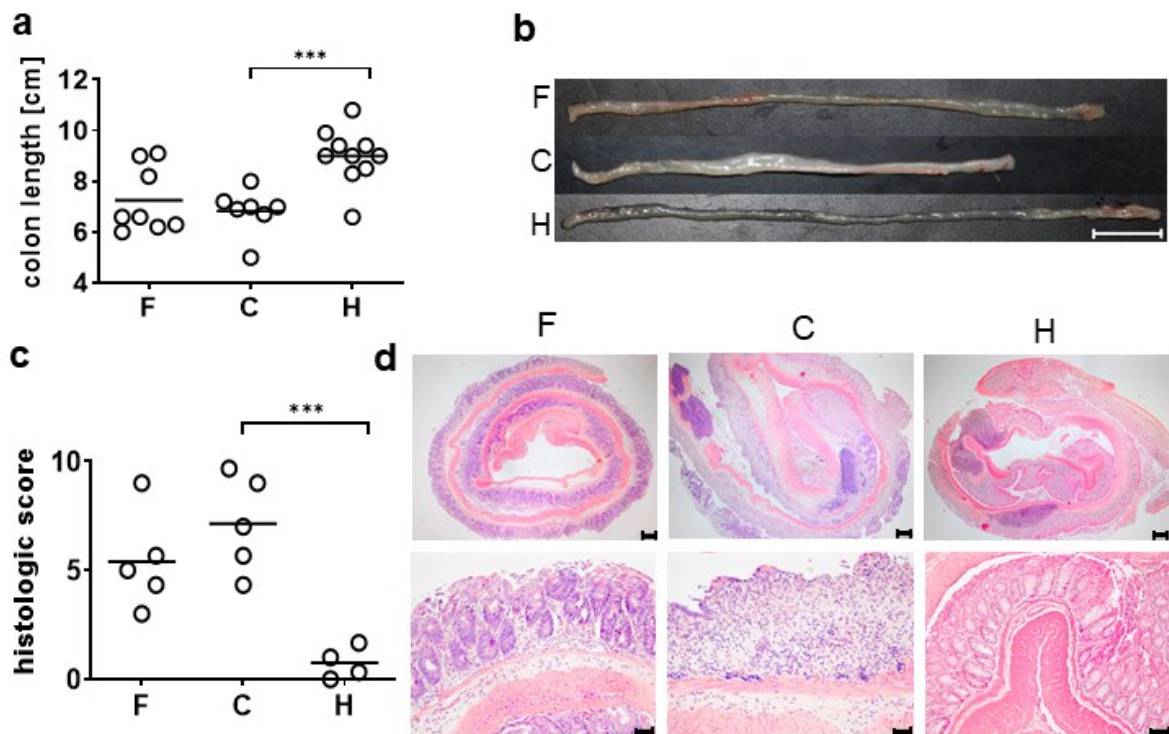


Figure 17: **Long-term changes of macroscopic and histopathologic features of colitis upon treatment with F-NPs.** Mice were given 3.75% (w/v) DSS in drinking water for 6 days and F-NPs (2.0 mg siRNA/kg BW) were administered intravenously to the respective groups on day 3. Investigations were performed six days later (day 9). F: F-NPs, colitis; C: no nanoparticles, colitis; H: no nanoparticles, healthy. (a) Colon length of all animals as single values and mean.  $n = 7 - 10$ . (b) representative images of colon length. Scale bar 2 cm. (c) histologic score for all groups. Shown are the single means for each animal scored from four blinded scientists as well as the mean from these means.  $n = 4 - 5$ . (d) representative images of histologic sections used for the scoring. Scale bar 200  $\mu\text{m}$  for upper panels, 50  $\mu\text{m}$  for lower panels. Statistical differences compared to control group C tested with an ANOVA and Dunnett-T (2-sided) post hoc test (\*\* $p < 0.001$ ).

In contrast to the short-term findings, on day 9 the protein expression of p65, as indicator of long-term therapeutic outcome, was downregulated in mice treated with F-NPs compared to the colitis group, towards the level of healthy mice (Figure 18a). In contrary, no significant change was seen for the level of phosphorylated I $\kappa$ B, as an indicator of the activation of the NF- $\kappa$ B signaling, for the treatment with F-NPs compared to untreated mice, while the level



in healthy animals was significantly higher. Moreover, the analysis of the expression of unphosphorylated I $\kappa$ B, the active form of the inhibitor, revealed a downregulation in mice treated with F-NPs compared to the colitis group towards the healthy level. Furthermore, the iNOS expression was substantially downregulated for the treatment with F-NPs compared to untreated mice towards the healthy level. Finally, no notable changes were found in the expression of COX-2 and Bcl-2 for all groups.

Additional immunohistological studies further highlighted that the expression of p65 in the healthy colon and after treatment with F-NPs was mainly found in the mucosa layer associated with goblet cells (Figure 18c). Due to the crypt loss seen in the colitis group, the distribution of p65 in the damaged mucosa was more diffuse.

Furthermore, in the whole colon tissue, the expression of most cytokines (e.g., TNF- $\alpha$ , IFN- $\gamma$  or IL-1 $\alpha/\beta$ ) was downregulated after treatment with F-NPs compared to the colitis group, and a comparable regulation was found for healthy mice (Figure 18b). Interestingly, IL-6 levels were upregulated in mice treated with F-NPs compared to untreated animals, while it was even downregulated for the healthy group. In contrast, the colonic expression of the cytokines IL-10 and IFN- $\beta$  were either unchanged or upregulated for both groups compared to mice with colitis. Notably, IL-23 levels were upregulated for both groups compared to group C.

The secretion of cytokines from the colon was generally downregulated in healthy mice compared to the colitis group. Similarly, the treatment with F-NPs showed comparable effect for most cytokines (e.g., IL-17A, IFN- $\gamma$ , IL27), with exception of GM-CSF and IL-23, which were upregulated. Strikingly, IL-1 $\alpha$  levels were only upregulated for mice treated with F-NPs.

Circulating levels of cytokines in the blood plasma were mostly downregulated in healthy mice compared to the colitis group, except for IL-1 $\alpha$ , which was strongly upregulated. Treatment with F-NPs led to enhanced circulatory levels for most inflammatory mediators (e.g., GM-CSF, IL-23, IL-1 $\alpha$ ). Interestingly, IL-10 levels were found to be lower after treatment with F-NPs compared to group C. Furthermore, IL-1 $\alpha$  was upregulated for all groups compared to mice with colitis.

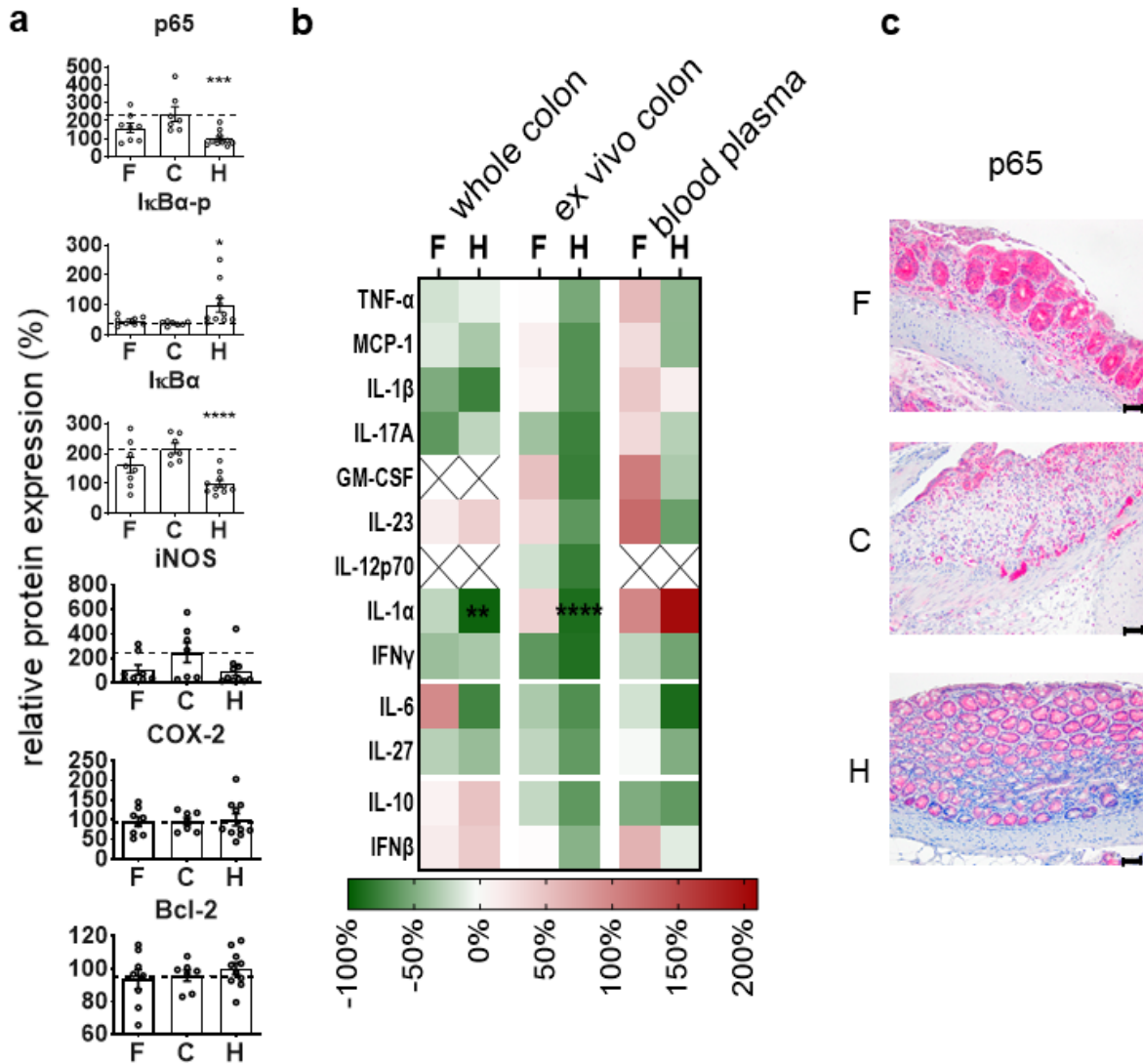


Figure 18: **Long-term impact of F-NPs on p65 NF-κB and related inflammatory mediators during colitis.** Mice were given 3.75% (w/v) DSS in drinking water for 6 days and F-NPs (2.0 mg siRNA/kg BW) were administered intravenously to the respective groups on day 3. Mice were sacrificed on day 9. F: F-NPs, colitis; C: no nanoparticles, colitis; H: no nanoparticles, healthy. (a) Protein expression in whole colon tissue. Expression was related to group H. Shown is the mean with values for each individual (n = 7 – 10). (b) Expression of inflammatory mediators in whole colon tissue, ex vivo cultivated colon tissue and blood plasma. Heat map showing the relative expression compared to mice with colitis (C). Red (scale): upregulation; green (scale): downregulation; X: cytokine level below detection threshold. Mean of n = 7 – 10. (c) Representative images of colonic tissue slides stained for p65. Scale bar 50 μm. Statistical differences compared to control group C tested with an ANOVA and Dunnett-T (2-sided) post hoc test (\*\* p < 0.01, \*\*\* p < 0.001; \*\*\*\* p < 0.0001).

### 4.3 Biodistribution of nanoparticles and side effects

Investigations concerning changes in the biodistribution of nanoparticles in the presence of colonic inflammation showed lower amounts of nanoparticles in spleen, liver, uterine tube, and uterus for mice with colitis compared to healthy mice after 3 h (Figure 19). In contrast, the presence of inflammation increased the nanoparticle accumulation in muscle, lung, small intestine, and especially in the appendix. These results highlight the fact that the

## Results

presence of local inflammation clearly affected the systemic distribution of the intravenously injected nanoparticles.

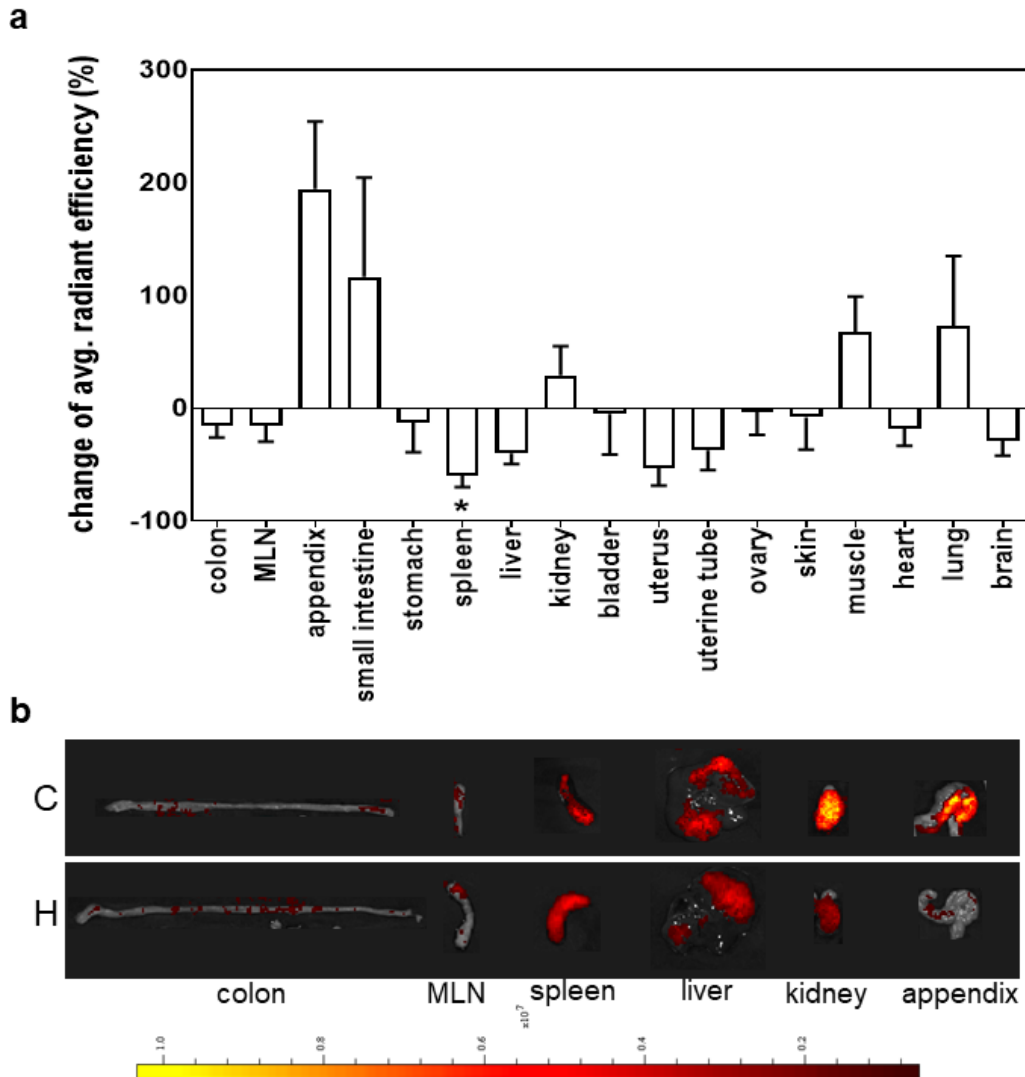


Figure 19: **Biodistribution of nanoparticles in mice with colitis compared to healthy mice.** Mice either received 3.75% (w/v) DSS in the drinking water or normal drinking water starting from day 0. On day 3, nanoparticles (2.6 mg Ca<sup>2+</sup>/ kg BW) were injected intravenously and after 3 hours mice were sacrificed. Organs were analyzed for the nanoparticle fluorescence intensity (Dy-734). (a) The change of average radiant efficiency for each organ in the colitis group was calculated with respect to healthy mice (set to zero). Shown is the mean with SEM for n = 10. (b) representative fluorescence images of colon, MLN, spleen, liver, kidney, and appendix for colitis group (C) and healthy group (H) with color scale for avg. radiant efficiency [p/s/cm<sup>2</sup>/sr] / [ $\mu$ W/cm<sup>2</sup>]. Statistical differences between groups tested with an ANOVA and Dunnett-T (2-sided) post hoc test (\* p < 0.05).

The analysis of the effects of the cargo siRNA *per se* by treating diseased mice with nanoparticles containing unspecific, scrambled siRNA (S-NPs) revealed no significant changes in the DAI, weight loss, colon length, or spleen weight, as indicators of the impact on the local inflammation, compared to mice treated with the p65-specific F-NPs (Figure 20a). Notably, the histological score as a measure for the extent of colonic

inflammation was even further decreased for the treatment with S-NPs compared to F-NPs. Furthermore, the p65 protein level, as direct target for the specific siRNA, was also even further reduced in mice treated with S-NPs with respect to F-NPs (Figure 20b). Treatment with S-NPs slightly increased the level of I $\kappa$ B $\alpha$  as an indicator of the activation of NF- $\kappa$ B signaling, compared to F-NPs, while the unphosphorylated protein, which represents the active inhibitor of NF- $\kappa$ B, was reversely regulated. As direct targets for NF- $\kappa$ B-mediated transcriptional activation and pro-inflammatory mediators, the level of iNOS was decreased for treatment with S-NPs compared to F-NPs, while there was no change for COX-2 and Bcl-2. Moreover, the expression of the inflammatory mediators TNF- $\alpha$ , IL-17A, IL-23, IL27, and IL-10 in the whole colon tissue was upregulated for mice treated with S-NPs compared to F-NPs, while IL-1 $\beta$ , IL-1 $\alpha$ , IL-6 and IFN- $\beta$  were downregulated by tendency (Figure 20c). Simultaneously, the secretion of inflammatory mediators in the blood plasma was found to be mostly downregulated for the treatment with S-NPs, except for IL-10, which was upregulated. Taken together, these results reveal the impact of nanoparticles on the colonic inflammation independent of the functionality of the incorporated siRNA. S-NPs even showed more favorable effects on the inflammation for some investigated factors compared to the nanoparticles carrying the functional p65 siRNA.

The assessment of potential side-effects of F-NPs revealed that neither the body weight, the feces consistency nor the rectal bleeding, as summarized by the DAI as general indicator for colonic inflammation, was influenced by the presence of F-NPs in healthy mice compared to untreated mice (Figure 21a). Moreover, the treatment with F-NPs did not have an impact on the colon length or spleen weight on day 9 as further indicators of inflammatory processes. Furthermore, no changes in the expression of p65 (as direct target of F-NPs), phosphorylated I $\kappa$ B $\alpha$  (indicating the activation of NF- $\kappa$ B), and unphosphorylated I $\kappa$ B $\alpha$  (active inhibitor of NF- $\kappa$ B) were detected for the treatment of healthy mice with F-NPs compared to the untreated healthy group (Figure 21b). Concerning the already previously investigated inflammatory proteins and direct targets of NF- $\kappa$ B-mediated transcriptional regulation, the iNOS expression was downregulation for the treatment with F-NPs, while COX-2 and Bcl-2 were slightly upregulated compared to untreated, healthy mice. Additionally, in the colon tissue, treatment of healthy mice with F-NPs mostly resulted in the unchanged or decreased expression of inflammatory mediators compared to the untreated group (Figure 21c). In contrast, levels of circulating cytokines, especially IL-27, in the blood plasma were upregulated after injection of F-NPs compared to untreated mice.

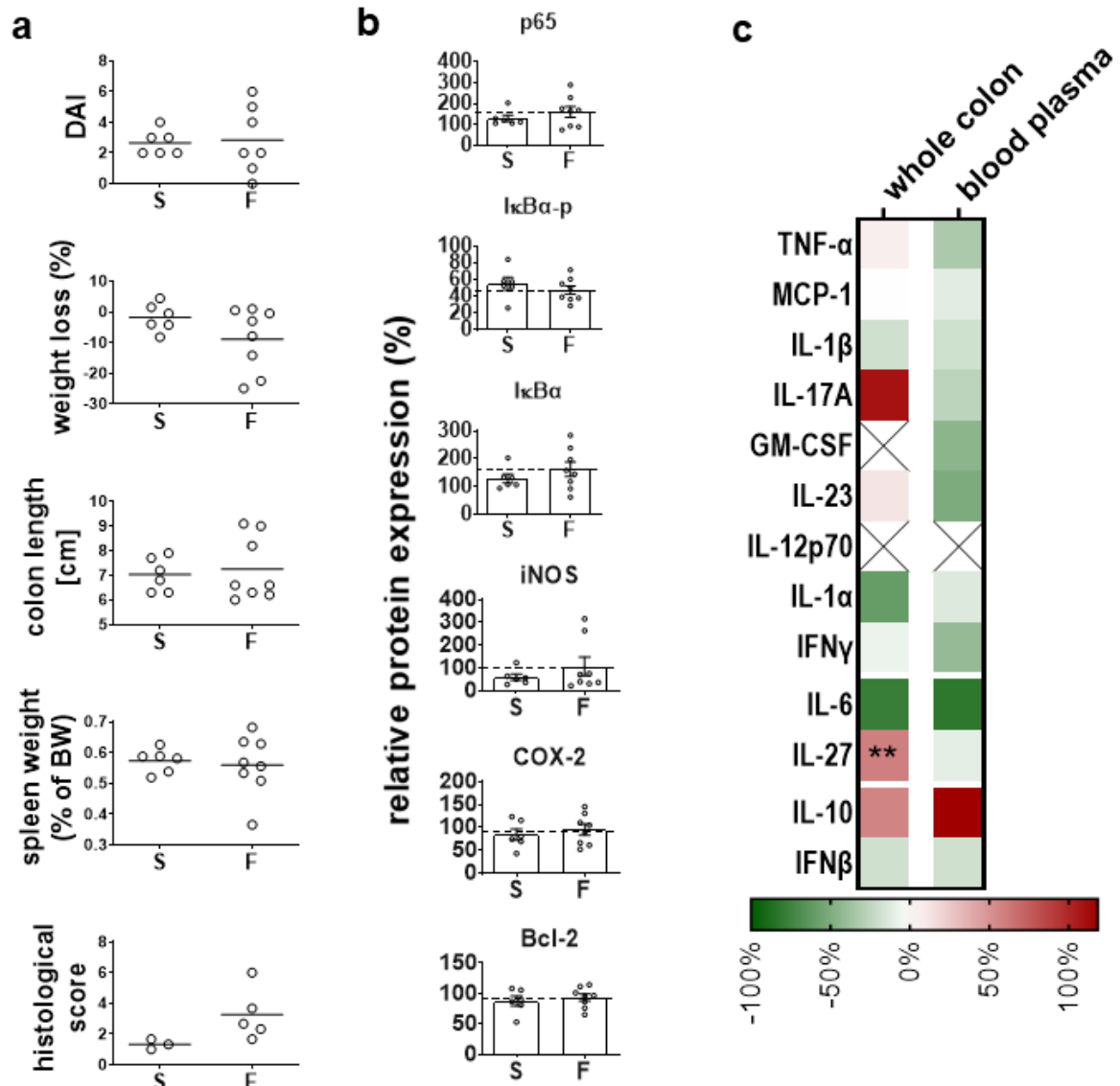


Figure 20: **Side-effects depending on the type of siRNA incorporated into the nanoparticles.** Nanoparticles (2.0 mg siRNA/kg BW) were administered intravenously to the respective groups on day 3. Mice were sacrificed on day 9. S: S-NPs, colitis; F: F-NPs, colitis. (a) Impact of the nanoparticles in healthy mice on parameters used to quantify the colonic inflammation (DAI, body weight, colon length, spleen weight and histologic score).  $n = 6 - 8$  (histological score  $n = 3 - 5$ ). (b) Protein expression of p65, IκB, iNOS, COX-2, and Bcl-2 in whole colon tissue. Expression was related to group H (see Figure 18). Shown is the mean with values for each individual ( $n = 6 - 8$ ). (c) Expression of inflammatory mediators in whole colon tissue, and blood plasma. Heat map showing the relative expression in mice with S-NPs (S) compared to mice with F-NPs (F). Red (scale): upregulation; green (scale): downregulation; X: cytokine level below detection threshold. Mean of the groups with  $n = 6 - 8$ . Statistical differences between groups tested with an ANOVA and Dunnett-T (2-sided) post hoc test (\*\*  $p < 0.01$ ).

Summarized, these results show that F-NPs indeed have no notable impact in healthy mice concerning the inflammatory parameters that were used to study the therapeutic efficiency of these nanoparticles. Nonetheless, during all above mentioned investigations, some mice suffered fatal adverse effects after intravenous injection of the nanoparticles that were independent of the inflammation status of the animals and the type of nanoparticles administered (Table A. 1, Table A. 2, Table A. 3, see appendix on pages 107 – 108).

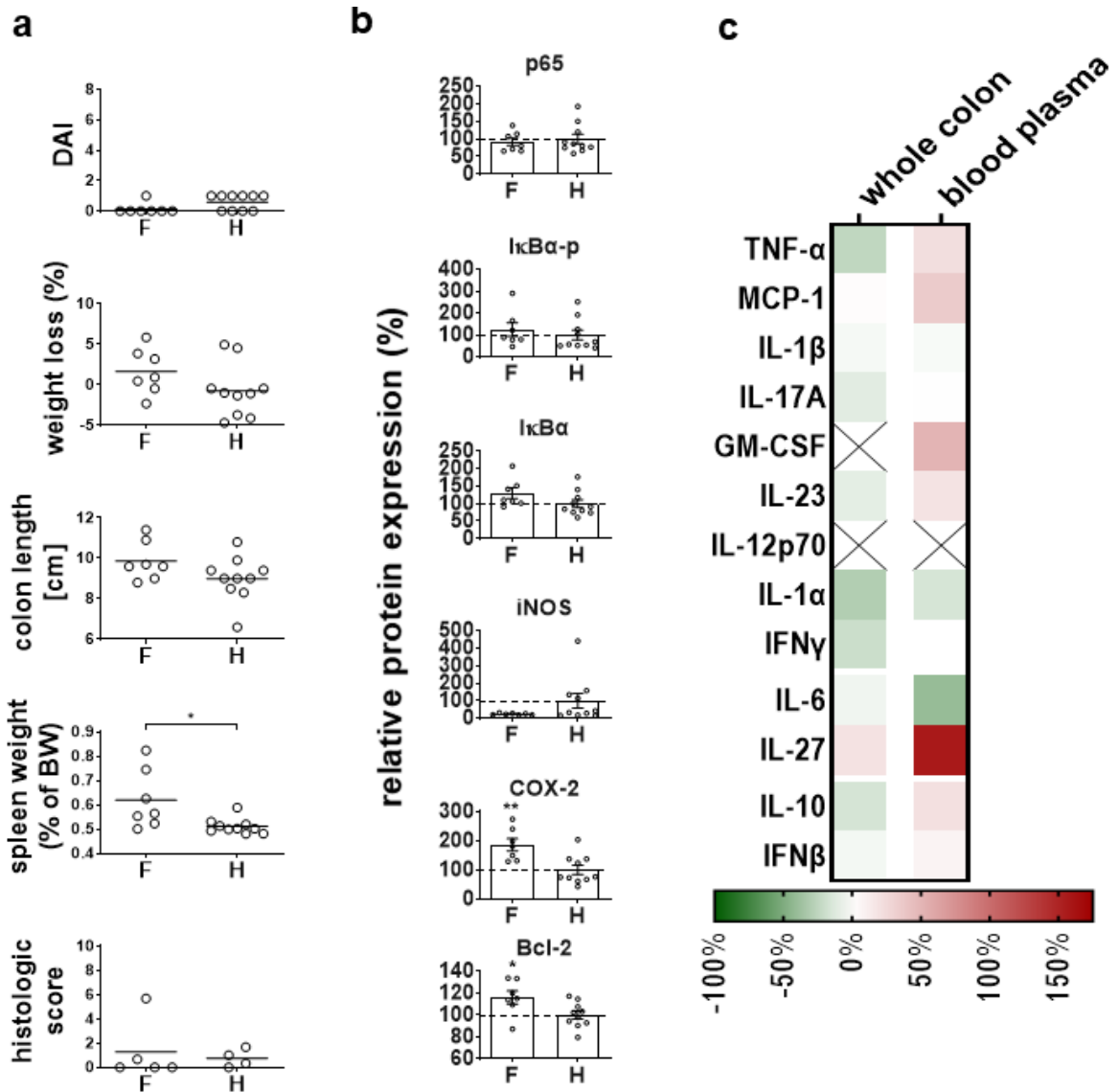


Figure 21: **Side-effects of F-NPs on inflammatory processes in healthy mice.** F-NPs (2.0 mg siRNA/kg BW) were administered intravenously to the respective groups on day 3. Mice were sacrificed on day 9. F: F-NPs, healthy; H: no nanoparticles, healthy. (a) Impact of the nanoparticles in healthy mice on parameters used to quantify the colonic inflammation (DAI, body weight, feces consistency, rectal bleeding, colon length and spleen weight).  $n = 7 - 10$  (histological score  $n = 4 - 5$ ). (b) Protein expression of p65, IκB, INOS, COX-2, and Bcl-2 in whole colon tissue. Expression was related to group H. Shown is the mean with values for each individual ( $n = 7 - 10$ ). (c) Expression of inflammatory mediators in whole colon tissue, ex vivo cultivated colon tissue and blood plasma. Heat map showing the relative expression compared to mice without nanoparticles compared to mice without nanoparticles (H). Red (scale): upregulation; green (scale): downregulation; X: cytokine level below detection threshold. Mean of the groups with  $n = 7 - 10$ . Statistical differences between groups tested with an ANOVA and Dunnett-T (2-sided) post hoc test (\*  $p < 0.05$ , \*\*  $p < 0.01$ ).

## 5 Discussion

In this study, it was shown that the nanoparticles were internalized into key cellular players of inflammation, and specific decoration even increased the uptake in some cell types. The nanoparticle internalization process was proven to be energy-dependent, and the cargo was found to be localized in the cytoplasm after uptake. The efficiency of siRNA-nanoparticles to downregulate p65 expression was dependent on the tested cell types. Investigations concerning the therapeutic efficiency in a murine colitis model revealed a clear amelioration of local inflammation after i.v. treatment with nanoparticles carrying p65 siRNA (F-NPs) with a distinct impact on the inflammatory signaling in the colon. The biodistribution of nanoparticles was clearly influenced by the local colonic inflammation. No notable off-target effects of F-NPs were found in the colon, while nanoparticles carrying non-functional, scrambled siRNA (S-NPs) also showed a distinct effect on the colonic inflammation.

### 5.1 Nanoparticles with functional siRNA and their impact on the p65 expression and inflammatory process in cellular players of inflammation

#### 5.1.1 Internalization of nanoparticles in the cellular players of inflammation

In general, the uptake of undecorated calcium phosphate nanoparticles (NPs) in the investigated key cellular players of inflammation was found to be dependent of the type of cells. Monocytes showed the highest uptake capacity, endothelial cells (ECs) and B cells exhibited intermediate internalization rates, while the uptake in T cells was very low. For all cell types the uptake was found to be dependent on the nanoparticle-concentration. Furthermore, the nanoparticle formulation was cytocompatible in all cell lines at least for the concentrations used in this study.

In detail, monocytes showed the highest whole population- as well as single cell nanoparticle uptake capacity of all investigated cell types. As a part of the mononuclear phagocytic system, monocytes/ macrophages recognize nanoparticles, which have been previously opsonized by the adsorption of blood serum components on the nanoparticles' surface (Mortimer *et al.* 2014, Hume 2006). Therefore, after injection of the nanoparticles into the blood stream, monocytes are expected to be the main cell type for the uptake and subsequent regulation of inflammatory processes via the downregulation of p65.

Moreover, endothelial cells showed distinct nanoparticle-uptake capacity, in the whole cell population as well as for single cells. Although ECs are generally non-phagocytic cells, they

are capable of internalizing foreign particles (Voigt *et al.* 2014, Landgraf *et al.* 2015). Therefore, ECs are also a good target for p65 downregulation via nanoparticles, since they play an important role in mediating inflammatory processes, especially in vascular diseases. Similarly, B cells also exhibited a good whole population-, and single cell nanoparticle uptake capacity. Since this cell type is known to be capable of endocytosis, especially of ligand-receptor complexes for ligand presentation to T cells (Zilker *et al.* 2017, Malhotra *et al.* 2009), a similar uptake process is proposed for the nanoparticles (Sokolova *et al.* 2010, Sokolova *et al.* 2013).

In contrast, for T cells no distinct accumulation of nanoparticles was measured. Therefore, this cell types will hardly be a target for the nanoparticle-based downregulation of p65 in inflammation processes.

In this context, especially for the T cells where the nanoparticle-uptake was very low, specific targeting with the nanoparticles can be attempted to enhance the cellular uptake, for example by decoration with specific antibodies against surface moieties on the target cells.

This study revealed that nanoparticles decorated with unspecific, xenogeneic IgG (Armenian hamster) were better internalized into all tested immune cell types compared to allogeneic IgG-NPs. Neither xenogeneic nor allogeneic IgG-NPs showed cytotoxic effects compared to undecorated NPs. In the view of this finding, it is reasonable to suggest that the enhanced uptake of targeted antibodies found in previous studies might also have been influenced by this species-dependent effect and not only by specific binding (Ivanova *et al.* 2021, Lee *et al.* 2021a, Lourenco *et al.* 2021, Notabi *et al.* 2021).

With consideration of this found species-dependent uptake of IgG-NPs, the mechanism involved in this internalization might be dependent on the formation of antibody aggregates. The uptake of soluble antibodies, especially after aggregation, was found to be mediated by MHCII recognition in B cells, and by non-specific uptake of foreign antigens by antigen-presenting cells and other cell types (Daha *et al.* 1982, Cheng *et al.* 1999). Therefore, it can be expected that the herein seen results are based on these uptake mechanisms seen for antibody aggregates, especially since antibodies immobilized on the NP-surface might simulate aggregate formation due to their proximity.

Nonetheless, also an unwanted activation of proinflammatory pathways, for example via the generation of anti-drug-antibodies associated with the recognition of foreign antigens, might occur. This in turn might lead to severe, life-threatening adverse effects which mitigate the positive effects of NP-decoration with xenogeneic antibodies.



A potential future strategy for the application of siRNA-nanoparticles might involve the decoration with very small doses of xenogeneic IgG as “subliminal baits” for immune cells while avoiding adverse effects. This strategy would increase the intracellular availability of siRNA in the cytoplasm of specific immune cells.

Interestingly, the presence of allogeneic IgG even masked the nanoparticles, thereby preventing the uptake compared to undecorated NPs. This effect renders a potential strategy to ensure longer circulation times by decoration with allogeneic IgG, which increases the contact time of nanoparticles with the target tissue and in turn might enhance the targeting efficiency (Yoo *et al.* 2010).

With consideration of the lower uptake of NPs in ECs, B cells and T cells compared to monocytes, a specific targeting of these cell lines with decorated nanoparticles is attempted to enhance the internalization.

On that account, in B cells an enhanced uptake of nanoparticles decorated with CD69-IgGh compared to undecorated NPs was demonstrated. CD69 was found to be expressed on the surface of B cells, and as a marker for early activated leukocytes it represents a good target for decorated nanoparticles (Cibrian and Sanchez-Madrid 2017). However, competition of binding with excess free CD69-IgGh revealed no notable decrease in the uptake of CD69-NPs. Taken together, these results indicate that the enhanced uptake of CD69-NPs is not caused by specific binding of CD69 and the antibody.

Interestingly, for the B cells an even stronger internalization of nanoparticles decorated with unspecific IgGh (isotype control) was seen compared to the specific CD69-NPs. Further competition experiments with excess free unspecific IgG indicated that the accumulation of IgGh-NPs in cells is mostly independent of FcγR binding. All together, these results suggest that the enhanced uptake of IgGh-NPs in B cells is mostly due to unspecific interactions with the antibody from xenogeneic species (as already discussed above) and further due to unspecific endocytosis or recognition by the B cell receptor and the MHCII antigen presentation pathway (Adler *et al.* 2017).

Moreover, in T cells also a marked increase in cellular uptake of nanoparticles decorated with CD69-IgGh was found compared to undecorated NPs. Nevertheless, this stronger internalization was still distinctively lower than in the other immune cell lines in this study. Considering the expression of CD69 on the surface of T cells, CD69 is suggested to be a good target for specific decorated nanoparticles. Nonetheless, competition with excess free CD69-IgG revealed that the IgG-mediated nanoparticle-binding was only in small parts specific for CD69. Since the receptor CD69 is internalized upon binding, specific binding to

CD69 might aid the nanoparticle internalization into the cells (Cibrian and Sanchez-Madrid 2017).

Remarkably, the uptake of nanoparticles decorated with unspecific IgGh was even higher than that of specific CD69-NPs in T cells, and the competition with free unspecific IgGh showed a weak specificity for IgG-mediated accumulation. All in all, these results indicate that nanoparticles decorated with antibodies are internalized into T cells to small parts mediated by Fc $\gamma$ R, though T cells express this receptor only during narrow window following the activation by T cell receptor signaling (Sandor and Lynch 1993). The nanoparticle accumulation is expected to be mostly non-specific, either by membrane invagination, receptor-mediated endocytosis, or due to unspecific interactions with the antibodies from xenogeneic species as discussed above.

Furthermore, in endothelial cells, nanoparticles decorated with the peptide cRGDfK were internalized to a higher extent than undecorated NPs. In this context, the EC cell line SVEC4-10 was shown to express integrin  $\alpha_v$  as a target for the peptide cRGDfK, which enables the specific targeting by RGD-NPs (Temming *et al.* 2006, Barczyk *et al.* 2010). This enhanced uptake was found to be, at least in parts, due to the specific binding of the RGD-peptide to integrin on the surface of the cells. Nonetheless some other unspecific internalization mechanisms are likely involved in the increased uptake of RGD-NPs in ECs.

Summarized, the targeting using different decorated nanoparticles markedly enhanced the uptake in all target cells to a different extent. Despite this, in B cells and T cells the enhanced internalization was not specific for the targeting moieties, but it generally increased with the presence of xenogeneic IgG on the surface of the nanoparticles.

On that account, the targeting was, especially for ECs and B cells, only effective for low nanoparticle-concentrations since higher concentrations led to saturation of the uptake, independently of the decoration of the nanoparticles. Nonetheless, the specific decoration is expected to have positive effects on the uptake in target cells for *in vivo* applications, since the concentration after systemic injection of the nanoparticles will be lower than that used for *in vitro* experiments.

### 5.1.2 Internalization mechanism of nanoparticles

A prerequisite for the application of calcium phosphate nanoparticles as transfection agents for siRNA molecules is the internalization of the nanoparticles into the target cells. In this context, results from this study indicated a high contribution of energy-dependent mechanisms in monocytes, and to a lower extent of processes related to phagocytosis and clathrin-mediated endocytosis.

In detail, nanoparticle internalization was affected by its inhibition with cytochalasin, which influences the actin depolymerization that plays a critical role for the adsorptive and fluid phase phagocytic and endocytic events (Gottlieb *et al.* 1993, Lamaze *et al.* 1997). Furthermore, inhibition with chlorpromazine showed distinct effects on the NP-uptake, where it reduces the presence of clathrin on the cell surface which decreases its availability for clathrin-mediated endocytosis (Vercauteren *et al.* 2010, Wang *et al.* 1993, Dutta and Donaldson 2012). Moreover, the effect of wortmannin in decreasing the uptake of nanoparticles can be attributed to the blockade of constitutive and stimulated micropinocytosis and phagocytosis (Ivanov 2008, Araki *et al.* 1996).

Overall, the observed mechanism for nanoparticle uptake in monocytes agrees well with the known size dependency of internalization processes (Foroozandeh and Aziz 2018). Besides this, previous studies suggest the reliance of the nanoparticle-uptake on the nanoparticle charge and also on the cell lines and its respective uptake characteristics (Sokolova *et al.* 2013, Rotan *et al.* 2017, Kollenda *et al.* 2020, Kopp *et al.* 2018).

Nonetheless, the internalization of nanoparticles in monocytes occurred at least in parts independently of the inhibited mechanisms and was also not completely blocked at 4°C. This indicates the involvement of non-endocytic pathways in the uptake of nanoparticles, possibly due to the interaction of positively charged nanoparticles with the anionic cell membrane or due to interactions with nanoparticle-components like silica or PEI.

With consideration of previous studies, the uptake of the cationic nanoparticles can occur via the formation of nanoscale holes in the negatively charged cell membrane (Chou *et al.* 2011, Hoet *et al.* 2004). Regarding this mechanism, the nanoparticles would be directly located in the cytoplasm circumventing the lysosomal location and digestion. Since no pronounced effects of the nanoparticles on the cell viability were seen, this suggested uptake via nanoscale holes should not have distinct negative impact on the cellular function.

Further studies highlight the possibility of cationic nanoparticles to be trapped on the negatively charged cell membrane without actual uptake (Pelaz *et al.* 2017, Patel *et al.* 2019, Behzadi *et al.* 2017, Beddoes *et al.* 2015, Nazarenius *et al.* 2014, Feliu *et al.* 2017, Kastl *et al.* 2013). However, in this study a clear intracellular localization of the nanoparticles could be shown, which indicates that most of the nanoparticles are indeed internalized despite the positive charge.

The uptake mechanism of nanoparticles in monocytes shown in this study is also postulated for the other key players of inflammation used herein. Since B cells are capable of endocytosis (Zilker *et al.* 2017, Malhotra *et al.* 2009), a similar uptake process as for

monocytes is reasonable and has been proposed earlier (Sokolova *et al.* 2010, Sokolova *et al.* 2013). Furthermore, for T cells, where the internalization of undecorated NPs was very low and decoration with IgG significantly increased the uptake, the internalization mechanisms most likely involves Fc-receptors and unspecific membrane invagination besides receptor-mediated endocytosis or antibody aggregate-mediated uptake as discussed above.

Previous studies showed the internalization of nanoparticles in endothelial cells via membrane invagination (Kozlova *et al.* 2012, Ge *et al.* 2014, Schraa *et al.* 2002, Xia *et al.* 2017). Therefore, it can be assumed that the intracellular uptake processes are comparable to the ones seen in monocytes. However, an alternative pathway was proposed for intracellular trafficking after RGD-mediated uptake of nanoparticles, which involved the immediate localization in the cytosol (Ge *et al.* 2014, Oba *et al.* 2008). This uptake pathway would circumvent the lysosomal entrapment and degradation of nanoparticles after uptake, comparably to the nanoscale holes discussed above.

Taken together, in monocytes, as the main target cell type for the nanoparticles and the most important cell type in immune surveillance, the internalization of the nanoparticles was mostly energy-dependent assumably leading to lysosomal processing of the internalized nanoparticles, though other uptake mechanisms are most likely also involved. The mechanisms of internalization of nanoparticles in other cell lines are considered to be similar.

### **5.1.3 Cytoplasmic availability of nanoparticles after internalization**

In this study, after cellular internalization, the nanoparticles were found to be colocalized with the endolysosomes after 3 to 6 hours of nanoparticle-incubation with a subsequent decrease of colocalization. Furthermore, the cargo-peptide was more evenly distributed in the cytoplasm for the longer incubation times. Together, these results indicate that the nanoparticles are degraded in the endolysosomes after cellular uptake and that subsequently the siRNA-cargo is released into the cytoplasm where it can exert its gene silencing function.

For the process of lysosomal escape, two possible mechanisms were proposed with the involvement of PEI as nanoparticle-component: the transient physical disruption of the negatively charged endosomal membrane or the proton sponge effect due to the protonation of the amino groups of PEI (Nimesh *et al.* 2011, Weng *et al.* 2020). Furthermore, the dissolution of basic calcium phosphate, which leads to an increase in calcium and phosphate ions and a subsequent increase in osmotic pressure inside endolysosomes, further facilitates the lysosomal escape of the nanoparticle components

(Neuhaus *et al.* 2016). The endolysosomal dissolution of the nanoparticles as a prerequisite for lysosomal escape was previously shown by incubating the nanoparticles in simulated endolysosomal medium (pH 4.7), where the dissolution rate was markedly higher than in neutral pH solutions (Białas *et al.* 2021).

In this context, the mechanism of lysosomal escape can be also assigned to the other cell types used in this study (endothelial cells, B cells and T cells), since the uptake mechanism is also assumed to mainly lead to lysosomal location (as discussed above), and the mechanisms of lysosomal rupture involving PEI and calcium phosphate are independent of the cell type, as it was already shown for other cell lines (Neuhaus *et al.* 2016).

However, the above-mentioned alternative routes for internalization via formation of nanoscale holes by PEI and the proposed RGD-mediated uptake in ECs would circumvent the lysosomal location of nanoparticles and therefore also bypass the step of nanoparticle degradation and the subsequent release of the components. Previously, a study showed the increase in gene silencing by enforcing the lysosomal escape via light irradiation (Zhang *et al.* 2020b), which indicates the importance and necessity of this step for efficient gene silencing via siRNA-nanoparticles. Therefore, the alternative routes of internalization of nanoparticles proposed above, that circumvent the lysosomal location, are probably not efficient for the transfection of siRNA since the siRNA would stay entrapped in the nanoparticles and would not be available for binding to the RISC complex to elicit subsequent gene silencing.

Summarized, the hereto shown lysosomal escape after internalization of the nanoparticles and the release of cargo siRNA into the cytosol enables the application of this siRNA-nanoparticle-system for gene silencing via RNAi.

### **5.1.4 Efficiency of siRNA-nanoparticles in downregulation of p65 expression**

The highest impact of p65 siRNA-nanoparticles on the protein expression was found after 72 h of incubation in monocytes. This result corresponds well with a previous study, where the efficiency of p65 siRNA (same vendor as in this study) was tested in TE-1 cells (human esophageal carcinoma cell line) at various time points, and the highest decrease in p65 protein expression was found at 72 h transfection time (Liu *et al.* 2014). Since in both cases different cell types were investigated, it indicates that the optimal time point of 72 h can be also transferred to the other immune cell lines used in this study.

In inflamed monocytes, endothelial cells and T cells, the treatment with p65 siRNA-containing F-NPs (undecorated, RGD-decorated or IgG-decorated, respectively) resulted in the downregulation of the p65 protein expression almost to the non-inflammatory state. Further investigations in inflamed monocytes revealed a distinct impact of the p65 siRNA also on the gene level. These results show the efficiency of transfection of these cell types with siRNA encapsulated in nanoparticles and the subsequent downregulation of target expression. In this context, these results are also an indirect confirmation that functional nanoparticle-bound siRNA is able to translocate from the endolysosomes to the cytoplasm after internalization. Therefore, these results support the findings for the lysosomal escape and following cytosolic location of the cargo already discussed above.

In contrast, for inflamed B cells no change in the p65 expression was found after incubation with F-NPs, either decorated with CD69-IgG or with unspecific IgGh. Since a downregulation of p65 was seen using functional p65 siRNA transfected with Lipofectamine™, the transfection with nanoparticles seems to be inefficient in these cells not the p65 siRNA *per se*. One explanation for this finding may be the internalization of nanoparticles into B cells via unfavorable uptake routes, where the lysosomal escape is not efficient, like through nanosized holes evoked by PEI as discussed above. This alternative internalization would prevent the relocation of siRNA into the cytoplasm and subsequently the execution of its function. Another explanation is that the calcium phosphate nanoparticles *per se* exhibit stimulatory effects in the cells which impede the effects of the p65 siRNA.

Indeed, such stimulatory effect was also seen in inflamed monocytes, endothelial cells, and B cells for the incubation with non-functional nanoparticles (either carrying scrambled siRNA or no cargo with the respective decoration dependent on the cell type), where the p65 protein expression was even upregulated beyond the inflamed level. This indicates the stimulatory effects of nanoparticle components, like calcium phosphate, PEI, or silica. Although in many previous studies siRNA-carrying calcium phosphate nanoparticles were used to treat different inflammation-associated diseases (Tenkumo *et al.* 2020, Zhang *et al.* 2020a, Duan and Li 2018, Frede *et al.* 2016), there are also reports of stimulating effects of calcium phosphate on the immune response in inflammatory cells (Velard *et al.* 2013), and calcium phosphate nanoparticles are also widely used as adjuvants for vaccines to enhance the stimulation of the immune system (Kopp *et al.* 2018, He *et al.* 2002, Ahmadpour *et al.* 2017). Another study showed that high silica concentrations were rather prone to activate NF- $\kappa$ B pathways via the production of oxidative stress (Liu and Sun 2010), but the overall low silica concentrations used herein indicate that the immune stimulation by silica at most only marginally contributes to the overall stimulatory effects of nanoparticles. Another explanation for this immune stimulation by nanoparticles is the unwanted activation of

proinflammatory pathways in the cells associated with the recognition of the nanoparticles as foreign material, which would lead to an increased activation of inflammatory signaling pathways and subsequently to an increased expression of NF- $\kappa$ B. In this context, the siRNA as foreign cargo of the nanoparticles can be recognized by intracellular TLRs and induce an immune reaction (Kanasty *et al.* 2012), while the nanoparticles *per se* can be identified as foreign by the complement system and also trigger the immune system (Parhiz *et al.* 2018). In case of ECs especially, the binding of RGD on the nanoparticle-surface to integrin might exert further stimulatory effect on the NF- $\kappa$ B expression, since previous studies already demonstrated an increased NF- $\kappa$ B activity upon binding of the peptide to integrin (Mussbacher *et al.* 2019, Scatena *et al.* 1998). Furthermore, for B cells specifically, a further upregulation of p65 via the crosstalk between different signaling pathways and the NF- $\kappa$ B signaling seems reasonable, as the activation of the immune signaling via FcR-binding (Ben Mkaddem *et al.* 2019), MHCII-binding (Cheng *et al.* 1999) or CD69-binding (Cibrian and Sanchez-Madrid 2017) might counteract the efficiency of p65 siRNA by upregulation of the p65 expression downstream of these receptors. Taken together, this indicates a potential stimulating effect of different components of the calcium phosphate nanoparticles on the inflammatory process by increasing the expression of NF- $\kappa$ B in the different cell types.

In contrast, in inflamed T cells the incubation with non-functional but CD69-targeted nanoparticles even decreased the p65 expression beyond the level reached with F-NPs independent of the decoration. Instead, for undecorated non-cargo SH-NPs the p65 expression was rather upregulated in accordance with the stimulatory effects of nanoparticles found in the other cell lines discussed above. Together with the finding that the internalization was at least partially dependent on the specific binding to CD69, this finding indicates that only the CD69-antibody-component of the nanoparticles is involved in the downregulation of p65, not the other nanoparticle parts. The signaling of CD69 was shown to regulate the differentiation of regulatory T cells (Cibrian and Sanchez-Madrid 2017), and binding of the specific antibodies might induce this signaling cascade and transform the cells into a Treg-phenotype. In these cells, the activation of the transcription factor forkhead box protein 3 (FOXP3) attenuates the canonical NF- $\kappa$ B signaling pathway by attenuating the p65 phosphorylation and nuclear translocation (Ziegler *et al.* 2021). Due to this decrease in the NF- $\kappa$ B signaling, the expression of p65 might be downregulated due to the feedback loop, where NF- $\kappa$ B enhances the expression of itself, which explains the downregulation of p65 seen for CD69-targeted nanoparticles in T cells independent of the cargo-loading.

Interestingly, the transfection with functional p65 siRNA and Lipofectamine™ as control for the nanoparticle-mediated transfection was only efficient in endothelial cells and B cells.

This supports previous findings, where different transfection susceptibilities for Lipofectamine™ were found in different cell types (Neuhaus *et al.* 2016).

Summarizing, the four different immune-relevant cell types showed different efficiency of p65 siRNA-nanoparticles in downregulation of NF- $\kappa$ B p65. On the one hand, this can be attributed to the proinflammatory effects of the nanoparticle-components *per se* as already discussed above. On the other hand, the varying susceptibility of different cell types to the transfection by calcium phosphate nanoparticles as described previously has to be taken into account (Neuhaus *et al.* 2016).

### 5.1.5 Impact of siRNA-nanoparticles on inflammatory signaling

For the cytokine secretion downstream of p65 signaling in monocytes, the influence of not only the functional p65 siRNA but of all nanoparticle-components was shown on the mediator and cytokine secretion. After internalization and lysosomal escape, the NP degradation products, like PEI, Ca<sup>2+</sup>, phosphate, and silica, are released into the cytoplasm or deposited in intracellular storages, which can impact the cytokine secretion of these cells in different ways.

In this context, the secretion of TNF- $\alpha$ , IL-6, and IFN- $\beta$  from monocytes was downregulated towards the non-inflamed level in presence of nanoparticles, regardless of the composition of the nanoparticle. Previous studies revealed an increase in intracellular calcium concentration after internalization of CaP-NPs (Neumann *et al.* 2009). Furthermore, it is well known that calcium is involved in many regulatory processes during inflammation (Hendy and Canaff 2016, Feske *et al.* 2003, Jennings *et al.* 2009) and that the regulation specificity is generally assumed to be controlled by variations in the oscillation amplitude and frequency (Dolmetsch *et al.* 1998). Subsequently, an increase in intracellular calcium levels was shown to increase cytoplasmic calcineurin concentrations (Biswas *et al.* 2003), which was shown to regulate the cells' inflammatory response dependent on the cell type (Jennings *et al.* 2009). In detail, in monocytes/ macrophages calcineurin acts as a negative regulator of the inflammatory response, since a constitutive activation of this enzyme led to the inhibition of LPS-induced activation of monocytes and the reduction of secretion of many pro-inflammatory mediators, like TNF- $\alpha$ , iNOS, or IL-12 (Conboy *et al.* 1999). Summarizing, the uptake of CaP-NPs in monocytes led to a transient spike in intracellular calcium levels, which in turn increased the activity of calcineurin, thereby inhibiting the proinflammatory cytokines, as shown in this study for TNF- $\alpha$ , IL-6 and IFN- $\beta$ . This finding hints towards a synergistic effect of siRNA and calcium in the nanoparticles in downregulating the inflammatory response downstream of NF- $\kappa$ B.



In contrast, the secretion of IL-1 $\beta$  in inflamed monocytes was increased for all nanoparticles, independent whether siRNA was incorporated, or which type of siRNA was used. Remarkably, the stimulation with LPS alone had no distinct effect on the IL-1 $\beta$  secretion. There is a reported relation between intracellular calcium levels and the expression of IL-1 (De Dios *et al.* 2020). In detail, increased extra-, or intracellular calcium concentration, hereto due to incubation with CaP-NPs, was found to be linked with the activation of the NLRP3 inflammasome, which in turn enhances the release of high levels of IL-1 $\beta$  from monocytes during inflammation (Rossol *et al.* 2012, Lee *et al.* 2012).

Taken together, for all tested inflammation-associated cell types, a profound effect of the nanoparticles without cargo siRNA was found on the inflammatory reaction and on the target protein expression. In this study, by testing the effect of non-cargo nanoparticles, we found that the components of the nanoparticles seem to have their own distinct effect on the inflammatory signaling, depending on the investigated cell type. Other studies investigating the application of CaP-NPs as carriers for siRNA have either not tested the unloaded nanoparticles for their inherent impact on the investigated target (Tenkumo *et al.* 2020, Wu *et al.* 2018) or did not find an effect of the nanoparticles *per se* on the specific target expression (Wang *et al.* 2019, Li *et al.* 2019). Therefore, the impact of the CaP-NPs on the target expression seems to be dependent on the target itself and also on the target cell type. In this context, NF- $\kappa$ B as a target for siRNA-mediated downregulation seems to be uniquely affected by the components of the herein used nanoparticles. Nevertheless, further investigations of the mechanism of action by which the nanoparticle-components distinctively influence the immune signaling in different cell types might further elucidate the efficiency of application of these nanoparticles to treat inflammation.

It has to be noted that the reason for the discrepancy in the influence of the nanoparticles on the NF- $\kappa$ B expression and cytokine secretion may be due to the activation of different signaling pathways independent of NF- $\kappa$ B or due to the impact of the components of the nanoparticles, which were shown to increase the p65 protein expression in most cell lines, while showing distinct downregulation of proinflammatory mediators, at least in monocytes.

Summarized, the silica-coated calcium phosphate nanoparticles are able to suppress pro-inflammatory reactions in different inflammatory cell types due to their favorable intracellular carrier functions and their feasibility of NF- $\kappa$ B p65 downregulation as well as their distinct impact on key proinflammatory mediators. Therefore, this nanoparticle-based system seems to be suitable for the treatment of acute and chronic inflammatory diseases in the future.

## 5.2 Therapeutic efficiency of nanoparticles with p65 siRNA in DSS-induced colitis in mice

### 5.2.1 Impact of F-NPs on the development of colitis

The investigation of the therapeutic efficiency of the siRNA-NP formulation revealed the effective alleviation of DSS-induced clinical features of colitis in mice for the treatment with F-NPs, such as DAI (disease activity index) and fecal Lcn-2 (Lipocalin-2) concentration. Especially, the treatment with F-NPs had distinct positive effect on the primary signs of colitis, such as the feces consistency and rectal bleeding, which are summarized in the DAI.

Furthermore, F-NPs markedly decreased the Lcn-2 levels in the feces. Lcn-2 was found to be a sensitive and robust biomarker for colitis in mice (Chassaing *et al.* 2012), and its human counterpart NGAL is also increased in fecal samples of patients with ulcerative colitis (Nielsen *et al.* 1999). Since Lcn-2 is also a direct target gene for NF- $\kappa$ B (Gilmore-Lab Boston University), the reduction of its fecal concentration can be either the result of specific inhibition of p65 in the cells secreting Lcn-2 or due to the general amelioration of colonic inflammation as the result of treatment. Since Lcn-2 is highly expressed in and secreted from colonic epithelial cells (Raffatellu *et al.* 2009), the effect of treatment with F-NPs on its fecal level is indeed probably only indirectly correlated to the downregulation of p65 by the nanoparticles as the epithelial cells are not a primary target for transfection. Instead, the effects can be contributed to the influence of the nanoparticles on the inflammatory signaling in the whole colon originating in the primary target cells of the nanoparticles (probably monocytes) and being transmitted to the epithelial cells, where the secretion of Lcn-2 is influenced.

However, substantial intraindividual differences in the development of DSS-induced colitis were seen in the animals. To ensure the best possible comparability during experiments, all possible parameters that may influence the development of colitis were kept unchanged (e.g., DSS concentration and batch, mouse strain and gender and vendor, housing conditions). Nonetheless, some parameters, especially the microbiological state and intestinal flora of the animals, are not ultimately controllable, and have distinct impact on the development of DSS-induced colitis (Perše and Cerar 2012, Li *et al.* 2018). In detail, the intestinal flora may play an important role in the susceptibility and responsiveness to DSS-induced damage of epithelial cells (Perše and Cerar 2012).

Furthermore, a significant shortening of the colon for mice with colitis compared to healthy mice was visible for short-term and long-term investigation points. The treatment with F-NPs was able to distinctively ameliorate this colonic shortening, especially after 72 h. In this

context, the colon length is an optimal indicator of colitis since this disease is characterized by the presence of marked hypertrophy of the longitudinal muscularis mucosae. The forceful contraction of this hypertrophied layer further shortens the whole colon together with a separation of the mucosa and the muscularis propria, which further narrows the lumen (Gore 1992).

Similarly, the histological score was significantly changed for mice with colitis compared to the healthy group, while the treatment with F-NPs substantially lowered these histopathological differences, especially for the short-term investigation. Remarkably pronounced was the effect of F-NPs on the crypt damage since lesser overall crypt damage and especially total crypt loss was seen for the treated animals. These findings indicate the notable impact of the treatment with F-NPs in the epithelial cells forming the crypts.

Both colon length and histological score clearly demonstrate the positive impact of F-NPs on the local development of colonic inflammation for both observation points. Interestingly, the impact of the treatment was less significant for the longer observation time than for the short-term investigation. This effect can be explained by self-healing processes that may have already started for the longer examination period after the DSS-administration had stopped. This finding is also in accordance with the cessation of rectal bleeding detected for untreated mice with colitis at day 9.

In contrast, no distinct effect of the treatment with F-NPs was found on the amount of white blood cells, lymphocytes, platelets, or monocytes in the blood for various time points. This indicates that the impact of the nanoparticles is predominant directly at the site of inflammation and has no effect on the overall composition of the cellular blood components.

Summarized, the clear amelioration of local colonic inflammation by treatment with F-NPs could be shown with different independent parameters with no notable effect on the global cellular composition in the circulation.

### **5.2.2 Impact of F-NPs on the inflammatory protein expression in the colonic tissue**

For short-term investigation (72 h after nanoparticle administration), distinct effects of the treatment with F-NPs were found on the expression of inflammatory proteins in the colon. Interestingly, the expression in isolated colonic leukocytes and the whole colonic tissue was differentially regulated. Since the nanoparticles were administered systemically, it is reasonable to assume that leukocytes, especially monocytes, are the primary target cells for the nanoparticles in the blood stream. After recruitment to the site of inflammation, these cells will elicit the direct effects (so called “primary effects”) of the nanoparticles, while other

cell types will be subsequently influenced indirectly by the nanoparticle-affected secretion of inflammatory mediators (as so called “secondary effects” of the nanoparticles).

In this context, in colonic leukocytes as primary effector cells of the nanoparticles, the treatment with F-NPs distinctively influenced the expression of inflammatory proteins for the short-term observation period. The alleviation of the DSS-induced changes of p65, phosphorylated I $\kappa$ B $\alpha$ , Bcl-2 and COX-2 protein expression by the F-NPs-treatment could be related to the suppressed proinflammatory activities which are not only related to the p65-mediated canonical NF- $\kappa$ B activation pathway, but rather to other regulative mechanisms, such as the noncanonical pathway (Sun 2011). In detail, the upregulation of phosphorylated I $\kappa$ B $\alpha$  in colitis is an indication of activated NF- $\kappa$ B canonical signaling, while the reverse regulation seen for the treatment with F-NPs is a sign for the increasing inactivation of this inflammatory pathway. Furthermore, the significant downregulation of COX-2 expression to the healthy level for the treatment group indicates a decreased potential for the production of prostaglandins, especially PGE2 (Meyer-Kirchrath and Schrör 2000, Masferrer *et al.* 1994), which is typically present in IBD patients (Wiercinska-Drapalo *et al.* 1999). Moreover, the decreased iNOS activity during mucosal injury in colitis could improve blood flow, reduce leukocytes and platelet recruitment as well as oxidative stress, which can reduce the inflammation in the colon (Kolios *et al.* 2004).

In contrast, the secondary effects of the treatment with F-NPs in the whole colon tissue revealed a different regulation of the inflammatory proteins as in leukocytes for the short-term investigation. Since at this time point during the development of colitis, substantial mucosal injury and crypt loss was found in the colon, the changes detected in the expression of inflammatory mediators in whole colon, especially in mucosal epithelial cells, are probably related to these events. In detail, treatment with F-NPs slightly upregulated the p65 expression, indicating that the NF- $\kappa$ B activity in the whole colon tissue is generally required for tissue repair processes, like the initiation of reparative proliferation of mucosal epithelial cells and of extracellular matrix synthesis (Pasparakis 2008, Kolachala *et al.* 2007). Furthermore, the suppression of the DSS-mediated increase of iNOS expression could be related to the presence of oxidative stress as a result of DSS-mediated injury which does not have a distinct impact on the NF- $\kappa$ B activation (Parikh *et al.* 2000). Interestingly, the expression of I $\kappa$ B $\alpha$  was located primarily in the apical mucosa in healthy colon tissue, which is comparable to the findings in a previous study (Ren *et al.* 2015), and could be attributed to the higher susceptibility of coming into contact with PAMPs or DAMPs on the apical side and the subsequent induction of signaling primarily at this site.

Similarly, the long-term effects of F-NPs in the whole colon tissue reduced the protein expression of p65 and its associated proteins I $\kappa$ B $\alpha$  and iNOS compared to the colitis group.

In this context, a decreased p65 expression after treatment is coupled with less activation of NF- $\kappa$ B and its subsequent signaling. It has to be noted that this effect was detected despite the presence of NF- $\kappa$ B inducers (e.g., TNF- $\alpha$ , IL-1), which leads to the activation of IKK and to the subsequent degradation of I $\kappa$ B $\alpha$  (Christian *et al.* 2016). Furthermore, the decrease of I $\kappa$ B $\alpha$  expression is strongly related to the strong IL-1 $\alpha$  expression in the whole colon found on day 6, which fosters the degradation of I $\kappa$ B (Parikh *et al.* 2000). Moreover, the suppressed expression of iNOS after treatment with F-NPs is an indication of the reduced NO-mediated proinflammatory potential in the whole colon tissue, in particular since this enzyme is regulated by NF- $\kappa$ B activity (Gilmore-Lab Boston University, Bacher and Schmitz 2004).

Summarized, after the short-term observation (72 h), the treatment with F-NPs revealed a primary impact in colonic leukocytes by decreasing the production of PGE<sub>2</sub>, reducing the oxidative stress and improving blood flow, which in turn enhanced tissue repair processes in the whole colon tissue as a secondary effect of the treatment. For the long-term investigation, the treatment with F-NPs led to less overall inflammatory signaling in the whole colon tissue.

### **5.2.3 Impact of F-NPs on the level of inflammatory mediators in colon and blood plasma**

In agreement with the alleviative inflammatory potential during DSS-mediated induction of colitis mentioned above, the administration of F-NPs influenced several proinflammatory mediators after the short-term observation period. In detail, the stimulation of IL-1 $\beta$  secretion in the whole colon tissue after treatment with F-NPs suggests the stimulation of the NF- $\kappa$ B pathway in intestinal epithelial cells (Parikh *et al.* 2000). This finding is well in accordance with the slight increase in p65 expression in whole colon tissue discussed above. Also, the increase of IL-1 $\alpha$  in the colon tissue after the treatment can be connected to the decreased I $\kappa$ B $\alpha$  expression found for the later time point discussed above. Furthermore, the stimulation of IFN $\gamma$  secretion on the whole colon tissue for F-NP treatment can be attributed to the support of epithelial regeneration following acute colonic injury, which is also connected to increased NF- $\kappa$ B activity (McElrath *et al.* 2021). Moreover, the increased IL-6 expression in the blood is related to the induction of acute phase reactions and neutrophilia, which is needed for the stimulation of B cells to induce antibody production and of hepatocytes to support acute phase reactions (Kishimoto 2006, Hashizume *et al.* 2011).

After the long-term observation, the administration of F-NPs inhibited several inflammatory mediators in the colon and the blood plasma. In detail, the local stimulation of IL-6 expression in the colon tissue is related to repair processes in the colonic mucosa, as IL-6 is known to stimulate intestinal epithelial proliferation and repair after injury (Kuhn *et al.* 2014). Furthermore, the stimulation of GM-CSF expression in the colon and blood plasma can lead to the enhanced maturation and polarization of inflammatory intestinal macrophages, which promotes anti-microbial functions and suppresses wound healing (Castro-Dopico *et al.* 2020). Also, the stimulation of IL-23 secretion in the colon and especially in the blood plasma is related to neutrophil recruitment after DSS-administration (Cox *et al.* 2012) and is produced by dendritic cells and macrophages to promote proinflammatory and regenerative activities of T helper and innate lymphoid cells (Lim *et al.* 2020). Moreover, the treatment with F-NPs suppressed the secretion of IL-17A from the colon tissue, which is associated with a protective role for the injured intestinal mucosa (Song *et al.* 2019, Fournier and Parkos 2012). Additionally, the decreased IL-10 secretion in the colon and blood plasma after the treatment shows the alleviation of DSS-induced effects on this cytokine back to the healthy level, as it was shown to be significantly upregulated in UC patients (Rana *et al.* 2014).

Taken together, the cytokine expression profiles for short- and long-term observation times both show that the treatment with F-NPs influences the signaling in the colon regarding the proliferation and repair of colonic mucosa and epithelium, epithelial stimulation, and regeneration, but also the further stimulation and recruitment of immune cells, like macrophages, neutrophils, and B cells.

It was beyond the scope of this study to investigate the therapeutic efficiency of the different specific decorated nanoparticles to target different cell types. But it is expected that the specifically decorated nanoparticles will elicit similar effects on the colonic inflammation as the undecorated ones, since similar mechanisms for both types of nanoparticles were found in the *in vitro* studies discussed above. Nonetheless, the *in vivo* situation is much more complex, therefore detailed investigations have to be performed to further elucidate the impact of the decorated nanoparticles on the specific target cell types and the inflammation in general.

Summarized, the treatment with F-NPs led to overall less inflammation in the colon with less inflammatory signaling as well as increased proliferation, regeneration, and repair processes for both short- and long-term observation periods. Therefore, a clear amelioration of local colonic inflammation by the F-NPs could be verified.

## 5.3 Potential off-target effects of the nanoparticles for the treatment of inflammation

### 5.3.1 Biodistribution of nanoparticles in mice with local inflammation

In this study, a distinct impact of the local colonic inflammation was found on the early biodistribution of the nanoparticles (3 h) after i.v. injection, which represents the immediate distribution in the organs prior to any redistribution. A previous study with comparable nanoparticles already revealed that 5 hours after i.v. application in healthy mice, the nanoparticles are mainly located in the spleen, lung, and liver (Kollenda *et al.* 2020).

In this context, a distinct enhanced nanoparticle accumulation, particularly in the appendix, was found in the diseased animals compared to healthy animals. Previous research provided evidence that the appendix, as a secondary lymphoid tissue, plays an important role in the initiation and sustainability of ulcerative colitis (Krieglstein *et al.* 2001). Despite being generally regarded as a rudimentary part of the intestine, previous literature suggests the involvement of this organ in the immune system in humans is comparable to the well-established connection in the murine organism (Kooij *et al.* 2016). Further investigations of biopsies from UC patients also hint to the involvement of the appendix as a priming site for the development of colonic inflammation (Matsushita *et al.* 2005) and a previous appendectomy correlates with an overall lower risk for the development of colitis as shown in murine models (Krieglstein *et al.* 2001). Therefore, the increase of the phagocytic potential of immune cells in the appendix during the development of colitis and subsequent uptake of F-NPs might mediate the secondary effects seen after treatment with the nanoparticles, since an inhibition of p65 in these immune cells might subsequently impact the inflammation in the colon.

In contrast, no notable change in the NP-accumulation in the colon and mesenteric lymph nodes was detected in the presence of colonic inflammation. This finding indicates that the nanoparticles have not yet reached the site of inflammation 3 h after application, suggesting that most of the ameliorating effects of F-NPs seen in colitis can be attributed to the secondary effects (as already discussed above) provoked by the migration of immune cells that internalized the nanoparticles in the blood or in lymphoid organs (e.g., the appendix), where the nanoparticle accumulation was prominent. Therefore, it is possible that for longer investigation times after injection, the nanoparticles can be detected at the site of inflammation due to migration of the immune cells with internalized nanoparticles.

Furthermore, the nanoparticle accumulation was increased in the small intestine in presence of colonic inflammation, which can be associated with the presence of gut-associated lymphoid tissues (GALT) as mediators of the inflammation (Mörbe *et al.* 2021).

Further increased accumulation in the lung in animals with colonic inflammation suggests the additional involvement of this lymphoid organ in the regulation of colonic inflammation. Interestingly, the accumulation of the nanoparticles in the spleen was decreased in presence of colitis, indicating that other lymphoid organs, like the appendix, play the predominant role in the mediation of colonic inflammation, not the spleen. Moreover, no notable change in the accumulation of nanoparticles in the stomach, bladder, ovaries, skin, heart, and brain in mice with colitis shows that the biodistribution in these organs is not influenced by the presence of local inflammation in the colon. Notably, the increase, by tendency, in the nanoparticle-accumulation in the kidney in colitis mice suggests an enhanced secretion of nanoparticles in the presence of local colonic inflammation.

Summarized, in this study distinct changes in the biodistribution of the nanoparticles after 3 h in the presence of colonic inflammation were shown with a notable involvement of different lymphoid organs, especially the appendix and also the small intestine and lung. This indicates that the local inflammation shifts the biodistribution of the nanoparticles towards the adjacent lymphoid organs as priming sites to impact the inflammation.

### **5.3.2 Impact of siRNA *per se* on the inflammation process**

Curiously, the treatment with S-NPs containing unspecific, scrambled siRNA, was found to have similar, or even higher effects on DSS-induced colitis as the F-NPs with functional p65 siRNA. The difference was most notable for the weight loss, the histologic score and for the p65 and iNOS protein expression in the colon. These effects might be attributed to a less-specific suppression of coding mRNAs, which might include inflammation players other than p65-related ones. Since the sequence of the purchased scrambled siRNA is not known, certain sequence similarities with other proteins cannot be excluded.

Furthermore, the expression profiles of inflammatory mediators in the colon and blood were notably affected by the treatment with S-NPs compared to F-NPs. Most inflammatory mediators were even downregulated with treatment of S-NPs. In contrast, IL-10 expression was upregulated both in the colon and blood with S-NPs. Since IL-10 was found to be downregulated for the treatment with F-NPs compared to untreated mice, this finding indicates that pathways independent of NF- $\kappa$ B might be influenced by S-NPs to regulate different cytokines. Additionally, IL-27 was found to be upregulated in the colon for S-NP treatment, which was found to be related to the suppression of differentiation of Th17 cells by the further suppression of several inflammatory cytokines (Sasaoka *et al.* 2011). With consideration of this different regulation of cytokine expression for the treatment with S-NPs compared to F-NPs, it is reasonable to assume that the efficiency of S-NPs is mediated at least in parts by pathways independent of NF- $\kappa$ B.



Moreover, the IL-17A expression in the colon was upregulated for the treatment with S-NPs compared to F-NPs, which indicates less protection for the injured intestinal mucosa as seen for F-NPs already discussed above (Song *et al.* 2019, Fournier and Parkos 2012). Additionally, IL-6 was found to be downregulated in the colon and plasma for S-NPs compared to F-NPs. Since the treatment with F-NPs even stimulated the IL-6 production in the colon (as discussed above), the S-NPs seem to have less impact on repair mechanisms in the colonic mucosa as F-NPs.

Summarized, the treatment with S-NPs elicits a similar impact on the overall colonic inflammation compared to F-NPs, but other mechanisms seem to be involved since the inflammatory mediators are differentially regulated.

As discussed above, a profound effect of the nanoparticles without cargo siRNA was found on the inflammatory reaction and especially on the siRNA-target p65 on cellular level. Therefore, it is reasonable to assume that *in vivo* the nanoparticles without cargo would also elicit a distinct effect on the inflammatory reaction, and that the herein seen amelioration of inflammation by S-NPs can also be attributed to the effects of the nanoparticles *per se* not only the scrambled siRNA. Future studies are needed to further investigate the effects of the different components of the nanoparticles on the amelioration of colonic inflammation, and which component is the most efficient in treating the inflammation.

### **5.3.3 Off-target effects of nanoparticles in healthy mice**

Overall, the off-target effects of F-NPs in the colon of healthy animals were very low. In detail, an increased COX-2 expression in the whole colon compared to untreated healthy mice may be related to certain proinflammatory reactions, which seem to be very weak, since the anti-apoptotic protein Bcl-2 was increasingly expressed, together with a lower expression of iNOS. Furthermore, the increased expression of IL-27 in the blood for the treatment with F-NPs demonstrates the recognition of the nanoparticles in the body as foreign agents, since this mediator is linked to the signaling regulating the immune response to extracellular protozoan infections (Liu *et al.* 2015).

Taken together, no distinct off-target effects of the F-NPs in the colonic region of healthy mice could be seen. It was beyond the scope of this study to investigate the off-target effects in the whole body and therefore additional investigations are needed to further elucidate the biological safety of these nanoparticles.

In this context it has to be mentioned that during the herein presented experiments, some mice suffered fatal adverse effects after intravenous injection of the nanoparticles. Though

the reasons for these events could not be verified, possible explanations include an anaphylactic shock elicited from the nanoparticle solution, or an agglomeration of the nanoparticles after injection resulting in thrombotic events in the body. These findings highlight that intravenous application, especially due to the high siRNA-nanoparticle concentration needed, is not applicable for further investigations. Therefore, other application forms, like rectal injection, administration *per orale*, or via suppositories should be tested.

In brief, the presence of colonic inflammation influenced the biodistribution of nanoparticles towards adjacent lymphoid organs. Moreover, the nanoparticles with scrambled siRNA elicited distinct ameliorating effects in the colitis, but further investigations are needed to investigate the impact of single components of the nanoparticles on the inflammation. Furthermore, no distinct off-target effects of the F-NPs in the colonic region of healthy mice were seen.

## 6 Conclusion & Outlook

In the herein presented study, the application of a novel nanoparticle-based treatment for inflammation was investigated. The nanoparticles with incorporated p65 siRNA were shown to be efficient in downregulating p65 expression in the main cellular players of inflammation as well as in ameliorating colitis in mice.

Additional optimization of the composition of the herein used nanoparticles could further enhance the biological efficiency. For example, the incorporation of more siRNA molecules per nanoparticle during synthesis could decrease the needed nanoparticle concentration without influencing the efficiency, thereby minimize potential side effects of the NP-components. Furthermore, alternative decorations of the nanoparticles could further enhance the targeting of specific cell types or tissues, which also decreases possible off-target effects.

Moreover, since the intravenous application of nanoparticles in this study elicited few fatal adverse effects after injection, other routes of delivery should be investigated. In this context, especially the oral administration or delivery via suppositories seems to be promising to treat colonic inflammation while reducing severe off-target effects from systemic administration.

Since in this study the therapeutic efficiency of the p65 siRNA nanoparticles was tested only in the murine DSS-colitis model, in the future also other inflammatory diseases connected to the NF- $\kappa$ B signaling, like arthritis or various cardiovascular diseases, should be investigated for the nanoparticles' potential as novel treatment modality.

The herein described experiments evaluated the potential of the p65 siRNA nanoparticles to treat inflammatory diseases. Prior to any clinical application, the nanoparticles will have to be investigated concerning their pharmacodynamics, pharmacokinetics, and toxicology to provide detailed safety and efficiency information of this treatment and also further elucidate the biological effect, both in *in vitro* and *in vivo* preclinical studies (Shah and Agnihotri 2011). Following this, the treatment can be tested in clinical studies with phases I, II, and III prior to regulatory approval.

## References

- Abraham C, Cho JH. 2009. Inflammatory bowel disease. *N Engl J Med*, 361 (21):2066-2078.
- Adler LN, Jiang W, Bhamidipati K, Millican M, Macaubas C, Hung SC, Mellins ED. 2017. The Other Function: Class II-Restricted Antigen Presentation by B Cells. *Frontiers in Immunology*, 8.
- Ahmadpour E, Sarvi S, Hashemi Soteh MB, Sharif M, Rahimi MT, Valadan R, Tehrani M, Khalilian A, Montazeri M, Fasihi-Ramandi M, Daryani A. 2017. Enhancing immune responses to a DNA vaccine encoding *Toxoplasma gondii* GRA14 by calcium phosphate nanoparticles as an adjuvant. *Immunology Letters*, 185:40-47.
- Akhtar S, Benter IF. 2007. Nonviral delivery of synthetic siRNAs in vivo. *Journal of Clinical Investigation*, 117 (12):3623-3632.
- Aksamitiene E, Hoek JB, Kholodenko B, Kiyatkin A. 2007. Multistrip Western blotting to increase quantitative data output. *Electrophoresis*, 28 (18):3163-3173.
- Araki N, Johnson MT, Swanson JA. 1996. A role for phosphoinositide 3-kinase in the completion of macropinocytosis and phagocytosis by macrophages. *J Cell Biol*, 135 (5):1249-1260.
- Bacher S, Schmitz ML. 2004. The NF- $\kappa$ B Pathway as a Potential Target for Autoimmune Disease Therapy. *Current Pharmaceutical Design*, 10:2827-2837.
- Barczyk M, Carracedo S, Gullberg D. 2010. Integrins. *Cell and Tissue Research*, 339 (1):269-280.
- Basil MC, Levy BD. 2016. Specialized pro-resolving mediators: endogenous regulators of infection and inflammation. *Nat Rev Immunol*, 16 (1):51-67.
- Beddoes CM, Case CP, Briscoe WH. 2015. Understanding nanoparticle cellular entry: A physicochemical perspective. *Advances in Colloid and Interface Science*, 218:48-68.
- Behzadi S, Serpooshan V, Tao W, Hamaly MA, Alkawareek MY, Dreaden EC, Brown D, Alkilany AM, Farokhzad OC, Mahmoudi M. 2017. Cellular uptake of nanoparticles: Journey inside the cell. *Chemical Society Reviews*, 46 (14):4218-4244.
- Ben Mkaddem S, Benhamou M, Monteiro RC. 2019. Understanding Fc Receptor Involvement in Inflammatory Diseases: From Mechanisms to New Therapeutic Tools. *Frontiers in Immunology*, 10:811.
- Białas N, Müller EK, Epple M, Hilger I. 2021. Silica-coated calcium phosphate nanoparticles for gene silencing of NF- $\kappa$ B p65 by siRNA and their impact on cellular players of inflammation. *Biomaterials*, 276:121013.
- Biswas G, Anandatheerthavarada HK, Zaidi M, Avadhani NG. 2003. Mitochondria to nucleus stress signaling: a distinctive mechanism of NF $\kappa$ B/Rel activation through calcineurin-mediated inactivation of I $\kappa$ B $\beta$ . *The Journal of cell biology*, 161 (3):507-519.
- Brenner PS, Krakauer T. 2003. Regulation of Inflammation: A Review of Recent Advances in Antiinflammatory Strategies. *Curr Med Chem – Anti-Inflammatory & Anti-Allergy Agents*, 2:274-283.
- Buckley CD, Gilroy DW, Serhan CN. 2014. Proresolving lipid mediators and mechanisms in the resolution of acute inflammation. *Immunity*, 40 (3):315-327.
- Carthew RW, Sontheimer EJ. 2009. Origins and Mechanisms of miRNAs and siRNAs. *Cell*, 136 (4):642-655.
- Castro-Dopico T, Fleming A, Dennison TW, Ferdinand JR, Harcourt K, Stewart BJ, Cader Z, Tuong ZK, Jing CZ, Lok LSC, Mathews RJ, Portet A, Kaser A, Clare S, Clatworthy MR. 2020. GM-CSF Calibrates Macrophage Defense and Wound Healing Programs during Intestinal Infection and Inflammation. *Cell Reports*, 32 (1).
- Chassaing B, Aitken JD, Malleshappa M, Vijay-Kumar M. 2014. Dextran sulfate sodium (DSS)-induced colitis in mice. *Curr Protoc Immunol*, 104:Unit 15 25.

- Chassaing B, Srinivasan G, Delgado MA, Young AN, Gewirtz AT, Vijay-Kumar M. 2012. Fecal Lipocalin 2, a Sensitive and Broadly Dynamic Non-Invasive Biomarker for Intestinal Inflammation. *Plos One*, 7 (9).
- Chen F, Castranova V, Shi X. 2001. New insights into the role of nuclear factor-kappaB in cell growth regulation. *The American journal of pathology*, 159 (2):387-397.
- Cheng PC, Steele CR, Gu L, Song W, Pierce SK. 1999. MHC class II antigen processing in B cells: accelerated intracellular targeting of antigens. *J Immunol*, 162 (12):7171-7180.
- Chou LY, Ming K, Chan WC. 2011. Strategies for the intracellular delivery of nanoparticles. *Chem Soc Rev*, 40 (1):233-245.
- Christian F, Smith EL, Carmody RJ. 2016. The Regulation of NF-kappa B Subunits by Phosphorylation. *Cells*, 5 (1).
- Cibrian D, Sanchez-Madrid F. 2017. CD69: from activation marker to metabolic gatekeeper. *European Journal of Immunology*, 47 (6):946-953.
- Conboy IM, Manoli D, Mhaikar V, Jones PP. 1999. Calcineurin and vacuolar-type H<sup>+</sup>-ATPase modulate macrophage effector functions. *Proc Natl Acad Sci U S A*, 96 (11):6324-6329.
- Conte R, Marturano V, Peluso G, Calarco A, Cerruti P. 2017. Recent Advances in Nanoparticle-Mediated Delivery of Anti-Inflammatory Phytocompounds. *Int J Mol Sci*, 18 (4).
- Cooper HS, Murthy SN, Shah RS, Sedergran DJ. 1993. Clinicopathologic study of dextran sulfate sodium experimental murine colitis. *Lab Invest*, 69 (2):238-249.
- Corbo C, Cromer WE, Molinaro R, Toledano Furman NE, Hartman KA, De Rosa E, Boada C, Wang X, Zawieja DC, Agostini M, Salvatore F, Abraham BP, Tasciotti E. 2017. Engineered biomimetic nanovesicles show intrinsic anti-inflammatory properties for the treatment of inflammatory bowel diseases. *Nanoscale*, 9 (38):14581-14591.
- Cox JH, Kljavin NM, Ota N, Leonard J, Roose-Girma M, Diehl L, Ouyang W, Ghilardi N. 2012. Opposing consequences of IL-23 signaling mediated by innate and adaptive cells in chemically induced colitis in mice. *Mucosal Immunology*, 5 (1):99-109.
- Daha MR, van EL, Hazevoet HM, Kijlstra A. 1982. Degradation of soluble immunoglobulin aggregates in vitro by monocytes from normal subjects and from patients with systemic lupus erythematosus. *Scand J Immunol*, 16 (2):117-122.
- De Dios R, Nguyen L, Ghosh S, McKenna S, Wright CJ. 2020. CpG-ODN-mediated TLR9 innate immune signalling and calcium dyshomeostasis converge on the NF kappa B inhibitory protein I kappa B beta to drive IL1 alpha and IL1 beta expression. *Immunology*:14.
- Dejban P, Nikravangolsefid N, Chamanara M, Dehpour A, Rashidian A. 2021. The role of medicinal products in the treatment of inflammatory bowel diseases (IBD) through inhibition of TLR4/NF-kappaB pathway. *Phytotherapy Research*, 35 (2):835-845.
- Diakos CI, Charles KA, McMillan DC, Clarke SJ. 2014. Cancer-related inflammation and treatment effectiveness. *Lancet Oncol*, 15 (11):e493-503.
- Dolmetsch RE, Xu K, Lewis RS. 1998. Calcium oscillations increase the efficiency and specificity of gene expression. *Nature*, 392 (6679):933-936.
- Donath MY. 2014. Targeting inflammation in the treatment of type 2 diabetes: time to start. *Nat Rev Drug Discov*, 13 (6):465-476.
- Dong Y, Yu T, Ding L, Laurini E, Huang Y, Zhang M, Weng Y, Lin S, Chen P, Marson D, Jiang Y, Giorgio S, Pricl S, Liu X, Rocchi P, Peng L. 2018. A Dual Targeting Dendrimer-Mediated siRNA Delivery System for Effective Gene Silencing in Cancer Therapy. *J Am Chem Soc*, 140 (47):16264-16274.
- Dowdy SF. 2017. Overcoming cellular barriers for RNA therapeutics. *Nature Biotechnology*, 35 (3):222-229.
- Duan WF, Li H. 2018. Combination of NF-kB targeted siRNA and methotrexate in a hybrid nanocarrier towards the effective treatment in rheumatoid arthritis. *Journal of Nanobiotechnology*, 16.
- Dutta D, Donaldson JG. 2012. Search for inhibitors of endocytosis: Intended specificity and unintended consequences. *Cell Logist*, 2 (4):203-208.

- Epple M. 2018. Review of potential health risks associated with nanoscopic calcium phosphate. *Acta Biomater*, 77:1-14.
- Epple M, Ganesan K, Heumann R, Klesing J, Kovtun A, Neumann S, Sokolova V. 2010. Application of calcium phosphate nanoparticles in biomedicine. *Journal of Materials Chemistry*, 20 (1):18-23.
- Feliu N, Sun X, Alvarez Puebla RA, Parak WJ. 2017. Quantitative Particle–Cell Interaction: Some Basic Physicochemical Pitfalls. *Langmuir*, 33 (27):6639-6646.
- Feske S, Okamura H, Hogan PG, Rao A. 2003. Ca<sup>2+</sup>/calcineurin signalling in cells of the immune system. *Biochem Biophys Res Commun*, 311 (4):1117-1132.
- Fire A, Xu S, Montgomery MK, Kostas SA, Driver SE, Mello CC. 1998. Potent and specific genetic interference by double-stranded RNA in *Caenorhabditis elegans*. *Nature*, 391 (6669):806-811.
- Foroozandeh P, Aziz AA. 2018. Insight into Cellular Uptake and Intracellular Trafficking of Nanoparticles. *Nanoscale Research Letters*, 13.
- Fournier BM, Parkos CA. 2012. The role of neutrophils during intestinal inflammation. *Mucosal Immunology*, 5 (4):354-366.
- Frede A, Neuhaus B, Klopffleisch R, Walker C, Buer J, Muller W, Epple M, Westendorf AM. 2016. Colonic gene silencing using siRNA-loaded calcium phosphate/PLGA nanoparticles ameliorates intestinal inflammation in vivo. *J Control Release*, 222:86-96.
- Fullerton JN, Gilroy DW. 2016. Resolution of inflammation: a new therapeutic frontier. *Nat Rev Drug Discov*, 15 (8):551-567.
- Gao Y, Ouyang ZJ, Yang C, Song C, Jiang CJ, Song SL, Shen MG, Shi XY. 2021. Overcoming T Cell Exhaustion via Immune Checkpoint Modulation with a Dendrimer-Based Hybrid Nanocomplex. *Advanced Healthcare Materials*.
- Gareb B, Otten AT, Frijlink HW, Dijkstra G, Kosterink JGW. 2020. Review: Local Tumor Necrosis Factor-alpha Inhibition in Inflammatory Bowel Disease. *Pharmaceutics*, 12 (6):34.
- Ge Z, Chen Q, Osada K, Liu X, Tockary TA, Uchida S, Dirisala A, Ishii T, Nomoto T, Toh K, Matsumoto Y, Oba M, Kano MR, Itaka K, Kataoka K. 2014. Targeted gene delivery by polyplex micelles with crowded PEG palisade and cRGD moiety for systemic treatment of pancreatic tumors. *Biomaterials*, 35 (10):3416-3426.
- Gerondakis S, Siebenlist U. 2010. Roles of the NF-kappaB pathway in lymphocyte development and function. *Cold Spring Harbor perspectives in biology*, 2 (5):a000182-a000182.
- Gilmore-Lab. Boston University. NF-kB Target Genes: <https://www.bu.edu/nf-kb/gene-resources/target-genes/> (September 2021).
- Gore RM. 1992. Colonic Contour Changes in Chronic Ulcerative-Colitis - Reappraisal of Some Old Concepts. *American Journal of Roentgenology*, 158 (1):59-61.
- Gottlieb TA, Ivanov IE, Adesnik M, Sabatini DD. 1993. Actin microfilaments play a critical role in endocytosis at the apical but not the basolateral surface of polarized epithelial cells. *J Cell Biol*, 120:695-710.
- Guo JF, Fisher KA, Darcy R, Cryan JF, O'Driscoll C. 2010. Therapeutic targeting in the silent era: advances in non-viral siRNA delivery. *Molecular Biosystems*, 6 (7):1143-1161.
- Gurcan S, Tsapis N, Reynaud F, Denis S, Vergnaud J, Ozer O, Fattal E. 2021. Combining dexamethasone and TNF-alpha siRNA within the same nanoparticles to enhance anti-inflammatory effect. *International Journal of Pharmaceutics*, 598:9.
- Hashizume M, Higuchi Y, Uchiyama Y, Mihara M. 2011. IL-6 plays an essential role in neutrophilia under inflammation. *Cytokine*, 54 (1):92-99.
- Hattori Y, Hattori K, Suzuki T, Matsuda N. 2017. Recent advances in the pathophysiology and molecular basis of sepsis-associated organ dysfunction: Novel therapeutic implications and challenges. *Pharmacol Ther*, 177:56-66.
- Hayden MS, Ghosh S. 2008. Shared principles in NF-kappaB signaling. *Cell*, 132 (3):344-362.

- He Q, Mitchell A, Morcol T, Bell SJD. 2002. Calcium phosphate nanoparticles induce mucosal immunity and protection against herpes simplex virus type 2. *Clinical and Diagnostic Laboratory Immunology*, 9 (5):1021-1024.
- Headland SE, Norling LV. 2015. The resolution of inflammation: Principles and challenges. *Semin Immunol*, 27 (3):149-160.
- Hendy GN, Canaff L. 2016. Calcium-sensing receptor, proinflammatory cytokines and calcium homeostasis. *Seminars in Cell & Developmental Biology*, 49:37-43.
- Hmar EL, Paul S, Boruah N, Sarkar P, Borah S, Sharma HK. 2021. Apprehending Ulcerative Colitis Management With Springing Up Therapeutic Approaches: Can Nanotechnology Play a Nascent Role? *Current Pathobiology Reports*, 9 (1):9-32.
- Hoet PH, Brüske-Hohlfeld I, Salata OV. 2004. Nanoparticles - known and unknown health risks. *J Nanobiotechnology*, 2 (1):12.
- Hu B, Zhong L, Weng Y, Peng L, Huang Y, Zhao Y, Liang X-J. 2020. Therapeutic siRNA: state of the art. *Signal Transduction and Targeted Therapy*, 5 (1):101.
- Huang KW, Hsu FF, Qiu JTT, Chern GJ, Lee YA, Chang CC, Huang YT, Sung YC, Chiang CC, Huang RL, Lin CC, Dinh TK, Huang HC, Shih YC, Alson D, Lin CY, Lin YC, Chang PC, Lin SY, Chen YC. 2020. Highly efficient and tumor-selective nanoparticles for dual-targeted immunogene therapy against cancer. *Science Advances*, 6 (3):13.
- Huang Y, Guo J, Gui S. 2018. Orally targeted galactosylated chitosan poly(lactic-co-glycolic acid) nanoparticles loaded with TNF- $\alpha$  siRNA provide a novel strategy for the experimental treatment of ulcerative colitis. *Eur J Pharm Sci*, 125:232-243.
- Hume DA. 2006. The mononuclear phagocyte system. *Curr Opin Immunol*, 18 (1):49-53.
- Ivanov AI. 2008. Exocytosis and endocytosis. Preface. *Methods Mol Biol*, 440:v-vi.
- Ivanova AV, Nikitin AA, Gabashvily AN, Vishnevskiy DA, Abakumov MA. 2021. Synthesis and intensive analysis of antibody labeled single core magnetic nanoparticles for targeted delivery to the cell membrane. *Journal of Magnetism and Magnetic Materials*, 521.
- Jennings C, Kusler B, Jones PP. 2009. Calcineurin inactivation leads to decreased responsiveness to LPS in macrophages and dendritic cells and protects against LPS-induced toxicity in vivo. *Innate Immun*, 15 (2):109-120.
- Jess T, Rungoe C, Peyrin-Biroulet L. 2012. Risk of colorectal cancer in patients with ulcerative colitis: a meta-analysis of population-based cohort studies. *Clin Gastroenterol Hepatol*, 10 (6):639-645.
- Jinek M, Doudna JA. 2009. A three-dimensional view of the molecular machinery of RNA interference. *Nature*, 457 (7228):405-412.
- Kaileh M, Sen R. 2012. NF-kappa B function in B lymphocytes. *Immunological Reviews*, 246:254-271.
- Kanasty RL, Whitehead KA, Vegas AJ, Anderson DG. 2012. Action and reaction: the biological response to siRNA and its delivery vehicles. *Mol Ther*, 20 (3):513-524.
- Kastl L, Sasse D, Wulf V, Hartmann R, Mircheski J, Ranke C, Carregal-Romero S, Martínez-López JA, Fernández-Chacón R, Parak WJ, Elsasser H-P, Rivera\_Gil P. 2013. Multiple Internalization Pathways of Polyelectrolyte Multilayer Capsules into Mammalian Cells. *ACS Nano*, 7 (8):6605-6618.
- Kim DH, Rossi JJ. 2007. Strategies for silencing human disease using RNA interference. *Nat Rev Genet*, 8 (3):173-184.
- Kim SH, Lee W, Kwon D, Lee S, Son SW, Seo M-S, Kim KS, Lee Y-H, Kim S, Jung Y-S. 2020. Metabolomic Analysis of the Liver of a Dextran Sodium Sulfate-Induced Acute Colitis Mouse Model: Implications of the Gut-Liver Connection. *Cells*, 9 (2):341.
- Kim SS, Ye C, Kumar P, Chiu I, Subramanya S, Wu H, Shankar P, Manjunath N. 2010. Targeted delivery of siRNA to macrophages for anti-inflammatory treatment. *Mol Ther*, 18 (5):993-1001.
- Kircheis R, Haasbach E, Lueftenegger D, Heyken WT, Ocker M, Planz O. 2020. NF-kappa B Pathway as a Potential Target for Treatment of Critical Stage COVID-19 Patients. *Frontiers in Immunology*, 11:11.

- Kishimoto T. 2006. Interleukin-6: discovery of a pleiotropic cytokine. *Arthritis Res Ther*, 8 Suppl 2 (Suppl 2):S2.
- Kitajima S, Takuma S, Morimoto M. 2000. Histological analysis of murine colitis induced by dextran sulfate sodium of different molecular weights. *Exp Anim*, 49 (1):9-15.
- Kolachala VL, Bajaj R, Wang L, Yan Y, Ritzenthaler JD, Gewirtz AT, Roman J, Merlin D, Sitaraman SV. 2007. Epithelial-derived Fibronectin Expression, Signaling, and Function in Intestinal Inflammation \*. *Journal of Biological Chemistry*, 282 (45):32965-32973.
- Kolios G, Valatas V, Ward SG. 2004. Nitric oxide in inflammatory bowel disease: a universal messenger in an unsolved puzzle. *Immunology*, 113 (4):427-437.
- Kollenda SA, Klose J, Knuschke T, Sokolova V, Schmitz J, Staniszewska M, Costa PF, Herrmann K, Westendorf AM, Fendler WP, Epple M. 2020. In vivo biodistribution of calcium phosphate nanoparticles after intravascular, intramuscular, intratumoral, and soft tissue administration in mice investigated by small animal PET/CT. *Acta Biomaterialia*, 109:244-253.
- Kooij IA, Sahami S, Meijer SL, Buskens CJ, Te Velde AA. 2016. The immunology of the vermiform appendix: a review of the literature. *Clin Exp Immunol*, 186 (1):1-9.
- Kopp E, Ghosh S. 1994. Inhibition of NF-kappa B by sodium salicylate and aspirin. *Science*, 265 (5174):956-959.
- Kopp M, Aufderhorst UW, Alt M, Dittmer U, Eis-Hubinger AM, Giebel B, Roggendorf M, Epple M, Krawczyk A. 2018. Induction of herpes simplex virus type 1 cell-to-cell spread inhibiting antibodies by a calcium phosphate nanoparticle-based vaccine. *Nanomedicine*, 16:138-148.
- Kozlova D, Chernousova S, Knuschke T, Buer J, Westendorf AM, Epple M. 2012. Cell targeting by antibody-functionalized calcium phosphatnanoparticles. *J Mater Chem*, 22 (2):396-404.
- Kriegstein CF, Cerwinka WH, Laroux FS, Grisham MB, Schurmann G, Bruwer M, Granger DN. 2001. Role of appendix and spleen in experimental colitis. *Journal of Surgical Research*, 101 (2):166-175.
- Kuhn KA, Manieri NA, Liu TC, Stappenbeck TS. 2014. IL-6 Stimulates Intestinal Epithelial Proliferation and Repair after Injury. *Plos One*, 9 (12).
- Lamaze C, Fujimoto LM, Yin HL, Schmid SL. 1997. The actin cytoskeleton is required for receptor-mediated endocytosis in mammalian cells. *J Biol Chem*, 272:20332-20335.
- Landgraf L, Müller I, Ernst P, Schäfer M, Rosman C, Schick I, Köhler O, Oehring H, Breus VV, Basché T, Sönnichsen C, Tremel W, Hilger I. 2015. Comparative evaluation of the impact on endothelial cells induced by different nanoparticle structures and functionalization. *Beilstein Journal of Nanotechnology*, 6:300-312.
- Layek B, Singh J. 2019. Editorial of Special Issue "Surface-Functionalized Nanoparticles as Drug Carriers". *International Journal of Molecular Sciences*, 20 (24):5.
- Lee G-S, Subramanian N, Kim AI, Aksentijevich I, Goldbach-Mansky R, Sacks DB, Germain RN, Kastner DL, Chae JJ. 2012. The calcium-sensing receptor regulates the NLRP3 inflammasome through Ca<sup>2+</sup> and cAMP. *Nature*, 492 (7427):123-127.
- Lee NK, Wang CPJ, Lim J, Park W, Kwon HK, Kim SN, Kim TH, Park CG. 2021a. Impact of the conjugation of antibodies to the surfaces of polymer nanoparticles on the immune cell targeting abilities. *Nano Convergence*, 8 (1).
- Lee RC, Feinbaum RL, Ambros V. 1993. The C-Elegans Heterochronic Gene Lin-4 Encodes Small Rnas with Antisense Complementarity to Lin-14. *Cell*, 75 (5):843-854.
- Lee S, Shin HJ, Noh C, Kim SI, Ko YK, Lee SY, Lim C, Hong B, Yang SY, Kim DW, Lee WH, Kim YH. 2021b. IKBKB siRNA-Encapsulated Poly (Lactic-co-Glycolic Acid) Nanoparticles Diminish Neuropathic Pain by Inhibiting Microglial Activation. *International Journal of Molecular Sciences*, 22 (11):13.
- Levine BL, Mosca JD, Riley JL, Carroll RG, Vahey MT, Jagodzinski LL, Wagner KF, Mayers DL, Burke DS, Weislow OS, St. Louis DC, June CH. 1996. Antiviral Effect and Ex Vivo CD4<sup>+</sup> T Cell Proliferation in HIV-Positive Patients as a Result of CD28 Costimulation. *Science*, 272 (5270):1939.



- Levingstone TJ, Herbaj S, Dunne NJ. 2019. Calcium Phosphate Nanoparticles for Therapeutic Applications in Bone Regeneration. *Nanomaterials*, 9 (11):22.
- Li CX, Parker A, Menocal E, Xiang S, Borodyansky L, Fruehauf JH. 2006. Delivery of RNA interference. *Cell Cycle*, 5 (18):2103-2109.
- Li M, Wu Y, Hu Y, Zhao L, Zhang C. 2018. Initial gut microbiota structure affects sensitivity to DSS-induced colitis in a mouse model. *Sci China Life Sci*, 61 (7):762-769.
- Li MS, Zhao PX, Fan T, Chen Y, Zhang XJ, He CC, Yang T, Lee RJ, Khan MW, Raza SM, Ma X, Lu Y, Xiang GY. 2019. Biocompatible co-loading vehicles for delivering both nanoplatin cores and siRNA to treat hepatocellular carcinoma. *International Journal of Pharmaceutics*, 572:9.
- Lim KS, Yong ZWE, Wang HJ, Tan TZ, Huang RYJ, Yamamoto D, Inaki N, Hazawa M, Wong RW, Oshima H, Oshima M, Ito Y, Voon DCC. 2020. Inflammatory and mitogenic signals drive interleukin 23 subunit alpha (IL23A) secretion independent of IL12B in intestinal epithelial cells. *Journal of Biological Chemistry*, 295 (19):6387-6400.
- Liu F, Wang CF, Gao YT, Li X, Tian F, Zhang YT, Fu MY, Li PF, Wang YL, Wang F. 2018. Current Transport Systems and Clinical Applications for Small Interfering RNA (siRNA) Drugs. *Molecular Diagnosis & Therapy*, 22 (5):551-569.
- Liu GG, Xu JJ, Wu H, Sun DL, Zhang XQ, Zhu XP, Magez S, Shi MQ. 2015. IL-27 Signaling Is Crucial for Survival of Mice Infected with African Trypanosomes via Preventing Lethal Effects of CD4(+) T Cells and IFN-gamma. *Plos Pathogens*, 11 (7).
- Liu H, Yang J, Yuan Y, Xia Z, Chen M, Xie L, Ma X, Wang J, Ouyang S, Wu Q, Yu F, Zhou X, Yang Y, Cao Y, Hu J, Yin B. 2014. Regulation of Mcl-1 by constitutive activation of NF-kappaB contributes to cell viability in human esophageal squamous cell carcinoma cells. *BMC Cancer*, 14:98.
- Liu T, Zhang L, Joo D, Sun SC. 2017. NF-kappaB signaling in inflammation. *Signal Transduct Target Ther*, 2.
- Liu X, Sun JA. 2010. Endothelial cells dysfunction induced by silica nanoparticles through oxidative stress via JNK/P53 and NF-kappa B pathways. *Biomaterials*, 31 (32):8198-8209.
- Lourenco BN, Pereira RF, Barrias CC, Fischbach C, Oliveira C, Granja PL. 2021. Engineering Modular Half-Antibody Conjugated Nanoparticles for Targeting CD44v6-Expressing Cancer Cells. *Nanomaterials*, 11 (2).
- Lu M, Zhang QP, Deng M, Miao J, Guo YH, Gao W, Cui QH. 2008. An Analysis of Human MicroRNA and Disease Associations. *Plos One*, 3 (10).
- MacFarlane LA, Murphy PR. 2010. MicroRNA: Biogenesis, Function and Role in Cancer. *Current Genomics*, 11 (7):537-561.
- Malhotra S, Kovats S, Zhang W, Coggeshall KM. 2009. B cell antigen receptor endocytosis and antigen presentation to T cells require Vav and dynamin. *J Biol Chem*, 284:24088-24097.
- Manicassamy S, Manoharan I. 2014. Mouse Models of Acute and Chronic Colitis. *Mouse Genetics: Methods and Protocols*, 1194:437-448.
- Martens TF, Remaut K, Demeester J, De Smedt SC, Braeckmans K. 2014. Intracellular delivery of nanomaterials: How to catch endosomal escape in the act. *Nano Today*, 9 (3):344-364.
- Martín I, Teixidó M, Giralt E. 2011. Design, Synthesis and Characterization of a New Anionic Cell-Penetrating Peptide: SAP(E). *ChemBioChem*, 12 (6):896-903.
- Masferrer JL, Zweifel BS, Manning PT, Hauser SD, Leahy KM, Smith WG, Isakson PC, Seibert K. 1994. Selective inhibition of inducible cyclooxygenase 2 in vivo is antiinflammatory and nonulcerogenic. *Proc Natl Acad Sci U S A*, 91 (8):3228-3232.
- Matricon J, Barnich N, Ardid D. 2010. Immunopathogenesis of inflammatory bowel disease. *Self/nonself*, 1 (4):299-309.
- Matsushita M, Takakuwa H, Matsubayashi Y, Nishio A, Ikehara S, Okazaki K. 2005. Appendix is a priming site in the development of ulcerative colitis. *World Journal of Gastroenterology*, 11 (31):4869-4874.

- McElrath C, Espinosa V, Lin JD, Peng JY, Sridhar R, Dutta O, Tseng HC, Smirnov SV, Risman H, Sandoval MJ, Davra V, Chang YJ, Pollack BP, Birge RB, Galan M, Rivera A, Durbin JE, Kotenko SV. 2021. Critical role of interferons in gastrointestinal injury repair. *Nature Communications*, 12 (1).
- Meyer-Kirchrath J, Schrör K. 2000. Cyclooxygenase-2 inhibition and side-effects of non-steroidal anti-inflammatory drugs in the gastrointestinal tract. *Curr Med Chem*, 7 (11):1121-1129.
- Mizoguchi A. 2012. Animal Models of Inflammatory Bowel Disease. In: Conn PM, Hrsg. *Progress in Molecular Biology and Translational Science*. Academic Press, 263-320.
- Mohamadzadeh M, DeGrendele H, Arizpe H, Estess P, Siegelman M. 1998. Proinflammatory stimuli regulate endothelial hyaluronan expression and CD44/HA-dependent primary adhesion. *Journal of Clinical Investigation*, 101 (1):97-108.
- Moolenbeek C, Ruitenber EJ. 1981. The Swiss Roll - a Simple Technique for Histological Studies of the Rodent Intestine. *Laboratory Animals*, 15 (1):57-59.
- Mörbe UM, Jørgensen PB, Fenton TM, von Burg N, Riis LB, Spencer J, Agace WW. 2021. Human gut-associated lymphoid tissues (GALT); diversity, structure, and function. *Mucosal Immunology*, 14 (4):793-802.
- Mortimer GM, Butcher NJ, Musumeci AW, Deng ZJ, Martin DJ, Minchin RF. 2014. Cryptic epitopes of albumin determine mononuclear phagocyte system clearance of nanomaterials. *ACS Nano*, 8:3357-3366.
- Mussbacher M, Salzmann M, Brostjan C, Hoesel B, Schoergenhofer C, Datler H, Hohensinner P, Basilio J, Petzelbauer P, Assinger A, Schmid JA. 2019. Cell Type-Specific Roles of NF-kappaB Linking Inflammation and Thrombosis. *Front Immunol*, 10:85.
- Nazarenus M, Zhang Q, Soliman MG, del Pino P, Pelaz B, Carregal-Romero S, Rejman J, Rothen-Rutishauser B, Cliff MJD, Zellner R, Nienhaus GU, Delehanty JB, Medintz IL, Parak WJ. 2014. In vitro interaction of colloidal nanoparticles with mammalian cells: What have we learned thus far? *Beilstein Journal of Nanotechnology*, 5:1477-1490.
- Neuhaus B, Tosun B, Rotan O, Frede A, Westendorf AM, Epple M. 2016. Nanoparticles as transfection agents: a comprehensive study with ten different cell lines. *Rsc Advances*, 6 (22):18102-18112.
- Neumann S, Kovtun A, Dietzel ID, Epple M, Heumann R. 2009. The use of size-defined DNA-functionalized calcium phosphate nanoparticles to minimise intracellular calcium disturbance during transfection. *Biomaterials*, 30 (35):6794-6802.
- Newton K, Dixit VM. 2012. Signaling in innate immunity and inflammation. *Cold Spring Harb Perspect Biol*, 4 (3).
- Nielsen OH, Gionchetti P, Ainsworth M, Vainer B, Campieri M, Borregaard N, Kjeldsen L. 1999. Rectal dialysate and fecal concentrations of neutrophil gelatinase-associated lipocalin, interleukin-8, and tumor necrosis factor-alpha in ulcerative colitis. *Am J Gastroenterol*, 94 (10):2923-2928.
- Nimesh S, Gupta N, Chandra R. 2011. Strategies and advances in nanomedicine for targeted siRNA delivery. *Nanomedicine (Lond)*, 6 (4):729-746.
- Notabi MK, Arnspang EC, Andersen MO. 2021. Antibody conjugated lipid nanoparticles as a targeted drug delivery system for hydrophobic pharmaceuticals. *European Journal of Pharmaceutical Sciences*, 161.
- Oba M, Aoyagi K, Miyata K, Matsumoto Y, Itaka K, Nishiyama N, Yamasaki Y, Koyama H, Kataoka K. 2008. Polyplex Micelles with Cyclic RGD Peptide Ligands and Disulfide Cross-Links Directing to the Enhanced Transfection via Controlled Intracellular Trafficking. *Molecular Pharmaceutics*, 5 (6):1080-1092.
- Oh H, Ghosh S. 2013. NF-κB: roles and regulation in different CD4(+) T-cell subsets. *Immunological reviews*, 252 (1):41-51.
- Pai S, Thomas R. 2008. Immune deficiency or hyperactivity-Nf-kappab illuminates autoimmunity. *J Autoimmun*, 31 (3):245-251.

- Parhiz H, Khoshnejad M, Myerson JW, Hood E, Patel PN, Brenner JS, Muzykantov VR. 2018. Unintended effects of drug carriers: Big issues of small particles. *Advanced Drug Delivery Reviews*, 130:90-112.
- Parikh AA, Moon MR, Pritts TA, Fischer JE, Szabo C, Hasselgren PO, Salzman AL. 2000. IL-1 beta induction of NF-kappa B activation in human intestinal epithelial cells is independent of oxyradical signaling. *Shock*, 13 (1):8-13.
- Pasparakis M. 2008. IKK/NF- $\kappa$ B signaling in intestinal epithelial cells controls immune homeostasis in the gut. *Mucosal Immunology*, 1 (1):S54-S57.
- Patel S, Kim J, Herrera M, Mukherjee A, Kabanov AV, Sahay G. 2019. Brief update on endocytosis of nanomedicines. *Advanced Drug Delivery Reviews*, 144:90-111.
- Pelaz B, Alexiou C, Alvarez-Puebla RA, Alves F, Andrews AM, Ashraf S, Balogh LP, Ballerini L, Bestetti A, Brendel C, Bosi S, Carril M, Chan WCW, Chen C, Chen X, Chen X, Cheng Z, Cui D, Du J, Dullin C, Escudero A, Feliu N, Gao M, George M, Gogotsi Y, Grünweller A, Gu Z, Halas NJ, Hampp N, Hartmann RK, Hersam MC, Hunziker P, Jian J, Jiang X, Jungebluth P, Kadhiresan P, Kataoka K, Khademhosseini A, Kopeček J, Kotov NA, Krug HF, Lee DS, Lehr C-M, Leong KW, Liang X-J, Ling Lim M, Liz-Marzán LM, Ma X, Macchiarini P, Meng H, Möhwald H, Mulvaney P, Nel AE, Nie S, Nordlander P, Okano T, Oliveira J, Park TH, Penner RM, Prato M, Puntès V, Rotello VM, Samarakoon A, Schaak RE, Shen Y, Sjöqvist S, Skirtach AG, Soliman MG, Stevens MM, Sung H-W, Tang BZ, Tietze R, Udugama BN, VanEpps JS, Weil T, Weiss PS, Willner I, Wu Y, Yang L, Yue Z, Zhang Q, Zhang Q, Zhang X-E, Zhao Y, Zhou X, Parak WJ. 2017. Diverse Applications of Nanomedicine. *ACS Nano*, 11 (3):2313-2381.
- Perše M, Cerar A. 2012. Dextran Sodium Sulphate Colitis Mouse Model: Traps and Tricks. *Journal of Biomedicine and Biotechnology*, 2012:718617.
- Pfaffl MW. 2001. A new mathematical model for relative quantification in real-time RT-PCR. *Nucleic Acids Research*, 29 (9).
- Raab RM, Stephanopoulos G. 2004. Dynamics of gene silencing by RNA interference. *Biotechnology and Bioengineering*, 88 (1):121-132.
- Raffatellu M, George MD, Akiyama Y, Hornsby MJ, Nuccio S-P, Paixao TA, Butler BP, Chu H, Santos RL, Berger T, Mak TW, Tsolis RM, Bevins CL, Solnick JV, Dandekar S, Bäumlér AJ. 2009. Lipocalin-2 resistance confers an advantage to *Salmonella enterica* serotype Typhimurium for growth and survival in the inflamed intestine. *Cell host & microbe*, 5 (5):476-486.
- Ramadass V, Vaiyapuri T, Tergaonkar V. 2020. Small Molecule NF- $\kappa$ B Pathway Inhibitors in Clinic. *International journal of molecular sciences*, 21 (14):5164.
- Rana SV, Sharma S, Kaur J, Prasad KK, Sinha SK, Kochhar R, Malik A, Morya RK. 2014. Relationship of cytokines, oxidative stress and GI motility with bacterial overgrowth in ulcerative colitis patients. *Journal of Crohns & Colitis*, 8 (8):859-865.
- Rauch DA, Harding JC, Ratner L, Wickline SA, Pan H. 2021. Targeting NF-kappa B with Nanotherapy in a Mouse Model of Adult T-Cell Leukemia/Lymphoma. *Nanomaterials*, 11 (6):15.
- Ren T, Tian T, Feng X, Ye S, Wang H, Wu W, Qiu Y, Yu C, He Y, Zeng J, Cen J, Zhou Y. 2015. An adenosine A3 receptor agonist inhibits DSS-induced colitis in mice through modulation of the NF- $\kappa$ B signaling pathway. *Scientific reports*, 5:9047.
- Rosenblat JD, Cha DS, Mansur RB, McIntyre RS. 2014. Inflamed moods: a review of the interactions between inflammation and mood disorders. *Prog Neuropsychopharmacol Biol Psychiatry*, 53:23-34.
- Rossol M, Pierer M, Raulien N, Quandt D, Meusch U, Rothe K, Schubert K, Schöneberg T, Schaefer M, Krügel U, Smajilovic S, Bräuner-Osborne H, Baerwald C, Wagner U. 2012. Extracellular Ca<sup>2+</sup> is a danger signal activating the NLRP3 inflammasome through G protein-coupled calcium sensing receptors. *Nature Communications*, 3 (1):1329.
- Rotan O, Severin KN, Popsel S, Peetsch A, Merdanovic M, Ehrmann M, Epple M. 2017. Uptake of the proteins HTRA1 and HTRA2 by cells mediated by calcium phosphate nanoparticles. *Beilstein J Nanotechnol*, 8:381-393.

- Ruparelia N, Chai JT, Fisher EA, Choudhury RP. 2017. Inflammatory processes in cardiovascular disease: a route to targeted therapies. *Nat Rev Cardiol*, 14 (3):133-144.
- Sandor M, Lynch RG. 1993. Lymphocyte Fc-Receptors - the Special Case of T-Cells. *Immunology Today*, 14 (5):227-231.
- Sasaoka T, Ito M, Yamashita J, Nakajima K, Tanaka I, Narita M, Hara Y, Hada K, Takahashi M, Ohno Y, Matsuo T, Kaneshiro Y, Tanaka H, Kaneko K. 2011. Treatment with IL-27 attenuates experimental colitis through the suppression of the development of IL-17-producing T helper cells. *American Journal of Physiology-Gastrointestinal and Liver Physiology*, 300 (4):G568-G576.
- Sato S, Sanjo H, Takeda K, Ninomiya-Tsuji J, Yamamoto M, Kawai T, Matsumoto K, Takeuchi O, Akira S. 2005. Essential function for the kinase TAK1 in innate and adaptive immune responses. *Nature Immunology*, 6 (11):1087-1095.
- Scatena M, Almeida M, Chaisson ML, Fausto N, Nicosia RF, Giachelli CM. 1998. NF- $\kappa$ B Mediates  $\alpha\beta$ 3 Integrin-induced Endothelial Cell Survival. *The Journal of Cell Biology*, 141 (4):1083-1093.
- Schmitz ML, Baeuerle PA. 1991. The p65 subunit is responsible for the strong transcription activating potential of NF-kappaB. *The EMBO Journal*, 10 (12):3805 - 3817.
- Schraa AJ, Kok RJ, Berendsen AD, Moorlag HE, Bos EJ, Meijer DKF, de Leij LFMH, Molema G. 2002. Endothelial cells internalize and degrade RGD-modified proteins developed for tumor vasculature targeting. *Journal of Controlled Release*, 83 (2):241-251.
- Schreiber S, Nikolaus S, Hampe J. 1998. Activation of nuclear factor kappa B inflammatory bowel disease. *Gut*, 42 (4):477-484.
- Schwarz DS, Hutvagner G, Du T, Xu ZS, Aronin N, Zamore PD. 2003. Asymmetry in the assembly of the RNAi enzyme complex. *Cell*, 115 (2):199-208.
- Sehnert B, Burkhardt H, Dübel S, Voll RE. 2020. Cell-Type Targeted NF-kappaB Inhibition for the Treatment of Inflammatory Diseases. *Cells*, 9 (7):1627.
- Senftleben U, Cao YX, Xiao GT, Greten FR, Krahn G, Bonizzi G, Chen Y, Hu YL, Fong A, Sun SC, Karin M. 2001. Activation by IKK alpha of a second, evolutionary conserved, NF-kappa B signaling pathway. *Science*, 293 (5534):1495-1499.
- Serhan CN. 2009. Systems approach to inflammation resolution: identification of novel anti-inflammatory and pro-resolving mediators. *J Thromb Haemost*, 7 Suppl 1:44-48.
- Setten RL, Rossi JJ, Han SP. 2019. The current state and future directions of RNAi-based therapeutics. *Nat Rev Drug Discov*, 18 (6):421-446.
- Shabalina SA, Koonin EV. 2008. Origins and evolution of eukaryotic RNA interference. *Trends in Ecology & Evolution*, 23 (10):578-587.
- Shah AK, Agnihotri SA. 2011. Recent advances and novel strategies in pre-clinical formulation development: An overview. *Journal of Controlled Release*, 156 (3):281-296.
- Sokolova V, Knuschke T, Kovtun A, Buer J, Epple M, Westendorf AM. 2010. The use of calcium phosphate nanoparticles encapsulating toll-like receptor ligands and the antigen hemagglutinin to induce dendritic cell maturation and T cell activation. *Biomaterials*, 31:5627-5633.
- Sokolova V, Kozlova D, Knuschke T, Buer J, Westendorf AM, Epple M. 2013. Mechanism of the uptake of cationic and anionic calcium phosphate nanoparticles by cells. *Acta Biomater*, 9 (7):7527-7535.
- Song YJ, Li Y, Xiao Y, Hu WG, Wang X, Wang P, Zhang XR, Yang JC, Huang Y, He WF, Huang CB. 2019. Neutralization of interleukin-17A alleviates burn-induced intestinal barrier disruption via reducing pro-inflammatory cytokines in a mouse model. *Burns & Trauma*, 7 (1).
- Sugimoto MA, Sousa LP, Pinho V, Perretti M, Teixeira MM. 2016. Resolution of Inflammation: What Controls Its Onset? *Front Immunol*, 7:160.
- Sun SC. 2011. Non-canonical NF-kappaB signaling pathway. *Cell Res*, 21 (1):71-85.
- Szelenyi I. 2012. Nanomedicine: evolutionary and revolutionary developments in the treatment of certain inflammatory diseases. *Inflamm Res*, 61 (1):1-9.

- Tabas I, Garcia-Cardena G, Owens GK. 2015. Recent insights into the cellular biology of atherosclerosis. *J Cell Biol*, 209 (1):13-22.
- Taeb AM, Hooper MH, Marik PE. 2017. Sepsis: Current Definition, Pathophysiology, Diagnosis, and Management. *Nutr Clin Pract*, 32 (3):296-308.
- Tatiparti K, Sau S, Kashaw SK, Iyer AK. 2017. siRNA Delivery Strategies: A Comprehensive Review of Recent Developments. *Nanomaterials*, 7 (4).
- Temming K, Lacombe M, van der Hoeven P, Prakash J, Gonzalo T, Dijkers ECF, Orfi L, Keri G, Poelstra K, Molema G, Kok RJ. 2006. Delivery of the p38 MAPkinase inhibitor SB202190 to angiogenic endothelial cells: Development of novel RGD-equipped and PEGylated drug - Albumin conjugates using platinum(II)-based drug linker technology. *Bioconjugate Chemistry*, 17 (5):1246-1255.
- Tenkumo T, Rojas-Sanchez L, Saenz JRV, Ogawa T, Miyashita M, Yoda N, Prymak O, Sokolova V, Sasaki K, Epple M. 2020. Reduction of inflammation in a chronic periodontitis model in rats by TNF-alpha gene silencing with a topically applied siRNA-loaded calcium phosphate paste. *Acta Biomaterialia*, 105:263-279.
- Tian XH, Angioletti-Uberti S, Battaglia G. 2020. On the design of precision nanomedicines. *Science Advances*, 6 (4):11.
- Torres J, Mehandru S, Colombel JF, Peyrin-Biroulet L. 2017. Crohn's disease. *Lancet*, 389 (10080):1741-1755.
- Ungaro R, Mehandru S, Allen PB, Peyrin-Biroulet L, Colombel JF. 2017. Ulcerative colitis. *Lancet*, 389 (10080):1756-1770.
- Van Belle K, Herman J, Boon L, Waer M, Sprangers B, Louat T. 2016. Comparative In Vitro Immune Stimulation Analysis of Primary Human B Cells and B Cell Lines. *Journal of immunology research*, 2016:5281823-5281823.
- Velard F, Braux J, Amedee J, Laquerriere P. 2013. Inflammatory cell response to calcium phosphate biomaterial particles: An overview. *Acta Biomaterialia*, 9 (2):4956-4963.
- Vercauteren D, Vandenbroucke RE, Jones AT, Rejman J, Demeester J, De Smedt SC, Sanders NN, Braeckmans K. 2010. The use of inhibitors to study endocytic pathways of gene carriers: optimization and pitfalls. *Mol Ther*, 18:561-569.
- Voigt J, Christensen J, Shastri VP. 2014. Differential uptake of nanoparticles by endothelial cells through polyelectrolytes with affinity for caveolae. *Proc Natl Acad Sci USA*, 111:2942-2947.
- Wang J, Lu Z, Wientjes MG, Au JL. 2010. Delivery of siRNA therapeutics: barriers and carriers. *Aaps j*, 12 (4):492-503.
- Wang LH, Rothberg KG, Anderson RG. 1993. Mis-assembly of clathrin lattices on endosomes reveals a regulatory switch for coated pit formation. *J Cell Biol*, 123:1107-1117.
- Wang YF, Wu QS, Wang JD, Li L, Sun X, Zhang ZR, Zhang L. 2020. Co-delivery of p38 alpha MAPK and p65 siRNA by novel liposomal glomerulus-targeting nano carriers for effective immunoglobulin a nephropathy treatment. *Journal of Controlled Release*, 320:457-468.
- Wang ZQ, Wang LC, Prabhakar N, Xing YX, Rosenholm JM, Zhang JX, Cai KY. 2019. CaP coated mesoporous polydopamine nanoparticles with responsive membrane permeation ability for combined photothermal and siRNA therapy. *Acta Biomaterialia*, 86:416-428.
- Weng YH, Huang QQ, Li CH, Yang YF, Wang XX, Yu J, Huang YY, Liang XJ. 2020. Improved Nucleic Acid Therapy with Advanced Nanoscale Biotechnology. *Molecular Therapy-Nucleic Acids*, 19:581-601.
- Whittem CG, Williams AD, Williams CS. 2010. Murine Colitis modeling using Dextran Sulfate Sodium (DSS). *J Vis Exp*, (35).
- Wiercinska-Drapalo A, Flisiak R, Prokopowicz D. 1999. Mucosal and plasma prostaglandin E2 in ulcerative colitis. *Hepato-Gastroenterology*, 46 (28):2338-2342.
- Wilson RC, Doudna JA. 2013. Molecular mechanisms of RNA interference. *Annu Rev Biophys*, 42:217-239.
- Wu JY, Wang ZX, Zhang G, Lu X, Qiang GH, Hu W, Ji AL, Wu JH, Jiang CP. 2018. Targeted co-delivery of Beclin 1 siRNA and FTY720 to hepatocellular carcinoma by

- calcium phosphate nanoparticles for enhanced anticancer efficacy. *International Journal of Nanomedicine*, 13:1265-1280.
- Wyss-Coray T, Rogers J. 2012. Inflammation in Alzheimer disease—a brief review of the basic science and clinical literature. *Cold Spring Harb Perspect Med*, 2 (1):a006346.
- Xia Y, Lin ZF, Li YH, Zhao MQ, Wang CB, Guo M, Zhang B, Zhu B. 2017. Targeted delivery of siRNA using RGDfC-conjugated functionalized selenium nanoparticles for anticancer therapy. *Journal of Materials Chemistry B*, 5 (33):6941-6952.
- Xiao W. 2004. Advances in NF-kappaB signaling transduction and transcription. *Cell Mol Immunol*, 1 (6):425-435.
- Xu X, Li Z, Zhao X, Keen L, Kong X. 2016. Calcium phosphate nanoparticles-based systems for siRNA delivery. *Regen Biomater*, 3 (3):187-195.
- Yang M, Zhang F, Yang CH, Wang LX, Sung J, Garg P, Zhang MZ, Merlin D. 2020. Oral Targeted Delivery by Nanoparticles Enhances Efficacy of an Hsp90 Inhibitor by Reducing Systemic Exposure in Murine Models of Colitis and Colitis-Associated Cancer. *Journal of Crohns & Colitis*, 14 (1):130-141.
- Yang YSS, Moynihan KD, Bekdemir A, Dichwalkar TM, Noh MM, Watson N, Melo M, Ingram J, Suh H, Ploegh H, Stellacci FR, Irvine DJ. 2019. Targeting small molecule drugs to T cells with antibody-directed cell-penetrating gold nanoparticles. *Biomaterials Science*, 7 (1):113-124.
- Yates LL, Gorecki DC. 2006. The nuclear factor-kappaB (NF-kappa B): from a versatile transcription factor to a ubiquitous therapeutic target. *Acta Biochimica Polonica*, 53 (4):651-662.
- Yoo JW, Chambers E, Mitragotri S. 2010. Factors that Control the Circulation Time of Nanoparticles in Blood: Challenges, Solutions and Future Prospects. *Current Pharmaceutical Design*, 16 (21):2298-2307.
- Zeyda M, Stulnig TM. 2009. Obesity, inflammation, and insulin resistance—a mini-review. *Gerontology*, 55 (4):379-386.
- Zhang J, Zhang HY, Jiang JQ, Cui N, Xue X, Wang TY, Wang XQ, He YP, Wang DK. 2020a. Doxorubicin-Loaded Carbon Dots Lipid-Coated Calcium Phosphate Nanoparticles for Visual Targeted Delivery and Therapy of Tumor. *International Journal of Nanomedicine*, 15:433-444.
- Zhang MM, Bahal R, Rasmussen TP, Manautou JE, Zhong XB. 2021. The growth of siRNA-based therapeutics: Updated clinical studies. *Biochem Pharmacol*, 189:114432.
- Zhang QF, Kuang GZ, Zhou DF, Qi YX, Wang MZ, Li XY, Huang YB. 2020b. Photoactivated polyprodrug nanoparticles for effective light-controlled Pt(IV) and siRNA codelivery to achieve synergistic cancer therapy. *Journal of Materials Chemistry B*, 8 (27):5903-5911.
- Zhang X, Bloch S, Akers W, Achilefu S. 2012. Near-infrared molecular probes for in vivo imaging. *Curr Protoc Cytom*, Chapter 12:Unit12.27.
- Zhao M, Gönczi L, Lakatos PL, Burisch J. 2021. The Burden of Inflammatory Bowel Disease in Europe in 2020. *Journal of Crohn's and Colitis*.
- Zhu C, Zhang S, Song C, Zhang Y, Ling Q, Hoffmann PR, Li J, Chen T, Zheng W, Huang Z. 2017. Selenium nanoparticles decorated with *Ulva lactuca* polysaccharide potentially attenuate colitis by inhibiting NF-kappaB mediated hyper inflammation. *J Nanobiotechnology*, 15 (1):20.
- Ziegler LS, Gerner MC, Schmidt RLJ, Trapin D, Steinberger P, Pickl WF, Sillaber C, Egger G, Schwarzwinger I, Schmetterer KG. 2021. Attenuation of canonical NF-kappa B signaling maintains function and stability of human Treg. *Febs Journal*, 288 (2):640-662.
- Zilker C, Kozlova D, Sokolova V, Yan H, Epple M, Uberla K, Temchura V. 2017. Nanoparticle-based B-cell targeting vaccines: Tailoring of humoral immune responses by functionalization with different TLR-ligands. *Nanomedicine*, 13 (1):173-182.
- Zu H, Gao DC. 2021. Non-viral Vectors in Gene Therapy: Recent Development, Challenges, and Prospects. *Aaps Journal*, 23 (4):12.

## Appendix

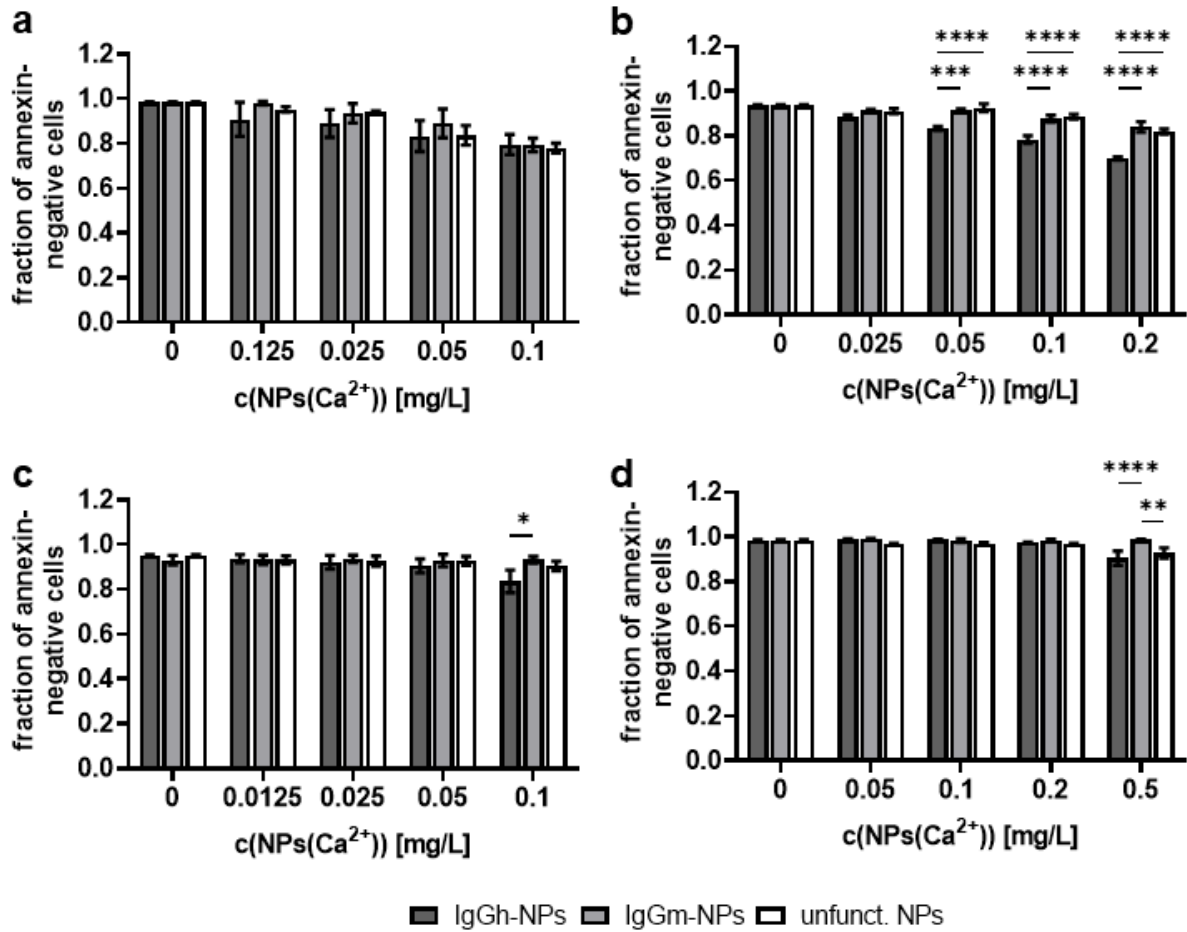


Figure A. 1: **Effects of the IgG-host species on the cytotoxicity of IgG-decorated nanoparticles.** B cells MOPC-315 (a), endothelial cells SVEC4-10 (b), monocytes J774A.1 (c) and T cells TK-1 (d) were incubated with nanoparticles decorated with unspecific Armenian hamster IgG (IgGh), murine IgG (IgGm) or undecorated NPs for 24 h prior to analysis by flow cytometry. Shown is the fraction of annexin-negative cells as the mean and SEM for 3 independent experiments with statistical differences between indicated groups (\*  $p < 0.05$ , \*\*  $p < 0.01$ , \*\*\*  $p < 0.001$ , \*\*\*\*  $p < 0.0001$ ).

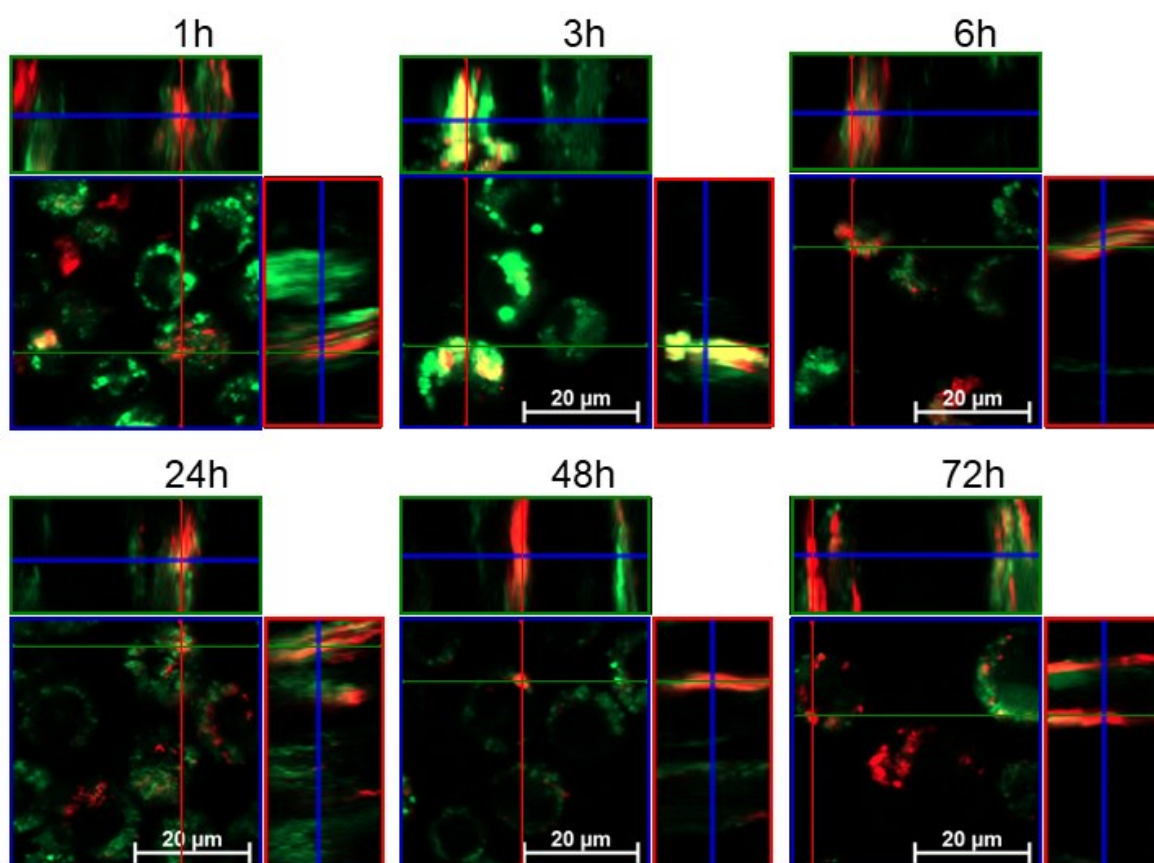


Figure A. 2: **Representative Z-stacks for the investigation of colocalization of nanoparticles with lysosomes** (Figure 8). J774A.1 cells were incubated with fluorescently labeled nanoparticles without cargo-peptide (0.5 mg/L Ca<sup>2+</sup>) for 1 – 72 h. Subsequently cells were stained with Lyso Tracker® Green DND-26 and Hoechst-33258. Living cells were directly analyzed by confocal laser scanning microscopy. red: Cy5 fluorescence (ex: 633 nm, em: 673 nm); blue: Hoechst fluorescence (ex: 405 nm; em: 450 nm); and green: Lyso-Tracker® Green DND-26 fluorescence (ex: 504 nm; em: 511 nm). Scale bar 20  $\mu$ m.

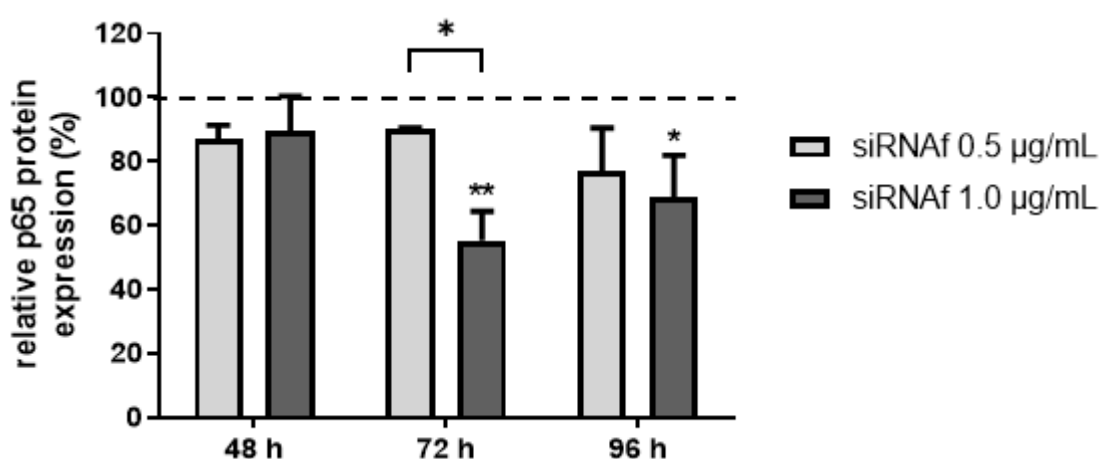


Figure A. 3: **Effect of siRNA concentration and incubation time on the efficiency of nanoparticles with incorporated NF- $\kappa$ B p65 siRNA in reversing p65 protein expression in inflamed monocytes.** J774A.1 cells were incubated with nanoparticles carrying different concentrations of siRNA for 48 to 96 h and stimulated with LPS. Protein expression of p65 was investigated relative to untreated cells. Shown is the mean with SEM from 3 independent experiments with statistical differences concerning the untreated control (100%) or between indicated groups (\*  $p < 0.05$ , \*\*  $p < 0.01$ ).



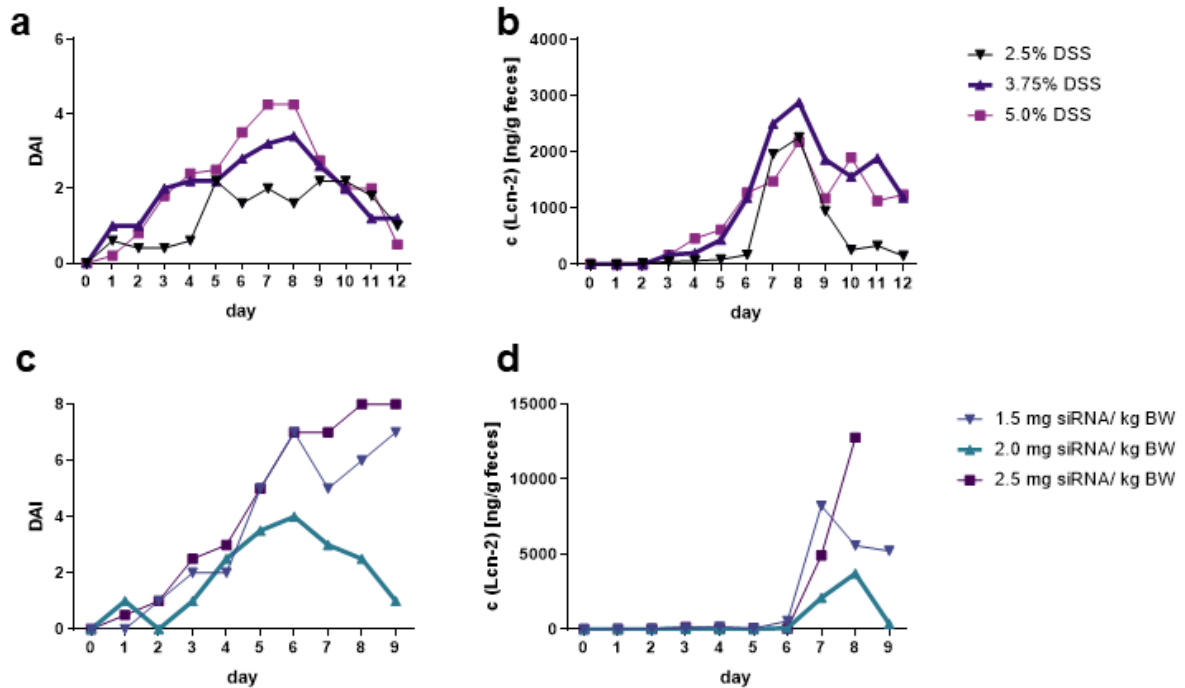


Figure A. 4: **Optimization of the murine DSS colitis model for investigating the efficiency of p65 siRNA-nanoparticles.** (a, b) Different DSS dosages (2.5%, 3.75%, or 5.0% (w/v)) were administered to mice ( $n = 5$ ) via drinking water for 6 days. DAI (a) and Lcn-2 levels in feces (b) were acquired every day for the observation time of 12 days. Shown is the mean of 5 mice. (c, d) Different siRNA-NP dosages (1.5, 2.0, 2.5 mg siRNA/ kg BW) were administered to mice via i.v. injection into the tail vein on day 3 while receiving 3.75% (w/v) DSS for the first 6 days. DAI (c) and Lcn-2 levels in feces (d) were acquired every day for the observation time of 9 days. Shown is the mean of 2 mice (exception 2.5 mg siRNA/ kg BW  $n = 1$ ). BW: body weight. DAI: disease activity index.

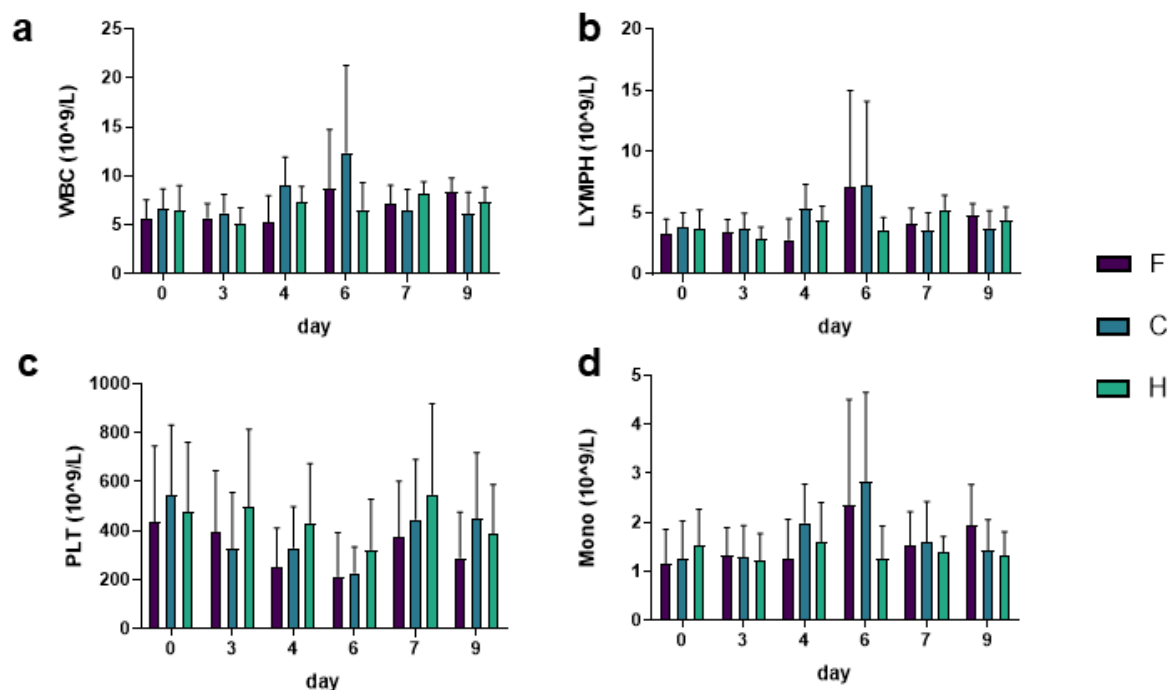


Figure A. 5: **Impact of F-NPs on the blood composition during the development of DSS-induced colitis in mice.** Mice were given 3.75% (w/v) DSS in drinking water for 6 days and F-NPs (2.0 mg siRNA/kg BW) were administered intravenously to the respective groups on day 3. F: F-NPs, colitis; C: no nanoparticles, colitis; H: no nanoparticles, healthy. Haemogram analyzed on indicated days. (a) white blood cell count. (b) lymphocyte count. (c) platelet count. (d) monocyte count. Shown is the mean and SD of 7 – 20 mice.

Table A. 1: **Detailed list of mice used for investigation of therapeutic efficiency of F-NPs.** Shown are the animal numbers per group for groups F (F-NPs, colitis), C (no nanoparticles, colitis), and H (no nanoparticles, healthy). 10 mice each group were originally planned for the study of short-term therapeutic efficiency (day 6) and 10 mice for the long-term investigations (day 9). Time-points where mice died during the experiments are indicated by \*.

DAY	0	1	2	3	4	5	6	7	8	9
F	20	20	20	20	15*	15	15	9	8*	8
C	20	20	20	20	20	20	20	9*	7*	7
H	20	20	20	20	20	20	20	10	10	10

Table A. 2: **Detailed list of mice used for investigation of side-effects of F-NPs.** Shown are the animal numbers per group for groups F (F-NPs, healthy), and H (no nanoparticles, healthy). 10 mice each group were originally planned for the long-term investigations (day 9). Group H is identical to the group for the study of therapeutic efficiency (see Table A. 1). Time-points where mice died during the experiments are indicated by \*.

DAY	0	1	2	3	4	5	6	7	8	9
F	10	10	10	10	7*	7	7	7	7	7
H	20	20	20	20	20	20	20	10	10	10

## Appendix

Table A. 3: **Detailed list of mice used for investigation of side-effects depending on type of siRNA incorporated into nanoparticles.** Shown are the animal numbers per group for groups S (S-NPs, colitis), and F (F-NPs, colitis). 10 mice each group were originally planned for the long-term investigations (day 9). Group H is identical to the group for the study of therapeutic efficiency (see Table A. 1). Time-points were mice died during the experiments are indicated by \*.

<b>DAY</b>	<b>0</b>	<b>1</b>	<b>2</b>	<b>3</b>	<b>4</b>	<b>5</b>	<b>6</b>	<b>7</b>	<b>8</b>	<b>9</b>
<b>S</b>	10	10	10	10	6*	6	6	6	6	6
<b>F</b>	20	20	20	20	15*	15	15	9	8*	8

## List of Figures

Figure 1: Scheme of the canonical NF- $\kappa$ B signaling pathway (own figure).....	8
Figure 2: Schematic depiction of the process of RNA interference (RNAi) (own figure). ....	11
Figure 3: Scheme for the application of calcium phosphate nanoparticles as transfection agents for siRNA against NF- $\kappa$ B p65 (own figure).....	14
Figure 4: Timeline of the procedure for in vivo experiments.....	37
Figure 5: Calcium phosphate nanoparticles (NPs) were readily taken up by most of the cells from the blood compartment while exhibiting low cytotoxicity effects.....	45
Figure 6: Uptake of IgG-decorated nanoparticles in target cells is mostly dependent on the IgG-host species. ....	46
Figure 7: Monocytes internalize nanoparticles via energy-dependent mechanisms and in parts by interplay of different endocytosis machineries.....	48
Figure 8: Nanoparticles are colocalized with lysosomes after internalization in monocytes and the cargo was released into the cytoplasm.....	49
Figure 9: Efficiency of nanoparticles with incorporated NF- $\kappa$ B p65 siRNA (F-NPs) in reversing p65 gene and protein expression on inflamed J774A.1 monocytes towards the non-inflamed condition. ....	51
Figure 10: Impact of the exposure of inflamed monocytes to NF- $\kappa$ B p65 siRNA-nanoparticles (F-NPs) on the secretion of pro- and anti-inflammatory mediators. ....	52
Figure 11: Target-specific nanoparticles with RGD-peptide (RGD-NPs) in endothelial cells (ECs).....	54
Figure 12: Target-specific nanoparticles decorated with CD69-IgG (CD69-NPs) and their impact on B cells. ....	56
Figure 13: Target-specific nanoparticles decorated with CD69-IgG (CD69-NPs) and their impact on T cells. ....	58
Figure 14: Effects of siRNA-loaded nanoparticles (F-NPs) on the development of DSS-induced colitis in mice.....	61
Figure 15: Short-term changes of macroscopic and histopathologic features of colitis upon treatment with F-NPs.....	62
Figure 16: Short-term impact of F-NPs on p65 NF- $\kappa$ B and related inflammatory mediators during colitis.....	64
Figure 17: Long-term changes of macroscopic and histopathologic features of colitis upon treatment with F-NPs.....	65
Figure 18: Long-term impact of F-NPs on p65 NF- $\kappa$ B and related inflammatory mediators during colitis.....	67

Figure 19: Biodistribution of nanoparticles in mice with colitis compared to healthy mice. ..68

Figure 20: Side-effects depending on the type of siRNA incorporated into the nanoparticles.  
..... 70

Figure 21: Side-effects of F-NPs on inflammatory processes in healthy mice. .... 71

Figure A. 1: Effects of the IgG-host species on the cytotoxicity of IgG-decorated nanoparticles. .... 104

Figure A. 2: Representative Z-stacks for the investigation of colocalization of nanoparticles with lysosomes (Figure 8). .... 105

Figure A. 3: Effect of siRNA concentration and incubation time on the efficiency of nanoparticles with incorporated NF-kB p65 siRNA in reversing p65 protein expression in inflamed monocytes. .... 105

Figure A. 4: Optimization of the murine DSS colitis model for investigating the efficiency of p65 siRNA-nanoparticles. .... 106

Figure A. 5: Impact of of F-NPs on the blood composition during the development of DSS-induced colitis in mice..... 107

## List of Tables

Table 1: Characteristics of nanoparticles for <i>in vitro</i> studies without decoration and with or without siRNA/ cargo peptide. ....	19
Table 2: Characteristics of nanoparticles for <i>in vitro</i> studies with cRGDfK peptide decoration and with or without siRNA to target endothelial cells. ....	20
Table 3: Characteristics of nanoparticles for <i>in vitro</i> studies with IgG decoration and without siRNA to target B cells and T cells. ....	20
Table 4: Characteristics of nanoparticles for <i>in vitro</i> studies with IgG decoration and with siRNA to target B cells and T cells. ....	21
Table 5: Characteristics of nanoparticles for <i>in vivo</i> studies without decoration and with or without siRNA. ....	21
Table 6: Used cell lines with origin and supplier. ....	22
Table 7: List of used equipment with supplier. ....	22
Table 8: List of consumption items with supplier. ....	23
Table 9: List of chemicals with supplier. ....	24
Table 10: Antibodies for Western Blot analyses, immunostainings, flow cytometric analyses, and other experiments with subtype/ clone, item number, LOT, and supplier. ....	27
Table 11: List of kits with supplier. ....	29
Table 12: List of buffers and solutions with composition and ingredients. ....	29
Table 13: Special software with supplier. ....	30
Table 14: Score parameters for the assessment of colitis. ....	38
Table 15: Dehydration steps using an automated tissue processor. ....	39
Table 16: Decreasing/ ascending alcoholic series: ....	39
Table 17: Histopathological scoring of H&E sections calculated by adding the scores of the listed parameters. ....	40
Table A. 1: Detailed list of mice used for investigation of therapeutic efficiency of F-NPs. ....	107
Table A. 2: Detailed list of mice used for investigation of side-effects of F-NPs. ....	107
Table A. 3: Detailed list of mice used for investigation of side-effects depending on type of siRNA incorporated into nanoparticles. ....	108

## Scientific publications and presentations

### Publications (peer-reviewed)

Białas N, **Müller EK**, Epple M, Hilger I. 2021. Silica-coated calcium phosphate nanoparticles for gene silencing of NF- $\kappa$ B p65 by siRNA and their impact on cellular players of inflammation. *Biomaterials*, 276:121013.

Gräfe C, **Müller EK**, Gresing L, Weidner A, Radon P, Friedrich RP, Alexiou C, Wiekhorst F, Dutz S, Clement JH. 2020. Magnetic hybrid materials interact with biological matrices. *Physical Sciences Reviews*.

Gawlitza AL, Speith J, Rinke J, Sajzew R, **Müller EK**, Schafer V, Hochhaus A, Ernst T. 2019. 5-Azacytidine modulates CpG methylation levels of EZH2 and NOTCH1 in myelodysplastic syndromes. *Journal of Cancer Research and Clinical Oncology*, 145 (11):2835-2843.

**Müller EK**, Grafe C, Wiekhorst F, Bergemann C, Weidner A, Dutz S, Clement JH. 2018. Magnetic Nanoparticles Interact and Pass an In Vitro Co-Culture Blood-Placenta Barrier Model. *Nanomaterials (Basel)*, 8 (2).

### Publications (submitted)

**Müller EK**, Białas N, Epple M, Hilger I. Gene silencing of NF- $\kappa$ B p65 in DSS-induced colitis in mice with calcium phosphate nanoparticles carrying siRNA. Submitted to *Nanoscale* 2021

**Müller EK**, Białas N, Epple M, Hilger I. Surface-decorated silica-coated calcium phosphate nanoparticles for siRNA-based gene silencing of NF- $\kappa$ B p65 in inflammatory cells. Submitted to *Biomacromolecules* 2021

(Poster) Presentations:

**Müller EK**, Białas N, Epple M, Hilger I. 2019. Cellular uptake and cytotoxicity of CaP-nanoparticles in immunological relevant cells. Tag der Nachwuchswissenschaftler des FZL (Jena)

**Müller EK**, Białas N, Epple M, Hilger I. 2018. Nanoparticle-induced gene-silencing for the suppression of inflammation. 1. Wissenschaftliches Werner Kaiser-Sommersymposium, IDIR (Jena)

**Müller EK**, Gräfe C, Hochhaus A, Clement, JH. 2016. Differential Behavior of BeWo and Pericytes during Incubation with SPIONs – an initial step for the Study of Nanoparticle Processing in an in vitro Blood-Placenta Barrier Model. 8th Postgraduate Symposium on Cancer Research (Dornburg)

**Müller EK**, Gräfe C, Hochhaus A, Clement, JH. 2016. Differential Behavior of BeWo and Pericytes during Incubation with SPIONs – an initial step for the Study of Nanoparticle Processing in an in vitro Blood-Placenta Barrier Model. Tag der Nachwuchswissenschaftler des FZL (Jena)



## Ehrenwörtliche Erklärung

Hiermit erkläre ich, dass mir die Promotionsordnung der Medizinischen Fakultät der Friedrich-Schiller-Universität bekannt ist,

ich die Dissertation selbst angefertigt habe und alle von mir benutzten Hilfsmittel, persönlichen Mitteilungen und Quellen in meiner Arbeit angegeben sind,

mich folgende Personen bei der Auswahl und Auswertung des Materials sowie bei der Erstellung des Manuskripts unterstützt haben:

- Prof. Dr. Ingrid Hilger unterstützte mich bei der Auswahl und Auswertung des Datenmaterials und der Erstellung des Manuskripts
- Julia Göring und Susann Burgold unterstützten mich mit technischer Assistenz während der Tierversuche sowie bei der Anfertigung von Gewebsschnitten und der Immunfärbung
- Nataniel Bialas und Prof. Dr. Matthias Eppe synthetisierten und charakterisierten die verwendeten Nanopartikel
- Prof. Dr. Peter Schlattmann stand bei den statistischen Auswertungen beratend zur Seite
- Dr. Susann Piehler unterstützte mich durch Korrekturlesen des Manuskripts

die Hilfe eines Promotionsberaters nicht in Anspruch genommen wurde und dass Dritte weder unmittelbar noch mittelbar geldwerte Leistungen von mir für Arbeiten erhalten haben, die im Zusammenhang mit dem Inhalt der vorgelegten Dissertation stehen,

dass ich die Dissertation noch nicht als Prüfungsarbeit für eine staatliche oder andere wissenschaftliche Prüfung eingereicht habe und

dass ich die gleiche, eine in wesentlichen Teilen ähnliche oder eine Abhandlung nicht bei einer anderen Hochschule als Dissertation eingereicht habe.

---

Ort, Datum

---

Elena Kerstin Müller